Cumulative Impacts of Watershed-Scale Hyporheic Stream Restoration on Nitrate Loading to Downstream Waterbodies

Michael L. Calfe

Thesis submitted to the faculty of the Virginia Polytechnic
Institute and State University in partial fulfillment of the
requirements for the degree of

Mater of Science
In
Civil Engineering

Erich T. Hester, Chair
Durelle T. Scott
Kyle B. Strom

December 16, 2019
Blacksburg, VA

Keywords: Stream Restoration, Hyporheic, Denitrification, Chesapeake Bay, Eutrophication

Cumulative Impacts of Watershed-Scale Hyporheic Stream Restoration on Nitrate Loading to Downstream Waterbodies

Michael L. Calfe

Abstract

Excess nutrient pollution and eutrophication are widespread problems that must be solved at watershed scales, and stream restoration is increasingly implemented as a solution. Yet few studies evaluate the cumulative effects of multiple individual restoration projects on watershed-scale nutrient loading. We constructed a HEC-RAS model of stream restoration implemented throughout a generic 4th order watershed typical of the Piedmont physiographic province of the eastern USA. We simulated restoration of hyporheic exchange as one increasingly popular technique that receives dissolved nitrate-nitrogen (NO_3^--N) mitigation credit under the Chesapeake Bay TMDL. We populated the model with hyporheic exchange (0.3% of surface flow per hyporheic-exchange inducing in-stream restoration structure) and NO_3^--N removal (supply-limited denitrification removes all NO_3^--N that enters the hyporheic zone) values from prior literature on in-stream structures and related restoration techniques. We then varied the percentage of stream channels in the watershed in which restoration occurred. For watersheds with less than 100% of stream channels restored, we also varied where in the watershed (i.e. stream order) that restoration occurred. We found that hyporheic restoration in our 4th order watersheds has the potential to reduce NO_3^--N loading to downstream waterbodies by up to 83%, but that a maximum of <100% reduction exists given certain watershed characteristics. Model results revealed a nonlinear relationship between percent of stream channels restored and percent NO_3^--N loading reduction that occurred at the watershed outlet. This indicates that the effects of individual projects are not linearly additive, and must be evaluated in the context of how much of the watershed has already been restored. We also found that restoration was more effective at reducing NO_3^--N loading when it occurred in higher order streams (e.g., 3rd and 4th order), yielding load reductions upward of 30% compared to < 10% in lower order streams (e.g., 1st and 2nd order). Thus, the location of an individual restoration project within a watershed is important in determining its effect on NO_3^--N. Overall, our results indicate that hyporheic restoration can have significant effects on watershed NO_3^--N loading to downstream waterbodies, yet the watershed must be viewed as a whole to understand the potential impacts of any particular project under consideration.

Cumulative Impacts of Watershed-Scale Hyporheic Stream Restoration on Nitrate Loading to Downstream Waterbodies

Michael L. Calfe

General Audience Abstract

Nutrient pollution and harmful algal blooms are widespread problems that must be solved at watershed scales, and stream restoration is increasingly implemented as a solution. Yet few studies evaluate the cumulative effects of multiple individual restoration projects on watershed-scale nutrient loading. We constructed a HEC-RAS model of stream restoration implemented throughout a generic watershed typical of the mid-Atlantic USA. We simulated restoration of nutrient-reducing groundwater flow cells along a stream corridor (hyporheic exchange) as one increasingly popular technique that is emphasized under the Chesapeake Bay TMDL. We populated the model with hyporheic exchange and nitrate-nitrogen (NO_3^--N) removal values from prior literature on in-stream structures and related restoration techniques. We then varied the percentage of stream channels in the watershed in which restoration occurred. For watersheds with less than 100% of stream channels restored, we also varied where in the watershed (i.e. stream order) that restoration occurred. We found that hyporheic restoration in our watershed has the potential to reduce NO_3^--N loading to downstream waterbodies by up to 83%, but that a maximum of less than 100% reduction exists given certain watershed characteristics. Model results revealed a nonlinear relationship between percent of stream channels restored and percent NO_3^--N load reduction that occurred at the watershed outlet. This indicates that the effects of individual projects are not linearly additive, and must be evaluated in the context of how much of the watershed has already been restored. We also found that restoration was more effective at reducing NO_3^--N loading when it occurred in larger streams, yielding load reductions upward of 30% compared to less than 10% in smaller streams. Thus, the location of an individual restoration project within a watershed is important in determining its effect on NO_3^--N. Understanding the maximum possible degree of NO_3^--N reducing hyporheic exchange is an important step for practitioners and policy-makers in choosing the most effective location for a stream restoration based on a project's goals, and cannot be done without analyzing the watershed as a whole. With more watershed-scale planning and a better understanding of certain physical characteristics, we can choose restoration locations and strategies that will ultimately work more efficiently toward reaching a nutrient reduction goal.

Acknowledgements

I would like to thank the Charles E. Via, Jr. Endowment at Virginia Tech and Dr. Paolo Scardina for providing me with support while completing my M.S. Thesis. I thank Dr. Tess Thompson for valuable classes on stream restoration and fluvial geomorphology that pointed me toward very useful literature and ideas implemented throughout my project. Additionally, I would like to thank my family and friends for all of their support. Finally, I would like to thank my advisor Dr. Erich Hester, as well as my other committee members Dr. Durelle Scott and Dr. Kyle Strom for all of their assistance on developing conceptual models, interpreting results, using HEC-RAS and NHD*Plus*, teaching valuable courses, and writing.

Table of Contents

List of Figures

List of Tables

List of Abbreviations

$\bar{A}$	Total average cross-sectional area between two cross-sections, (L^2)
A_c	Cross-sectional area of the channel, (L^2)
A_f	Cross-sectional area of the floodplain, (L^2)
A_t	Total cross-sectional area of the flow, (L^2)
BMP	Best Management Practice
C_{ho}	Concentration of the surface water that enters the hyporheic zone at the furthest upstream outflow location, (M/L^3)
C_{lat}	Concentration of the groundwater upwelling, (M/L^3)
D	Bankfull depth, (L)
DA	Drainage area, (L^2)
DO	Dissolved oxygen
DOC	Dissolved organic carbon
HABs	Harmful Algal Blooms
HEC-RAS	Hydrologic Engineering Center River Analysis System
HEC-HMS	Hydrologic Engineering Center Hydrologic Modeling System
HSPF	Hydrological Simulation Program – FORTRAN
HUC	Hydrologic Unit Code
K	Soil hydraulic conductivity, (L/T)
L	Stream length, (L)
N_i	Number of streams if order i in a given watershed, (#)
N_{i+1}	Number of streams if order i+1 in a given watershed, (#)
NHD	National Hydrography Dataset
Q	Surface water flow rate, (L^3/T)
Q_{hi}	Flow into surface water from the hyporheic zone after a restoration, (L^3/T)
Q_{ho}	Flow out of surface water into hyporheic zone at the upstream end of a restoration, (L^3/T)
$\bar{Q}_l$	Average lateral inflow between two cross-sections, (L^3/T)
Q_{lat}	Lateral inflow from groundwater, (L^3/T)
R_b	Bifurcation ratio, (-)
r_h	Percentage of surface water flowing through the hyporheic zone per in-stream feature, (%)
r_N	Percentage of denitrification in the hyporheic zone per in-stream feature, (%)
S	Average bankfull slope, (L/L)
$\bar{S}_f$	Average friction slope between two cross-sections, (L/L)
S_N	Any sources and sinks, (M/T)
S_Q	Storage from non-conveying portions of a cross-section, (L^3)
t	Time-step of the hydrograph, (T)
TMDL	Total Maximum Daily Load
USACE	United States Army Corps of Engineers
USDA	United States Department of Agriculture
USEPA	United States Environmental Protection Agency
USGS	United States Geological Survey
V	Flow velocity, (L/T)
$\forall$	Volume of the water quality cell, (L^3)

W	Bankfull width, (L)
x_c	Length of the main channel between two cross-sections, (L)
x_e	Equivalent flow path length, (L)
x_f	Length of the floodplain between two cross-sections, (L)
z	Channel bed elevation from datum, (L)
β	Velocity distribution factor, (-)
Γ	User-defined longitudinal dispersion coefficient, (L^2/T)
Φ	Arbitrary constituent concentration, (M/L^3)
ρ_b	Bulk density of soil in the hyporheic "box," (M/L^3)

1. Introduction

1.1 Literature Review

1.1.1 Stream Restoration as a Solution to Excess Nutrient Loading

Excess nutrient loading to coastal waters presents a worldwide threat to coastal ecological communities, and is largely a product of human impacts in response to the needs of a growing population [*Boyer et al.*, 2006]. Since the mid-1900s when the use of nitrogen-based fertilizers in agriculture became a more widespread practice, eutrophication in waterbodies up to the oceanic-scale (e.g. the Baltic Sea, Black Sea, East China Sea, Gulf of Mexico, etc.) has resulted in the development of hypoxic zones and harmful algal blooms (HABs) that significantly decrease the amount of dissolved oxygen (DO) available to aquatic organisms [*Diaz & Rosenberg*, 2008; *Howarth et al.*, 2000; *Oelsner & Stets*, 2019]. HABs are highly competitive and can alter every stage of growth in other aquatic organisms' lifespans [*Li et al.*, 2015], and when they die lead to the formation of "dead zones" where there is not sufficient DO to support any surviving aquatic life [*Diaz & Rosenberg*, 2008]. Higher riverine discharges and therefore higher nutrient loads are trending upward as a result of urbanization and global climate change, leading to potential exacerbation of the current consequences felt from these HABs [*Diaz & Rosenberg*, 2008; *Oelsner & Stets*, 2019]. These trends in HAB and hypoxic zone development have severe implications on human survival in regions that rely on coastal resources.

In 2010 the United States Environmental Protection Agency (USEPA) implemented the largest effort for water quality improvement in the agency's history on the 165,000 km^2 Chesapeake Bay watershed [*USEPA*, 2019]. Historically the Chesapeake Bay has been a valuable economic resource from its fisheries, and was recognized as one of the most diverse ecological communities in the United States, being home to over 3,600 unique species of plants and animals [*Chesapeake Bay Foundation*, 2019]. In the decades prior to the total maximum daily load (TMDL) legislation, excess nutrient and sediment loads from agriculture and urbanization greatly impacted the habitat that these important plants and animals rely on to survive [*Chesapeake Bay Foundation*, 2019; *USEPA*, 2019]. Excess nutrient loads in particular have led to eutrophication and the development of harmful algal blooms (HABs) throughout the Bay that block sunlight from reaching the marine grasses that provide the aquatic community with dissolved oxygen (DO) and are home to many of these important aquatic organisms [*Li et al.*, 2015]. These are the primary reasons that species like oysters are currently surviving at rates

less than 5% of what they were at their peak in the late 1800's [*Chesapeake Bay Foundation*, 2019; *Li et al.*, 2015]. The TMDL has called for a 25% reduction in nitrogen, 24% reduction in phosphorous, and a 20% reduction in sediment by 2025 as a final attempt to restore the Bay to its once diverse and bountiful condition [*USEPA*, 2010]. The midpoint assessment on the TMDL completed in 2017 passed its goals for phosphorous and sediment but failed to reach its nitrogen reduction goal [*USEPA*, 2018], which as a result has left the Bay still at risk for eutrophication and HAB development [*Bennett*, 2017; *Li et al.*, 2015].

Stream restoration has been looked at as one of the most effective potential strategies to meet the goals of the TMDL, specifically the nitrogen requirement [*Berg et al.*, 2014; *Bernhardt et al.*, 2005; *Craig et al.*, 2008; *Filoso & Palmer*, 2011; *Kasahara & Hill*, 2006; *Thompson et al.*, 2018]. Degraded East Coast streams tend to lack riparian buffers that protect the corridor from overland nutrient sources, and are highly incised – continually cutting into floodplains that consist of hundreds of years of legacy sediment deposits [*Walter & Merritts*, 2008]. Common strategies utilized in stream restoration act to stabilize banks and reduce legacy nutrient loads [*Donovan et al.*, 2015], reconnect the main channel to a vegetated floodplain that allows sediment to settle out during storm events with nutrients potentially undergoing denitrification in floodplain soils [*Hester et al.*, 2016], and induce hyporheic exchange into sediments that are home to denitrifying bacteria [*Crispell & Endreny*, 2009; *Herzog et al.*, 2016; *Hester & Doyle*, 2008]. Due to all the different mechanisms of nutrient removal that common stream restoration strategies employ, along with numerous other ecologically beneficial results such as increased fish passage and restored in-stream habitat [*Bernhardt et al.*, 2005], governmental bodies quickly developed mitigation credit standards for restoration [*Berg et al.*, 2014] such that stream restoration has blossomed into a billion dollar industry [*Thompson et al.*, 2018]. However, the ambiguity of the current protocol's mitigation credit rewarding system has created a race to obtain as many streams as possible to "restore" with an overall lack of watershed-scale planning [*Stack*, 2019].

Perhaps the most questionable protocol in the Chesapeake Bay nitrogen mitigation credit protocol [*Hester et al.*, 2016; *Stack*, 2019; *USEPA*, 2018] is Protocol 2: Instream Denitrification [*Berg et al.*, 2014]. In Protocol 2, the procedure for rewarding nitrogen removal credit depends on the successful implementation of a "hyporheic box" which extends the entire length of the restored reach at a uniform depth and is used along with a single denitrification rate to determine

the effectiveness of a restoration project [*Berg et al.*, 2014]. In nature, the hyporheic zone is the region surrounding the wetted perimeter of a channel where surface water flows through a groundwater flow cell and eventually re-enters the channel somewhere downstream according to the bed material and hydraulic head gradient [*Hester & Doyle*, 2008; *Wondzell*, 2011]. This zone often creates ideal conditions for the process of denitrification (oxidized nitrogen; i.e. nitrate transformed to dinitrogen gas) due to its oxygen depleted shallow sediments and ample dissolved organic carbon (DOC) sources from biomass (i.e. woody material, leaves, and/or dead aquatic life) [*Hester et al.*, 2018; *Newcomer Johnson et al.*, 2016; *Zarnetske et al.*, 2011]. Studies have shown that the hyporheic zone that exists in any alluvial system has significant effects on nutrient attenuation and the overall health of a stream ecosystems [*Hester & Gooseff*, 2011; *Hiscock & Grischek*, 2001; *Newcomer Johnson et al.*, 2016; *Stanford & Ward*, 1993]; hence the nutrient mitigation credit rewarded for proving the existence of said hyporheic zone [*Berg et al.*, 2014].

The issue with the Berg *et al.* (2014) protocol is that numerous reach-scale studies have shown that hyporheic exchange is a much more complicated and variable process than their current conceptualization that lacks any intricate functional considerations [*Hester et al.*, 2016; *Stack*, 2019]. A single restoration may have different orders of magnitude of hyporheic exchange resulting from every aspect that went into the design whether it be different in-stream structure type (fully-spanning weirs or J-vanes) [*Hester & Doyle*, 2008], meander bends [*Kiel & Bayani Cardenas*, 2014], bedforms [*Gomez-Velez et al.*, 2015], or step-pool configurations [*Kasahara & Hill*, 2006], among others. Without considering the differing degrees of denitrification occurring around each of these unique features, the protocol tends to overestimate the reductions being obtained by restoration projects [*Stack*, 2019], which likely contributed to the TMDL failing to meet its midpoint nitrogen removal goal [*USEPA*, 2018].

In addition to the overestimation problems of the mitigation protocol, there is very little watershed-scale planning within the industry [*Maryland Dept. of Information Technology*, 2019; *Stack*, 2019]. While there are numerous reach-scale studies that have successfully quantified stream restoration's ability to induce hyporheic exchange and increase denitrification rates [*Azinheira et al.*, 2014; *Boulton*, 2007; *Crispell & Endreny*, 2009; *Gordon et al.*, 2013; *Groffman et al.*, 2005; *Herzog et al.*, 2016; *Hester et al.*, 2018; *Morén et al.*, 2017], very few of those studies have investigated the cumulative impacts of restoration at the watershed-scale. We know

that watersheds are highly interconnected and interdependent systems, yet the only watershed-scale studies on restoration are for floodplain management and reconnection [*Bohn & Kershner*, 2002; *Christopher et al.*, 2017; *Singh et al.*, 2019]. The failure to meet the goals of the midpoint assessment and the knowledge gap between the reach and watershed-scales were the primary motivators behind this study.

1.1.2 Piedmont Physiographic Province Watershed and Stream Characteristics

We began with an in-depth study on specific watershed and stream characteristics so we could develop a realistic model domain to carry out our stream restoration scenarios. Watersheds are very spatially organized systems that are controlled externally by climate, plate tectonics, base level, and human activity; and are controlled internally by factors such as local geology, topography, and vegetation [*Charlton*, 2008]. The Chesapeake Bay Watershed in particular is a hotspot for stream restoration for water quality purposes given the landmark Chesapeake Bay TMDL [*USEPA*, 2010].

Regional similarities between these driving forces of geomorphologic process have led to the development of the physiographic provinces across the United States. The Chesapeake Bay Watershed is made up of multiple physiographic provinces spanning from New York to Virginia; including the Valley and Ridge, Piedmont, and Coastal Plain [*Hanson et al.*, 2016]. We focused on the eastern boundary of the Piedmont in particular, due to the high amount of stream restoration being carried out [*Maryland Dept. of Information Technology*, 2019], which in turn is due to a high proportion of single-threaded channels [*Cinotto*, 2003; *Lotspeich*, 2009; *USDA*, 2007], urbanization in and around growing cities (e.g., Baltimore and Washington), and proximity to the polluted Chesapeake Bay [*Howarth et al.*, 2000; *Oelsner & Stets*, 2019; *Thompson et al.*, 2018].

Lower order watersheds within each physiographic province tend to develop similar spatial patterns according to all these driving forces. The Piedmont consists of low, well-rounded hills and long, northeast trending valleys and ridges ranging from about 90 to 180 m above sea level, with stream reliefs in the range of 30 to 60 m [*Swain et al.*, 1991]. The more gentle topography and the geology of the region has led to more dendritic drainage networks as compared to the trellis patterns seen in the western-adjacent Valley and Ridge physiographic province [*Swain et al.*, 1991].

There are always more low order streams than high order streams in any given watershed based on the definition of Strahler ordering [*Strahler*, 1957]. Although individual high order streams are longer than low order reaches, there is often more cumulative stream length of lower order reaches in a given watershed; hence the focus of stream restoration being in lower order reaches (i.e., 1st – 3rd order streams) [*Craig et al.*, 2008]. The ratio of streams of order n to streams of order n+1 in a watershed is known as the bifurcation ratio and varies according to the type of watershed [*Morisawa*, 1962; *Strahler*, 1957].

Channel features are largely dependent on drainage area, which has led to the development of scalable Hortonian relationships to be used in prediction and design [*McCuen*, 2005]. Due to the similarities in geology and climate associated with the physiographic provinces, the USGS utilized stream gauge data and developed statistical relationships with drainage area for cross-sectional, flow, and longitudinal properties (bankfull discharge, width, depth, cross-sectional area, and slope) known as regional curves [*Cinotto*, 2003; *Lotspeich*, 2009]. Hack (1957) studied longitudinal profiles of streams in the Piedmont regions of Virginia and Maryland to develop Horton relationships for length according to drainage area. This dataset consisted of over 400 streams in the region. His findings in this paper and other studies on the Hortonian relationship between length and drainage area have held true within numerous different landscapes [*Hack*, 1957] to the point that the relationship is now known as Hack's Law. Finally, baseflow characteristics are also a function of drainage area and the USGS developed direct multipliers (units of discharge per unit drainage area) for different geologic and climatic settings [*Nelms et al.*, 1995]. All of these datasets and relationships were used to develop a hypothetical 4th order Piedmont watershed in HEC-RAS to implement different configurations of hyporheic restoration.

In-stream structures are typically implemented roughly every 30 m of channel when included in a restoration design [*Hester et al.*, 2018; *Hester et al.*, 2016; *USDA*, 2007]. Reach-scale studies have shown that a fully spanning weir ("cross-vane") installed in a mildly gaining stream with streambed hydraulic conductivity of ~10^{-4} m/s (gravel and cobble with some fines) induces ~0.3% of the surface water into the hyporheic zone [*Azinheira et al.*, 2014]. We chose the value from Azinheira *et al.* (2014) due to the study site's proximity to the Piedmont (Virginia Valley & Ridge province), yet its magnitude is similar to other studies including in-stream gravel bars in a 4th order mountain stream in Oregon (0.007% for storms - 0.79% for summer low

flows) [*Wondzell & Swanson*, 1996], and 2nd through 4th order streams with cross-vanes in central New York (~0.4%) [*Gordon et al.*, 2013]. Exchange and denitrification rates are highly variable depending on sediment hydraulic conductivity and residence time within the hyporheic flow cell [*Hester et al.*, 2018; *Zarnetske et al.*, 2011], yet many such cells are supply or transport-limited [*Hester et al.*, 2016] where denitrification is complete with upwelling back to the channel at 0 mg/L [*Herzog et al.*, 2016; *Hester et al.*, 2016].

1.2 Research Objectives

The purpose of our study was to investigate watershed-scale impacts of hyporheic restoration on denitrification using a method that can accurately simulate variation in induced hyporheic exchange among different in-stream features. While there are numerous reach-scale studies that successfully quantify effects of stream restoration on hyporheic exchange and denitrification [*Azinheira et al.*, 2014; *Boulton*, 2007; *Crispell & Endreny*, 2009; *Gordon et al.*, 2013; *Groffman et al.*, 2005; *Herzog et al.*, 2016; *Hester et al.*, 2018; *Morén et al.*, 2017], to our knowledge none have investigated the cumulative impacts of restoration at the watershed-scale. Additionally, the current Chesapeake Bay nitrogen mitigation credit system outlined in Protocol 2 of Berg *et al.* (2014) does not account for known spatial and temporal variability in hyporheic function (i.e., in removal magnitude and efficiency) [*Hester et al.*, 2016; *Stack*, 2019]. We chose HEC-RAS as a model that is well known by stream restoration practitioners. We chose it over more typical watershed models (e.g., HEC-HMS, HSPF) for its ability to model channel networks while accounting for detailed variation in spatially-explicit sources and sinks along the channel that can simulate water and contaminant exchange with the hyporheic zone. Thus, our specific objectives were to:

1. Develop a simulation approach using HEC-RAS that can mechanistically account for spatial variation in hyporheic exchange effects on denitrification at the watershed-scale;
2. Use the model to investigate how the effect of hyporheic restoration on nitrate-nitrogen (NO_3^--N) load reduction varies with percent of watershed stream length restored; and
3. among individual stream orders;
4. Compare our results to the current Chesapeake Bay nitrogen mitigation credit system outlined in Protocol 2 of Berg *et al.* (2014).

1.3 Organization of Thesis

This thesis is organized around a journal article that will be submitted for publication in *Ecological Engineering*. The journal article is located in Section 2 of this document and is the central component of the study. Section 1 is a more detailed literature review used to write the article introduction (Section 2.1) and Section 3 is an extension of the article conclusion (Section 2.5) on the greater engineering significance of the research. The thesis concludes with Appendices containing detailed methodology on running the model in HEC-RAS, our auxiliary R code, how to interpret results from different simulations, and raw data used in model simulations and figure development.

<u>Section 2</u>

Calfe, M.L., D.T. Scott, and E.T. Hester (2020). Cumulative Impacts of Watershed-Scale Hyporheic Stream Restoration on Nitrate Loading to Downstream Waterbodies. To be submitted to *Ecological Engineering*.

References

Azinheira, D. L., Scott, D. T., Hession, W., & Hester, E. T. (2014). Comparison of effects of inset floodplains and hyporheic exchange induced by in-stream structures on solute retention. Water Resources Research, 50(7), 6168-6190. doi:10.1002/2013WR014400

Bencala, K. E., & Walters, R. A. (1983). Simulation of solute transport in a mountain pool-and-riffle stream: A transient storage model. Water Resources Research, 19(3), 718-724. doi:10.1029/WR019i003p00718

Bennett, L. (2017). Algae, Cyanobacteria Blooms, and Climate Change. The Climate Institute.

Berg, J., Burch, J., Cappucciti, D., Filoso, S., Lisa, F.-M., Goerman, D., . . . Winters, J. (2014). Recommendations of the Expert Panel to Define Removal Rates for Individual Stream Restoration Projects. Retrieved from Chesapeake Bay Program:

Bernhardt, E. S., Palmer, M. A., Allan, J. D., Alexander, G., Barnas, K., Brooks, S., . . . Sudduth, E. (2005). Synthesizing U.S. River Restoration Efforts. Science, 308(5722), 636. doi:10.1126/science.1109769

Bohn, B. A., & Kershner, J. L. (2002). Establishing aquatic restoration priorities using a watershed approach. Journal of Environmental Management, 64(4), 355-363. doi:https://doi.org/10.1006/jema.2001.0496

Boulton, A. J. (2007). Hyporheic rehabilitation in rivers: restoring vertical connectivity. Freshwater Biology, 52(4), 632-650. doi:10.1111/j.1365-2427.2006.01710.x

Boyer, E. W., Howarth, R. W., Galloway, J. N., Dentener, F. J., Green, P. A., & Vörösmarty, C. J. (2006). Riverine nitrogen export from the continents to the coasts. Global Biogeochemical Cycles, 20(1). doi:10.1029/2005GB002537

Brunke, M. (1999). Colmation and Depth Filtration within Streambeds: Retention of Particles in Hyporheic Interstices. International Review of Hydrobiology, 84(2), 99-117. doi:10.1002/iroh.199900014

Bunte, K., & Abt, S. R. (2001). Sampling surface and subsurface particle-size distributions in wadable gravel-and cobble-bed streams for analyses in sediment transport, hydraulics, and streambed monitoring. Gen. Tech. Rep. RMRS-GTR-74. Fort Collins, CO: U.S. Department of Agriculture, Forest Service, Rocky Mountain Research Station.

Calver, A. (2001). Riverbed Permeabilities: Information from Pooled Data. Groundwater, 39(4), 546-553. doi:10.1111/j.1745-6584.2001.tb02343.x

Cardenas, M. B. (2009). A model for lateral hyporheic flow based on valley slope and channel sinuosity. Water Resources Research, 45(1). doi:10.1029/2008WR007442

Charlton, R. (2008). Fundamentals of fluvial geomorphology. London: Routledge.

Chesapeake Bay Foundation. (2019). Saving a National Treasure. Retrieved from https://www.cbf.org

Chesapeake Bay Program. (2018). Chesapeake Bay Program Quick Reference Guide for Best Management Practices (BMPs): Nonpoint Source BMPs to Reduce Nitrogen, Phosphorus and Sediment Loads to the Chesapeake Bay and its Local Waters. In.

Chow, V. T. (1959). Open Channel Hydraulics. McGraw-Hill, New York.

Christopher, S. F., Tank, J. L., Mahl, U. H., Yen, H., Arnold, J. G., Trentman, M. T., . . . Royer, T. V. (2017). Modeling nutrient removal using watershed-scale implementation of the two-stage ditch. Ecological Engineering, 108, 358-369. doi:https://doi.org/10.1016/j.ecoleng.2017.03.015

Cinotto, P. J. (2003). Development of regional curves of bankfull-channel geometry and discharge for streams in the non-urban, Piedmont Physiographic Province, Pennsylvania and Maryland (2003-4014). Retrieved from Reston, VA: http://pubs.er.usgs.gov/publication/wri034014

Craig, L. S., Palmer, M. A., Richardson, D. C., Filoso, S., Bernhardt, E. S., Bledsoe, B. P., . . . Wilcock, P. R. (2008). Stream restoration strategies for reducing river nitrogen loads. Frontiers in Ecology and the Environment, 6(10), 529-538. doi:10.1890/070080

Crispell, J. K., & Endreny, T. A. (2009). Hyporheic exchange flow around constructed in-channel structures and implications for restoration design. Hydrological Processes, 23(8), 1158-1168. doi:10.1002/hyp.7230

Diaz, R. J., & Rosenberg, R. (2008). Spreading Dead Zones and Consequences for Marine Ecosystems. Science, 321(5891), 926. doi:10.1126/science.1156401

Donovan, M., Miller, A., Baker, M., & Gellis, A. (2015). Sediment contributions from floodplains and legacy sediments to Piedmont streams of Baltimore County, Maryland. Geomorphology, 235, 88-105. doi:https://doi.org/10.1016/j.geomorph.2015.01.025

Dragun, J. (1998). The Soil Chemistry of Hazardous Materials (2nd ed.): Amherst Scientific.

Filoso, S., & Palmer, M. (2011). Assessing Stream Restoration Effectiveness at Reducing Nitrogen Export to Downstream Waters. Ecological applications: a publication of the Ecological Society of America, 21, 1989-2006. doi:10.2307/41416633

Genereux, D., Leahy, S., Mitasova, H., Kennedy, C., & Corbett, D. (2008). Spatial and temporal variability of streambed hydraulic conductivity in West Bear Creek, North Carolina, USA. Journal of Hydrology, 358, 332-353. doi:10.1016/j.jhydrol.2008.06.017

Godfrey, R. G., & Frederick, B. J. (1970). Stream dispersion at selected sites (433K). Retrieved from http://pubs.er.usgs.gov/publication/pp433K

Gomez-Velez, J. D., Harvey, J. W., Cardenas, M. B., & Kiel, B. (2015). Denitrification in the Mississippi River network controlled by flow through river bedforms. Nature Geoscience, 8, 941. doi:10.1038/ngeo2567 https://www.nature.com/articles/ngeo2567#supplementary-information

Gordon, R. P., Lautz, L. K., & Daniluk, T. L. (2013). Spatial patterns of hyporheic exchange and biogeochemical cycling around cross-vane restoration structures: Implications for stream

restoration design. Water Resources Research, 49(4), 2040-2055. doi:10.1002/wrcr.20185

Groffman, P. M., Dorsey, A. M., & Mayer, P. M. (2005). N processing within geomorphic structures in urban streams. Journal of the North American Benthological Society, 24(3), 613-625. doi:10.1899/04-026.1

Hack, J. T. (1957). Studies of longitudinal stream profiles in Virginia and Maryland (294B). Retrieved from http://pubs.er.usgs.gov/publication/pp294B

Hanson, J., Chair, R., Boomer, K., Mason, P., Clearwater, D., Denver, J., . . . Uybarreta, T. (2016). Wetlands and Wetland Restoration Recommendations of the Wetland Expert Panel for the incorporation of non-tidal wetland best management practices (BMPs) and land uses in the Phase 6 Chesapeake Bay Watershed Model Prepared for With: Additional Contract Support Provided by Wetland Expert Panel iii.

Herzog, S. P., Higgins, C. P., & McCray, J. E. (2016). Engineered Streambeds for Induced Hyporheic Flow: Enhanced Removal of Nutrients, Pathogens, and Metals from Urban Streams. Journal of Environmental Engineering, 142(1), 04015053. doi:10.1061/(ASCE)EE.1943-7870.0001012

Hester, E. T., Brooks, K. E., & Scott, D. T. (2018). Comparing reach scale hyporheic exchange and denitrification induced by instream restoration structures and natural streambed morphology. Ecological Engineering, 115, 105-121. doi:https://doi.org/10.1016/j.ecoleng.2018.01.011

Hester, E. T., & Doyle, M. W. (2008). In-stream geomorphic structures as drivers of hyporheic exchange. Water Resources Research, 44(3). doi:10.1029/2006WR005810

Hester, E. T., & Gooseff, M. (2011). Hyporheic Restoration in Streams and Rivers (Vol. 194).

Hester, E. T., Hammond, B., & Scott, D. T. (2016). Effects of inset floodplains and hyporheic exchange induced by in-stream structures on nitrate removal in a headwater stream. Ecological Engineering, 97, 452-464. doi:https://doi.org/10.1016/j.ecoleng.2016.10.036

Hiscock, K., & Grischek, T. (2001). Attenuation of groundwater pollution by bank filtration. Journal of Hydrology, 266, 139-144. doi:10.1016/S0022-1694(02)00158-0

Howarth, R. W., Anderson, D. B., Cloern, J. E., Elfring, C., Hopkinson, C. S., Lapointe, B., . . . Walker, D. (2000). Issues in ecology: Nutrient pollution of coastal rivers, bays, and seas.

Jones, C. N., Scott, D. T., Guth, C., Hester, E. T., & Hession, W. C. (2015). Seasonal Variation in Floodplain Biogeochemical Processing in a Restored Headwater Stream. Environmental Science & Technology, 49(22), 13190-13198. doi:10.1021/acs.est.5b02426

Kasahara, T., & Hill, A. R. (2006). Effects of riffle–step restoration on hyporheic zone chemistry in N-rich lowland streams. Canadian Journal of Fisheries and Aquatic Sciences, 63(1), 120-133. doi:10.1139/f05-199

Kiel, B. A., & Bayani Cardenas, M. (2014). Lateral hyporheic exchange throughout the Mississippi River network. Nature Geoscience, 7, 413. doi:10.1038/ngeo2157 https://www.nature.com/articles/ngeo2157#supplementary-information

Knust, A. E., & Warwick, J. J. (2009). Using a fluctuating tracer to estimate hyporheic exchange in restored and unrestored reaches of the Truckee River, Nevada, USA. Hydrological Processes, 23(8), 1119-1130. doi:10.1002/hyp.7218

Li, J., Glibert, P. M., & Gao, Y. (2015). Temporal and spatial changes in Chesapeake Bay water quality and relationships to Prorocentrum minimum, Karlodinium veneficum, and CyanoHAB events, 1991–2008. Harmful Algae, 42, 1-14. doi:https://doi.org/10.1016/j.hal.2014.11.003

Lotspeich, R. R. (2009). Regional curves of bankfull channel geometry for non-urban streams in the Piedmont Physiographic Province, Virginia. (51 p.). Reston, VA

Maryland Dept. of Information Technology. (2019). Maryland Trust Fund Restoration Mapper (DNR). Retrieved from https://data.imap.maryland.gov/datasets/5d35e10a473e4630b90f67f3511ccd38

McCuen, R. H. (2005). Hydrologic analysis and design (3rd ed). Upper Saddle River, NJ: Pearson Education Inc.

Morén, I., Wörman, A., & Riml, J. (2017). Design of Remediation Actions for Nutrient Mitigation in the Hyporheic Zone. Water Resources Research, 53(11), 8872-8899. doi:10.1002/2016WR020127

Morisawa, M. E. (1962). Quantitative Geomorphology of Some Watersheds in the Appalachian Plateau. GSA Bulletin, 73(9), 1025-1046. doi:10.1130/0016-7606(1962)73[1025:QGOSWI]2.0.CO;2

Nelms, D. L., Harlow Jr, G. E., & Hayes, D. C. (1995). Base-flow characteristics of streams in the Valley and Ridge, Blue Ridge, and Piedmont physiographic provinces of Virginia (95-298). Retrieved from http://pubs.er.usgs.gov/publication/ofr95298

Newcomer Johnson, T., Kaushal, S., Mayer, P., Smith, R., & Sivirichi, G. (2016). Nutrient Retention in Restored Streams and Rivers: Global Review and Synthesis.

Oelsner, G. P., & Stets, E. G. (2019). Recent trends in nutrient and sediment loading to coastal areas of the conterminous U.S.: Insights and global context. Science of the Total Environment, 654, 1225-1240. doi:https://doi.org/10.1016/j.scitotenv.2018.10.437

Pierson, S. M., Rosenbaum, B. J., McKay, L. D., & Dewald, T. G. (2008). Strahler Stream Order and Strahler Calculator Values in NHDPlus. In.

Robertson, W. D., & Merkley, L. C. (2009). In-Stream Bioreactor for Agricultural Nitrate Treatment. 38(1), 230-237. doi:10.2134/jeq2008.0100

Schumm, S. A. (1956). Evolution of Drainage Systems and Slopes in Badlands at Perth Amboy, New Jersey. GSA Bulletin, 67(5), 597-646. doi:10.1130/0016-7606(1956)67[597:EODSAS]2.0.CO;2

Sheibley, R. W., Ahearn, D. S., & Dahlgren, R. A. (2006). Nitrate loss from a restored floodplain in the Lower Cosumnes River, California. Hydrobiologia, 571(1), 261-272. doi:10.1007/s10750-006-0249-2

Singh, N. K., Gourevitch, J. D., Wemple, B. C., Watson, K. B., Rizzo, D. M., Polasky, S., & Ricketts, T. H. (2019). Optimizing wetland restoration to improve water quality at a regional scale. Environmental Research Letters, 14(6), 064006. doi:10.1088/1748-9326/ab1827

Stack, B. (Producer). (2019). Chesapeake Bay Program Stream Restoration Credits: Moving Toward Functional Lift? Retrieved from https://www.cwp.org/chesapeake-bay-program-stream-restoration-credits-moving-toward-functional-lift/

Stanford, J. A., & Ward, J. V. (1993). An Ecosystem Perspective of Alluvial Rivers: Connectivity and the Hyporheic Corridor. Journal of the North American Benthological Society, 12(1), 48-60. doi:10.2307/1467685

Strahler, A. N. (1957). Quantitative analysis of watershed geomorphology. Eos, Transactions American Geophysical Union, 38(6), 913-920. doi:10.1029/TR038i006p00913

StructX. (2019). Structural Engineering Resources - Density Ranges for Different Soil Types. Retrieved from https://structx.com/Soil_Properties_002.html

Swain, L. A., Hollyday, E. F., Daniel Iii, C. C., & Zapecza, O. S. (1991). Plan of study for the regional aquifer-system analysis of the Appalachian Valley and Ridge, Piedmont, and Blue Ridge physiographic provinces of the eastern and southeastern United States, with a description of study-area geology and hydrogeology (91-4066). Retrieved from http://pubs.er.usgs.gov/publication/wri914066

Thompson, J., Pelc, C. E., Brogan, W. R., & Jordan, T. E. (2018). The multiscale effects of stream restoration on water quality. Ecological Engineering, 124, 7-18. doi:https://doi.org/10.1016/j.ecoleng.2018.09.016

USACE. (2016a). HEC-RAS River Analysis System Hydraulic Reference Manual. U.S. Army Corps of Engineers Institute for Water Resources Hydrologic Engineering Center.

USACE. (2016b). HEC-RAS River Analysis System User's Manual. US Army Corps of Engineers Institue for Water Resources Hydrologic Engineering Center.

USDA. (2007). Stream Restoration Design. Part 654 National Engineering Handbook.

USEPA. (2010). Chesapeake Bay Total Maximum Daily Load for Nitrogen, Phosphorus and Sediment. . U.S. Environmental Protection Agency, Region 3.

USEPA. (2018). Midpoint Assessment of the Chesapeake Bay Total Maximum Daily Load. Retrieved from https://www.epa.gov/sites/production/files/2018-07/documents/factsheet-epa-midpoint-assessment-chesapeake-bay-tmdl.pdf

USEPA. (2019). Chesapeake Bay Total Maximum Daily Load (TMDL). Retrieved from https://www.epa.gov/chesapeake-bay-tmdl

USGS. (2019). Science in Your Watershed. Retrieved from https://water.usgs.gov/wsc/map_index.html

Walter, R. C., & Merritts, D. J. (2008). Natural Streams and the Legacy of Water-Powered Mills. Science, 319(5861), 299. doi:10.1126/science.1151716

Wondzell, S. M. (2011). The role of the hyporheic zone across stream networks. Hydrological Processes, 25(22), 3525-3532. doi:10.1002/hyp.8119

Wondzell, S. M., & Swanson, F. J. (1996). Seasonal and Storm Dynamics of the Hyporheic Zone of a 4th-Order Mountain Stream. II: Nitrogen Cycling. Journal of the North American Benthological Society, 15(1), 20-34. doi:10.2307/1467430

Zarnetske, J. P., Haggerty, R., Wondzell, S. M., & Baker, M. A. (2011). Dynamics of nitrate production and removal as a function of residence time in the hyporheic zone. Journal of Geophysical Research: Biogeosciences, 116(G1). doi:10.1029/2010JG001356

2. Cumulative Impacts of Watershed-Scale Hyporheic Stream Restoration on Nitrate Loading to Downstream Waterbodies

2.1 Introduction

Excess nutrient loading from human activities to coastal waters presents a threat to coastal ecological communities worldwide [*Boyer et al.*, 2006]. Since the use of nitrogen-based fertilizers in agriculture became widespread in the mid-1900s, eutrophication has resulted in hypoxic zones and harmful algal blooms (HABs) in waterbodies up to the oceanic-scale (e.g. Baltic Sea, Black Sea, East China Sea, Gulf of Mexico) [*Diaz & Rosenberg*, 2008; *Howarth et al.*, 2000; *Oelsner & Stets*, 2019]. HABs are aggressive, affecting growth of other aquatic organisms [*Li et al.*, 2015] and forming "dead zones" of low dissolved oxygen (DO) as they decompose [*Diaz & Rosenberg*, 2008]. Higher stream flow from urbanization and global climate change also increase nutrient loads and exacerbate these effects [*Diaz & Rosenberg*, 2008; *Oelsner & Stets*, 2019].

By 2010, more than 60% of U.S. coastal rivers and bays were classified as moderately or severely degraded by nutrient pollution [*Howarth et al.*, 2000] leading the United States Environmental Protection Agency (USEPA) to implement the monumental Chesapeake Bay total maximum daily load (TMDL) for excess nutrients and sediment [*Chesapeake Bay Foundation*, 2019; *USEPA*, 2019]. At that time, important commercial species such as oysters were surviving at rates less than 5% of their peak in the late 1800's [*Chesapeake Bay Foundation*, 2019; *Li et al.*, 2015]. The TMDL midpoint assessment in 2017 passed its goals for phosphorous and sediment but failed to reach its nitrogen reduction goal [*USEPA*, 2018], leaving the Bay still at risk for HAB development [*Bennett*, 2017; *Li et al.*, 2015].

Stream restoration is a multibillion dollar industry with goals of in-stream and riparian zone habitat improvement, flow modification, and water quality management [*Bernhardt et al.*, 2005; *Thompson et al.*, 2018]. In particular, it has recently been viewed as one of the most effective potential strategies to implement the TMDL, specifically the nitrogen requirement [*Berg et al.*, 2014; *Bernhardt et al.*, 2005; *Craig et al.*, 2008; *Filoso & Palmer*, 2011; *Kasahara & Hill*, 2006; *Thompson et al.*, 2018]. Common strategies include bank stabilization to reduce mobilization of legacy nutrients [*Craig et al.*, 2008; *Donovan et al.*, 2015], floodplain reconnection to allow settling of particulates and contact of dissolved nutrients with reactive soils during storm events [*Hester et al.*, 2016; *Jones et al.*, 2015; *Sheibley et al.*, 2006], and

inducing hyporheic exchange into sediments that are home to denitrifying bacteria [*Crispell & Endreny*, 2009; *Herzog et al.*, 2016; *Hester & Doyle*, 2008]. The Chesapeake Bay Program led the way by developing nutrient mitigation credits for these restoration practices [*Berg et al.*, 2014]. However, the ambiguity of these protocols created a race to maximize credits without appreciable watershed-scale planning [*Stack*, 2019].

The hyporheic zone exists beneath and adjacent to channels where bidirectional exchange of surface water and groundwater occurs [*Hester & Doyle*, 2008; *Wondzell*, 2011]. This exchange has significant effects on nutrient attenuation and the overall health of a stream ecosystems [*Hester & Gooseff*, 2011; *Hiscock & Grischek*, 2001; *Newcomer Johnson et al.*, 2016; *Stanford & Ward*, 1993]. Protocol 2 of Berg *et al.* (2014) credits denitrification in streambed and riparian hyporheic zones through implementation of a "hyporheic box" extending the length of the restored reach at uniform depth multiplied by a single denitrification rate [*Berg et al.*, 2014]. Yet numerous reach-scale studies have shown that hyporheic exchange is much more variable in space and time [*Hester et al.*, 2016; *Stack*, 2019]. The effect of a restoration project on hyporheic exchange and denitrification may vary over orders of magnitude depending on installed features, including in-stream structures (fully-spanning weirs or J-vanes) [*Hester & Doyle*, 2008], meander bends [*Kiel & Bayani Cardenas*, 2014], bedforms [*Gomez-Velez et al.*, 2015], and step-pool configurations [*Kasahara & Hill*, 2006]. Without accounting for this variation, the protocol tends to overestimate reductions [*Stack*, 2019], contributing to failure to meet the TMDL midpoint nitrogen removal goal.

The purpose of our study was to investigate watershed-scale impacts of hyporheic restoration on denitrification using a method that can accurately simulate variation in induced hyporheic exchange among different in-stream features. There are numerous reach-scale studies that successfully quantify effects of stream restoration on hyporheic exchange and denitrification [*Azinheira et al.*, 2014; *Boulton*, 2007; *Crispell & Endreny*, 2009; *Gordon et al.*, 2013; *Groffman et al.*, 2005; *Herzog et al.*, 2016; *Hester et al.*, 2018; *Morén et al.*, 2017], , and there are some recent studies that quantify the cumulative effect of hyporheic exchange and even hyporheic-induced denitrification at the watershed-scale, yet their methodology does not provide sufficient flexibility to simulate all restoration practices (e.g., in-stream structures) [*Gomez-Velez et al.*, 2015]. The only watershed-scale studies of restoration for water quality purposes are for floodplain management and reconnection [*Bohn & Kershner*, 2002; *Christopher et al.*, 2017;

Singh et al., 2019]. Our objectives were thus to 1) develop a simulation approach using HEC-RAS that can mechanistically account for spatial variation in hyporheic exchange effects on denitrification at the watershed-scale, 2) use the developed model to investigate how the effect of hyporheic restoration on nitrate load reduction varies with percent of watershed stream length restored, and 3) among individual stream orders, and 4) compare our results to the current Chesapeake Bay nitrogen mitigation credit system outlined in Protocol 2 of Berg *et al.* (2014).

2.2 Methods

We utilized the United States Army Corps of Engineers (USACE) Hydrologic Engineering Center's River Analysis System (HEC-RAS) in conjunction with an auxiliary R script to simulate hyporheic exchange and denitrification induced by stream restoration in a 4th order stream network. Restoration was simulated in different patterns throughout the network to evaluate effects on overall nitrate removal capacity of the watershed. To enhance generality, the stream network used average or typical stream characteristics representative of the Piedmont physiographic province of the eastern USA.

2.2.1 Watershed and Channel Network Characteristics

We focus on the Chesapeake Bay Watershed due to extensive stream restoration for water quality purposes given the landmark Chesapeake Bay TMDL [*USEPA*, 2010]. The Chesapeake Bay Watershed is composed of multiple physiographic provinces including the Valley and Ridge (~35% by area), Piedmont (~20%), and Coastal Plain (~25%) [*Hanson et al.*, 2016]. We focus on the eastern boundary of the Piedmont in particular, due to the greater amount of stream restoration being carried out, which in turn is due to a high proportion of single-threaded channels [*Cinotto*, 2003; *Lotspeich*, 2009; *USDA*, 2007], urbanization in and around growing cities (e.g., Baltimore and Washington), and proximity to the Chesapeake Bay [*Maryland Dept. of Information Technology*, 2019].

We developed a 4th order Piedmont watershed conceptual model. A simplified generic model approach was chosen rather than a site-specific model in order to increase the generality of our results to any similar-sized watershed in the Piedmont region, although we expect our results will be applicable in part to regions beyond the Piedmont. While stream restoration is most commonly carried out on 1st through 3rd order streams due to construction restraints and

higher cumulative stream lengths within a watershed [*Craig et al.*, 2008], we also included a 4th order stream for greater generality.

HEC-RAS requires a model channel network characterized by the number and length of channel reaches, channel cross-sectional geometries, and bed slopes. These channel characteristics are strongly correlated to basin drainage area by region-specific power-law relationships, i.e. Horton Laws [*McCuen*, 2005].

2.2.1.1 Bifurcation Ratios

The bifurcation ratio relates the number of streams of order *n* to the number of streams of order *n+1* in a watershed,

$$R_b = \frac{N_i}{N_{i+1}} \tag{1}$$

where R_b is the bifurcation ratio of streams of order *i* to order *i+1* (-), N_i is the number of streams of Strahler order *i* in a given watershed (-) [*Strahler*, 1957], and N_{i+1} is the number of streams of order *i+1* in a given watershed (-).

The bifurcation ratio exhibits very small variation among regions [*Strahler*, 1957], thus this parameter did not need to be as regionally specific as other parameters. Four sources were used to determine bifurcation ratios for the model's stream network (Table 1). Strahler (1957) provided general ranges of bifurcation ratios. Regional datasets were available for the adjacent Allegheny Plateau (15 watersheds) [*Morisawa*, 1962] and the Badlands of Perth Amboy, NJ (3 watersheds) [*Schumm*, 1956]. Finally, we analyzed data from the National Hydrography Dataset (NHD*Plus*) for the Piedmont physiographic province itself.

Table 1: Bifurcation ratios determined from [*Morisawa*, 1962; *Schumm*, 1956; *Strahler*, 1957] and NHD*Plus*.

Low Order – High Order (N_i/N_{i+1})	**Bifurcation Ratio (R_b)**				
	***Strahler*, 1957**	***Morisawa*, 1962**	***Schumm*, 1956**	**NHD*Plus***	**Selected for Model**
1/2	4.0 – 5.1	3.8	4.4	2.8	4.0
2/3	2.8 - 4.9	3.9	4.8	1.8	3.0
3/4	-	4.5	4.4	1.8	2.0

We chose bifurcation ratios within the range of values seen in the data but also integers that simplify the model (Table 1). This resulted in one 4th order river, two 3rd order rivers, six 2nd order rivers, and 24 1st order rivers (Figure 1). The model was assembled symmetrically to eliminate random variation in results due to geometry or spatial layout. Again for simplicity, the 3rd order rivers were split exactly in half at the 2nd order junctions (rather than some other ratio of lengths) and the 2nd order rivers were split exactly into thirds at the 1st order junctions.

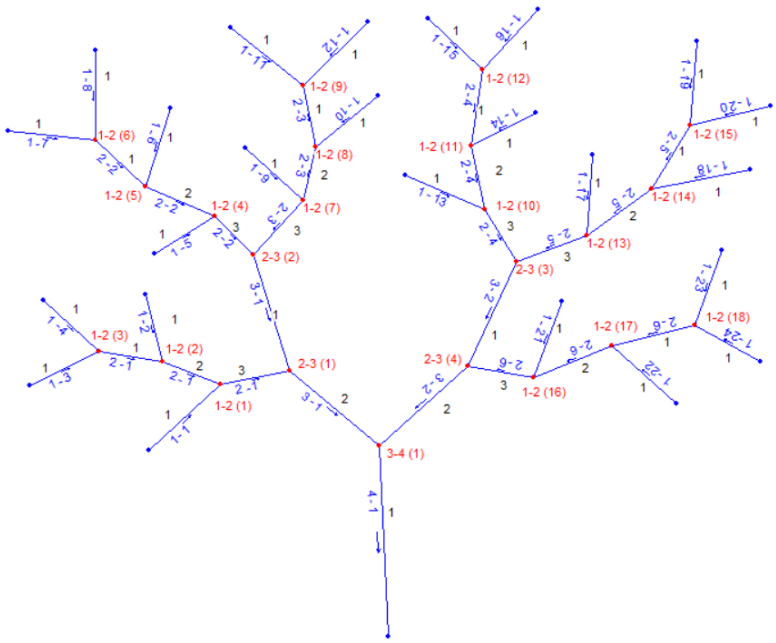

Figure 1: Plan view schematic of HEC-RAS channel network. "Rivers" are labeled in blue as "order-stream number out of total". For example, River 1-11 is the eleventh 1st order river in the model. "Reaches" are labeled by black numbers. For example, River 3-1 is split in half by River 2-1; the top half of that split is labeled with a 1 and the bottom half of that reach is labeled with a 2. "Junctions" are labeled in red as "low order-high order (junction number)". For example, junction 1-2(9) is the ninth junction between 1st and 2nd order rivers. Note that rivers are NOT drawn to scale per HEC-RAS output; for true lengths of each order river see Table 2.

2.2.1.2 Drainage Areas from Stream Orders

In order to utilize the USGS Piedmont Regional Curves [*Lotspeich*, 2009] to determine representative cross-sectional geometries, we first used the NHD*Plus* stream order and drainage area datasets [*Pierson et al.*, 2008] to find representative drainage areas. Data in NHD*Plus* is sorted based on 14-digit "ReachCodes," in which the first 8 digits are the flowline's Hydrologic Unit Code (HUC). The Piedmont is primarily made up of the 02-Mid Atlantic, and 03N-South Atlantic North HUCs. There are very small contributions from 06-Tennessee and 03W-South

Atlantic West that were not considered [*Cinotto*, 2003; *Lotspeich*, 2009; *USGS*, 2019]. We manually filtered data to the 8th digit in the HUCs to ensure data was only from the Piedmont.

The drainage areas for each stream order were right-tailed with a few outliers that we filtered out. Those outliers (~6% of the total number of streams) were at least an order of magnitude greater than the maximum from the filtered dataset, and would have resulted in ~15% greater drainage areas. Our resulting dataset included 50,839 1st order streams, 18,235 2nd order streams, 10,012 3rd order streams, and 5,511 4th order streams. Because of the high skew of the datasets, the median drainage area values were used rather than the mean (Table 2).

Table 2: 1st through 4th order representative drainage areas determined from the median of the filtered NHD*Plus* dataset, cross-sectional and longitudinal properties determined through the Virginia Piedmont USGS Regional Curves [*Lotspeich*, 2009], and stream lengths determined from Hack's Law for Piedmont Streams [*Hack*, 1957]

Stream Order	Representative drainage area (DA) [km^2]	Bankfull Width (W) [m]	Bankfull Mean Depth (D) [m]	Bankfull Slope (S) [m/m]	Model Stream Length (L) [m]
1	1.77	3.40	0.23	0.00656	1,830
2	9.74	7.00	0.46	0.00429	5,030
3	46.9	13.7	0.79	0.00289	12,800
4	202	25.6	1.4	0.00200	30,790

2.2.1.3 Channel Geometries and Slopes from Drainage Areas

We used the USGS Piedmont Regional Curves (Equations 2-4) [*Lotspeich*, 2009] to determine representative bankfull width, depth, and slope for 1st through 4th order streams (Table 2),

$$W = 12.964 * (DA)^{0.4294} \quad (2)$$

$$D = 0.891 * (DA)^{0.3721} \quad (3)$$

$$S = 0.006 * (DA)^{-0.2518} \quad (4)$$

where W is the bankfull width in (ft), D is the bankfull mean depth in (ft), S is the bankfull slope in (ft/ft), and DA is the drainage area in (mi^2). There are regional curves for the non-urban Piedmont in Maryland and Pennsylvania [*Cinotto*, 2003], and for the non-urban Piedmont in

Virginia [*Lotspeich*, 2009]. Calculations with our chosen drainage areas resulted in similar values for both sets of curves. However, we chose to use Equations 2-4 from the Virginia curves because they did not require extrapolation for the lower order streams. The lowest DA used to develop the Maryland and Pennsylvania curves in Cinotto (2003) was 6.66 km^2 which is higher than our 1st order DA (Table 2). Basins used to develop the Virginia curves ranged from 0.75 km^2 to 287 km^2, so no extrapolation was necessary for our chosen watershed areas [*Lotspeich*, 2009]. Note that while we used metric units in the HEC-RAS model, the regional curves and other USGS resources are in feet and square miles, so we used them in their native units and converted their output.

2.2.1.4 Stream Lengths from Drainage Areas

We used the Horton relationships of Hack (1957) (Hack's Law) between stream length and drainage area from over 400 streams in the Piedmont regions of Virginia and Maryland to determine the length of the 1st through 4th order rivers (Table 2),

$$L = 1.4 * (DA)^{0.6} \tag{5}$$

where L is the stream length in (mi), and DA is the drainage area in (mi^2).

2.2.2 Channel Flows from Drainage Area

Restoring hyporheic exchange using geomorphic features such as in-stream structures, gravel bars, and pool-riffle sequences will have the greatest effect on dissolved contaminants such as excess nitrate-nitrogen during baseflow conditions when the induced hyporheic exchange is the largest fraction of channel flow [*Azinheira et al.*, 2014; *Hester et al.*, 2018]. For this reason, we modeled annual average baseflow conditions that are representative of the majority of the annual cycle. To determine representative flows for each order reach in our model, we used the "mean baseflow" metric (long-term average contribution of groundwater to streams) from Virginia streams for drainage areas ranging from 1.2 to 5,996 km^2 [*Nelms et al.*, 1995]. Their dataset for the Piedmont was made up of 37 sites from the north Piedmont, 101 sites from the south Piedmont, and 40 sites from the Piedmont/Blue Ridge Transition. Each of those sub-regions had a unique mean baseflow value that we used to calculate an average of 6.16×10^{-3}

$m^3/s/km^2$ weighted by number of sites and multiplied by drainage area (Table 2) to determine surface water flow rates at the downstream end of each individual order river (Table 3).

Table 3: Channel flow rates determined from the mean baseflow characteristics of Piedmont streams in VA and the amount of lateral inflow from groundwater each of those streams needs in order to meet the conditions of continuity at each model junction.

Stream Order	Surface water flow rate at the outlet of each river (Q) [m^3/s]	Amount of gaining along each river (Q_{lat}) [m^3/s]
1	0.0113	0.00850
2	0.0596	0.0144
3	0.289	0.110
4	1.24	0.662

Given the nature of our chosen channel network (Figure 1), the flow values in Table 3 created a scenario where continuity was not met at every junction. For example, where two 1st order rivers come together, based on Table 3 that would result in a channel flow rate of 0.0226 m^3/s, which does not equal the value of 0.0595 m^3/s also in Table 3, and this issue propagated down the model. The reason for this is that the watersheds in Nelms et al. (1995) were generally gaining, and therefore also had baseflow coming into the channel between flow measurements. To correct this, we distributed this inferred baseflow as uniform gaining along each HEC-RAS river, where the flow at the upstream end of each river equaled the sum of the two lower order flow rates that join to form it, and the flow at the bottom each river equaled the corresponding value in Column 2 Table 3. The bifurcation ratios determined how much lateral inflow was needed along each reach as four 1st order rivers drained into each 2nd order river, three 2nd order rivers drained into each 3rd order river, and two 3rd order rivers drained into the 4th order river.

2.2.3 HEC-RAS Model

We chose HEC-RAS as a model that is well known by stream restoration practitioners. We chose it over more typical watershed models (e.g., HEC-HMS, HSPF) for its ability to model channel networks while accounting for detailed variation in spatially-explicit sources and sinks along the channel that can simulate water and contaminant exchange with the hyporheic zone. HEC-RAS also has the unique potential to be easily extended in the future for other restoration practices such as floodplain reconnection. Our hope is that the methods developed here can

facilitate more mechanistic determination of expected load and concentration reductions for awarding mitigation credit [*Berg et al.*, 2014; *Stack*, 2019]. Ambiguity in the current methods to determine nutrient removal credit has often resulted in over-predictions of removal [*Stack*, 2019], and is one reason the halfway total nitrogen reduction goals of the Chesapeake Bay TMDL have yet to be realized [*USEPA*, 2018].

2.2.3.1 Channel Network Geometry and Boundary Properties

We built the channel network with twenty-four 1st order HEC-RAS "rivers", six 2nd order rivers (each with 3 reaches), two 3rd order rivers (each with 2 reaches), and one 4th order river (Figure 1). Here we use HEC-RAS terms where "river" means one individual channel, and "reach" means the sections of that river after being split with a tributary junction. Each junction length was set at 200 feet to avoid overlapping of cross-sections which can cause model unsteadiness [USACE, 2016b]. This distance is considered negligible given the overall length of the watershed.

The slope of each HEC-RAS river (Table 2) was implemented by manually calculating cross-section elevations. For example, the downstream end of the 4th order channel had an elevation of 0 m. The length of the river (30,790 m) is then multiplied by the slope (0.0020 m/m) to determine the change in elevation in the z-direction (61.6 m). This then becomes the channel-bottom elevation for the downstream end of the 3rd order rivers. According to the lengths and slopes determined earlier, the 4th order river rises 61.6 m, the 3rd order rivers rise by 37.0 m, the 2nd order rivers rise 21.5 m, and the 1st order rivers rise 12.0 m. The highest overall relief in the watershed is 132.3 m between the downstream end of River 4-1 (the watershed outlet) and the upstream end of the highest 1st order rivers (Figure A - 3).

Cross-section stations and their corresponding elevations were determined from the widths and depths in Table 2. For simplicity we modeled straight (sinuosity = 1), rectangular channels throughout the watershed, with Manning's n of 0.03 [*Chow*, 1959]. We interpolated cross-sections between the manually implemented upstream and downstream cross-sections of each river in 15 m increments. This spacing was determined via a sensitivity study to reduce unsteadiness in the discretized continuity and momentum equations (Equations 6 and 7, see Section 2.2.3.2 below) as much as possible (+/- ~1.4×10^{-4} m^3/s).

2.2.3.2 Hydraulic Model and Parameters

Although our conceptual model was steady baseflow conditions, we utilized the HEC-RAS unsteady flow feature because that was necessary to allow us to specify gaining streams with baseflow uniformly distributed along the channel length. Thus we specified constant flows and ran the model until hydraulic conditions were steady throughout the entire channel network (i.e. warmup period [*USACE*, 2016a]). After a sensitivity analysis, we found that 20,000 warmup steps at 0.1 hours each allowed complete dissipation of transient numerical phenomena.

The HEC-RAS unsteady flow feature solves the 1D channel continuity and momentum equations using an implicit finite difference scheme (Equations 6 and 7, respectively) [*USACE*, 2016a].

$$\Delta Q + \frac{\Delta A_c}{\Delta t}\Delta x_c + \frac{\Delta A_f}{\Delta t}\Delta x_f + \frac{\Delta S_Q}{\Delta t}\Delta x_f - \bar{Q}_l = 0 \tag{6}$$

where Q is the channel flow rate (m^3/s), A_c is the cross-sectional area of the channel (m^2), x_c is the length of the main channel between two cross-sections (m), A_f is the cross-sectional area of the floodplain (m^2), x_f is the length of the floodplain between two cross-sections (m), S_Q is the storage from non-conveying portions of a cross-section (m^3), $\bar{Q}_l$ is the average lateral inflow between two cross-sections (m^3/s), and t is the time-step of the hydrograph (s). Since the floodplain was never inundated, the A_f term went to zero, but was included so storm events could be tested in future studies.

$$\frac{\Delta(Q_c\Delta x_c + Q_f\Delta x_f)}{\Delta t\Delta x_e} + \frac{\Delta(\beta VQ)}{\Delta x_e} + g\bar{A}\Delta z + g\bar{A}(\frac{\Delta z}{\Delta x_e} + \bar{S}_f) = 0 \tag{7}$$

where β is a velocity distribution factor (-), V is the flow velocity (m/s), $\bar{A}$ is the total average cross-sectional area between two cross-sections (m^2), z is the channel bed elevation (m), $\bar{S}_f$ is the average friction slope between two cross-sections (m/m), and x_e is the equivalent flow path (m).

At the furthest upstream cross-section of every 1st order river, an arbitrary constant flow hydrograph was implemented at 0.0028 m^3/s. Summed across all 1st order rivers this represents only ~10% of the outflow from the 4th order river, but was necessary to run the model. The downstream boundary condition of the watershed (at the final cross-section of River 4-1) was set

to be the normal depth at a slope of 0.0020 m/m. We then specified equal water surface elevations at every junction. We left all initial conditions blank and let the model use the boundary conditions as initial conditions, but because we ran the model until steady state, this choice did not affect the results.

We specified baseflow gaining from groundwater using the uniform lateral inflow feature available in the unsteady mode of HEC-RAS. The most upstream and downstream cross-sections of each river were occupied by boundary/initial conditions and used in the routing computations within junctions, respectively. Uniform lateral inflow hydrographs were thus added to the remaining cross-sections in between. For example, the cumulative lateral inflows for all 1st order cross-sections in a given 1st order river summed to 0.0085 m^3/s (Table 3). Similarly, the cumulative lateral inflows for each reach of the 2nd through 4th order rivers were set to 0.0048 m^3/s, 0.055 m^3/s, and 0.662 m^3/s, respectively. These lateral inflows, along with the point flow inputs at intermediate junctions sum to the Q values in Table 3.

2.2.3.3 Water Quality Model and Parameters

The HEC-RAS water quality module utilizes the 1D advection-dispersion equation [*USACE*, 2016b].

$$\frac{\partial}{\partial t}(\forall \Phi) = -\frac{\partial}{\partial x}(Q\Phi)\Delta x + \frac{\partial}{\partial x}\left(\Gamma A_t \frac{\partial \Phi}{\partial x}\right)\Delta x \pm S_N \tag{8}$$

where $\forall$ is the volume of the water quality cell (L), Φ is the arbitrary constituent concentration (mg/L), Q is the flow rate (L/s), Γ is the user-defined longitudinal dispersion coefficient (m^2/s), A_t is the total cross-sectional area of the flow (m^2), and S_N are any sources and sinks from upwelling or hyporheic restoration (mg/s).

$$S_N = -Q_{ho}C_{ho} + Q_{lat}C_{lat} \tag{9}$$

where Q_{ho} is the amount of water flowing through a restoration's hyporheic zone (L), C_{ho} is the concentration of the surface water that enters the hyporheic zone at the furthest upstream outflow location (mg/L), Q_{lat} is the amount of groundwater upwelling along a restored reach (Table 3 values multiplied by the fraction of stream length restored) (L), and C_{lat} is the concentration of

the groundwater upwelling (constant 1 mg/L in our model). We modeled nitrate-nitrogen (NO_3^--N) transport in the channel as an arbitrary conservative (non-reacting) constituent consistent with our conceptual model of nitrate reacting only in hyporheic (groundwater) flow. Similar to the hydraulic model, we ran the water quality model until steady state, when concentrations were no longer changing.

Concentration boundary conditions were needed at the upstream end of each river, at every flow change location, and for all uniform lateral inflows. We set all these boundary conditions to the same value to simulate a uniformly polluted watershed. This was a reasonable starting point when trying to isolate the effect of spatially-varying stream restoration practice (Section 2.2.4.2 below). We chose 1 mg/L as a typical representative value for human-impacted streams where denitrification approximately follows first order kinetics [*Hester et al.*, 2018; *Hester et al.*, 2016]. Initial conditions were needed only at the upstream end of each reach, and were set to 1 mg/L, although because we ran the model until steady state, they do not affect our results.

The final parameter needed was Γ of each reach. This parameter does not affect steady-state transport conditions, but does affect the approach to steady-state [*Bencala & Walters*, 1983]. Since we were only interested in the results after the system has reached steady-state, we chose a relatively low dispersion coefficient of 0.02 m^2/s to decrease model run times and achieve steady state more quickly. Sensitivity analyses were completed to ensure this value had no effect on the final steady state of the model.

2.2.4 Implementing Hyporheic Restoration with Aid of an Auxiliary R Script

We utilized HEC-RAS's uniform lateral inflows in conjunction with an auxiliary script written in R to simulate hyporheic exchange induced by stream restoration practices. We simulated restoration both in individual stream orders and also throughout the entire watershed to test the effect of restoration placement and cumulative watershed effects.

2.2.4.1 Simulating Hyporheic Exchange and Denitrification

Stream restoration can increase hyporheic exchange, allowing channel water to access subsurface sediment where natural bacteria carry out denitrification [*Boulton*, 2007; *Groffman et al.*, 2005; *Hester & Doyle*, 2008]. We simulated in-stream restoration structures that induce

hyporheic flow cells in the subsurface [*Crispell & Endreny*, 2009; *Hester & Doyle*, 2008], yet our simulations apply more generally to any stream restoration technique that similarly induces exchange, e.g., pool-riffle sequences, in-channel bars, and meanders [*Cardenas*, 2009; *Kasahara & Hill*, 2006; *Knust & Warwick*, 2009]. Exchange and denitrification rates are highly variable depending on sediment hydraulic conductivity and residence time within the hyporheic flow cell, yet many such cells are supply or transport-limited where denitrification is complete with upwelling back to the channel at 0 mg/L [*Herzog et al.*, 2016; *Hester et al.*, 2018; *Hester et al.*, 2016; *Zarnetske et al.*, 2011]. Thus, we assumed 100% denitrification of nitrate that entered the hyporheic zone from the channel (Figure 2).

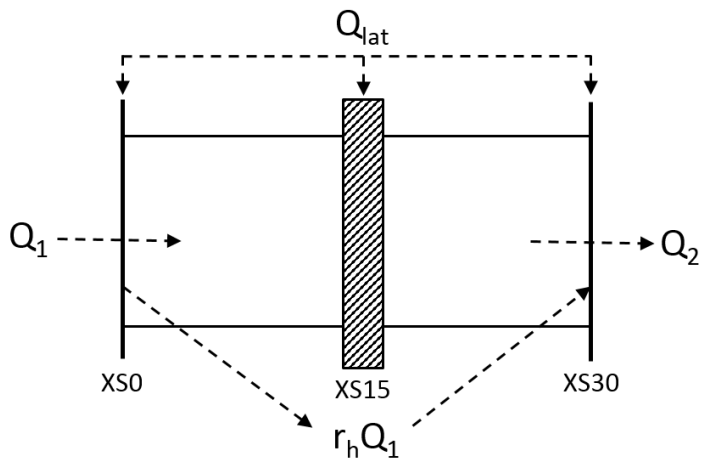

Figure 2: Plan view of channel and hyporheic flow around a fully-spanning in-stream structure (shaded rectangle) as it would be modeled in HEC-RAS. Q_1 is channel flow from upstream, Q_{lat} is a fraction of the total groundwater upwelling into the channel from all directions that is evenly distributed from the top to the bottom of each river according to Table 3 (shown here at the side of the channel for simplicity), Q_2 is channel flow to downstream, and r_h is the percentage of surface flow that leaves the channel with nitrate, flows beneath the structure in a hyporheic flow cell, and re-enters the channel downstream of the structure without nitrate. XS0, XS15, and XS30 represent HEC-RAS cross-sections.

We assumed the common restoration practice of implementing in-stream structures roughly every 30 m of channel throughout the model [*Hester et al.*, 2018; *Hester et al.*, 2016; *USDA*, 2007]. Reach-scale studies have shown that a fully spanning weir ("cross-vane") installed in a mildly gaining stream with streambed hydraulic conductivity of ~10^{-4} m/s (gravel and cobble with some fines) induces ~0.3% of the surface water into the hyporheic zone [*Azinheira et al.*, 2014]. We chose the value from Azinheira *et al.* (2014) due to the study site's proximity to the Piedmont (Virginia Valley & Ridge province with similar baseflow and soil characteristics), yet

its magnitude is similar to other studies including in-stream gravel bars in a 4th order mountain stream in Oregon (0.007% for storms - 0.79% for summer low flows) [*Wondzell & Swanson*, 1996], and 2nd through 4th order streams with cross-vanes in central New York (~0.4%) [*Gordon et al.*, 2013]. We simulated a series of structures in an R script (Figure B - 3) using a cumulative water balance based on this exchange rate and the uniform lateral inflows (Figure 3) (Equations 9-10).

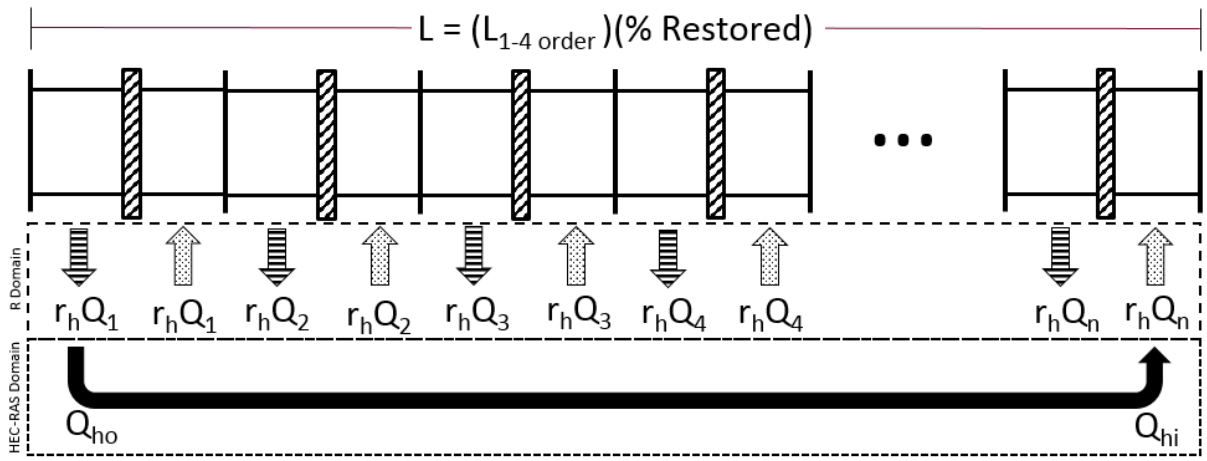

Figure 3: Conceptual model of hyporheic exchange induced by multiple restoration structures along a given HEC-RAS river. Calculations are split between the R code (upper dashed box simulating the hyporheic exchange and nitrate mass loss to the subsurface) and HEC-RAS (lower dashed box showing how the cumulative effects of the hyporheic exchange simulated by R were implemented in the water quality module of HEC-RAS). Q_{lat} is omitted for simplicity.

$$Q_{ho} = Q_{hi} = r_h(Q_1) + r_h(Q_2) + r_h(Q_3) + \ r_h(Q_4) \ldots + r_h(Q_n) \tag{10}$$

$$Q_{ho} = Q_{hi} = r_h[(Q_1) + (Q_2) + (Q_3) + (Q_4) + \cdots + (Q_n)] \tag{11}$$

where Q_{ho} is the cumulative amount of surface water with nitrate going into the hyporheic zone for each percent restored (m^3/s), and Q_{hi} is the amount of water without nitrate re-entering the channel at the downstream end of a restoration (m^3/s), and n is the number of structures spaced 30 m apart corresponding to a certain length (and percentage) of channel restored.

Since HEC-RAS requires a water quality boundary condition at every flow change location (i.e. every R domain arrow in Figure 3), and the long channel lengths in the model, we treated the entire length of restored channel within a given HEC-RAS river as a single unit. We did this by sending the cumulative amount of hyporheic exchange (with nitrate) for that length of

restored channel out of the model as a lateral outflow ($Q_{ho}C_{ho}$, as in Equation 9) at the 3rd cross-section from the upstream end of each river (XS1 was occupied by the upstream flow boundary condition and XS2 was occupied by the boundary condition for the uniform lateral inflows that spanned the entire river), and having all that hyporheic water (without nitrate) re-enter all at once at the furthest downstream cross-section of the restored section of the river (Q_{hi}). Because reaction did not occur in the channel, and reaction was complete within the hyporheic zone, this had the same net effect on flow and nitrate concentrations in the channel as would occur if the hyporheic exchange induced by each structure was accounted for individually, but was computationally simpler. The R script essentially did the work of HEC-RAS within the restored length of channel and determined what lateral outflows and inflows for input to HEC-RAS were necessary at the upstream and downstream end of the restored channel length, respectively, to equal what they would have if HEC-RAS were able to directly implement the hyporheic exchange processes described in Figure 2 and shown in the "R domain" of Figure 3. The R script and HEC-RAS were coupled manually. We then repeated this process for each HEC-RAS river in the model.

2.2.4.2 Restoration Scenarios

Our first set of scenarios determined how the effect of hyporheic restoration varied by stream order (headwaters vs mainstem). We implemented restoration starting at the upstream end of every river and increased downstream in increments of 10% of the cumulative overall distance present for the given stream order. For example, restoring 10% of 1st order rivers entailed restoring the upstream-most 10% of each of 24 total 1st order rivers, equal to 4,560 m of restoration, or roughly 190 m per individual 1st order river. Table D - 1 through Table D - *4* show these percentages and their corresponding restored lengths, number of structures, and induced hyporheic exchange.

In the 3rd and 4th order restorations, water began to be recycled through the hyporheic zone. In other words, more water was cumulatively cycling through the induced hyporheic zone than was flowing down the channel at the most upstream cross-section, such that some channel water would cycle through the hyporheic zone more than once. Starting at 60% restored in the 3rd order simulations and 30% restored in the 4th order simulations, more water needed to be sent into the hyporheic zone than was available at the top of the river. For this reason, after the

simulation was completed for 50% and 20% restored, respectively, a new hyporheic inflow point was needed in the form of a new Q_{ho} point as in Figure 3. At this point, the difference between the amount of water that had already been through the hyporheic zone, and the amount needed for the corresponding percent restored was sent out at the cross-section following the 50% and 20% restored cross-section. This water was sent back out with a water quality boundary condition equal to the surface water concentration at the end of the 50% and 20% restored model run. This was only needed once in the 3rd order rivers, but was needed every 20% restored in the 4th order river. This procedure for implementing recycling in the model was benchmarked against hand calculations for small reaches to confirm the procedure was giving expected results.

Next we evaluated the effect of restoring the entire watershed starting in the 1st order rivers working down to the outlet of the 4th order river. After a lower order river was fully restored, new hyporheic outflow points (Q_{ho}) were added in each successive higher order river, with everything done prior being left in the model. The same lengths, number of structures, and amount of water into and out of the hyporheic zone for each order river remained the same as in the individual order restorations, but the corresponding percent restored values were rescaled to the watershed-scale. After each lower order river had been fully restored, the final surface water concentration in that order then became the upstream boundary condition in the water quality model at the top of the next order river moving further down the watershed.

Reductions throughout the model were gross load reductions, i.e. we did not consider any pre-existing hyporheic denitrification around meander bends, lateral storage zones, or natural steps. Therefore, any hyporheic exchange deemed to exist in a pre-watershed analysis would need to be subtracted from our gross results to determine the net effect of the new hyporheic restoration implemented in our model.

2.3 Results

2.3.1 Effect of Percent Restored

As the percent of channel restored in each stream order increased, the percent reduction of nitrate-nitrogen (NO_3^--N) load or concentration at the downstream end of that river predictably increased for all stream orders (Figure 4). These trends were often nonlinear, and overall went from concave up for the 1st order rivers to concave down for the 4th order river. In particular, the trends were all concave-up for 1st and 2nd order rivers (Figure 4A and B). Trends

in the 3rd order rivers were very slightly concave-up in the upper reaches (<50% restored) and became more linear where surface water began to recycle through the hyporheic zone (>50% restored, Figure 4C). The full 4th order river trend was slightly concave up in the upper reach (<20% restored), and became linear with slight breaks in slope at each new recycling point (every 20% restored after the first recycling point, Figure 4D); hence the concave-down appearance. As discussed more in Section 2.2.4.2 above, by recycling we mean more water was cumulatively cycling through the induced hyporheic zone than was flowing down the channel at the most upstream cross-section, such that some channel water would cycle through the hyporheic zone more than once.

The effect of NO_3^--N reductions from restoration in the low order rivers decreased moving downstream to the 4th order outlet as more water containing NO_3^--N at 1 mg/L entered via diffuse gaining from groundwater (Q_{lat}) (Figure 4A through C). For example, when all 24 1st order rivers were fully restored, the reduction at the downstream end of the 1st and 4th order rivers was 12% and 2.5% respectively, because 0.968 m^3/s of 1 mg/L water entered from groundwater in the 2nd through 4th order rivers (Table 3). Thus, restoration of higher order channels was more effective in reducing mass load and concentration at the outlet of the 4th order watershed (e.g., 83% reduction in 4th order, Figure 4D) because a higher percentage of NO_3^--N from upstream surface water and upwelling groundwater cycled through the hyporheic zone (Appendix D, Table D - 1 through Table D - 4), due in turn to greater length of these rivers and their proximity to the overall watershed outlet.

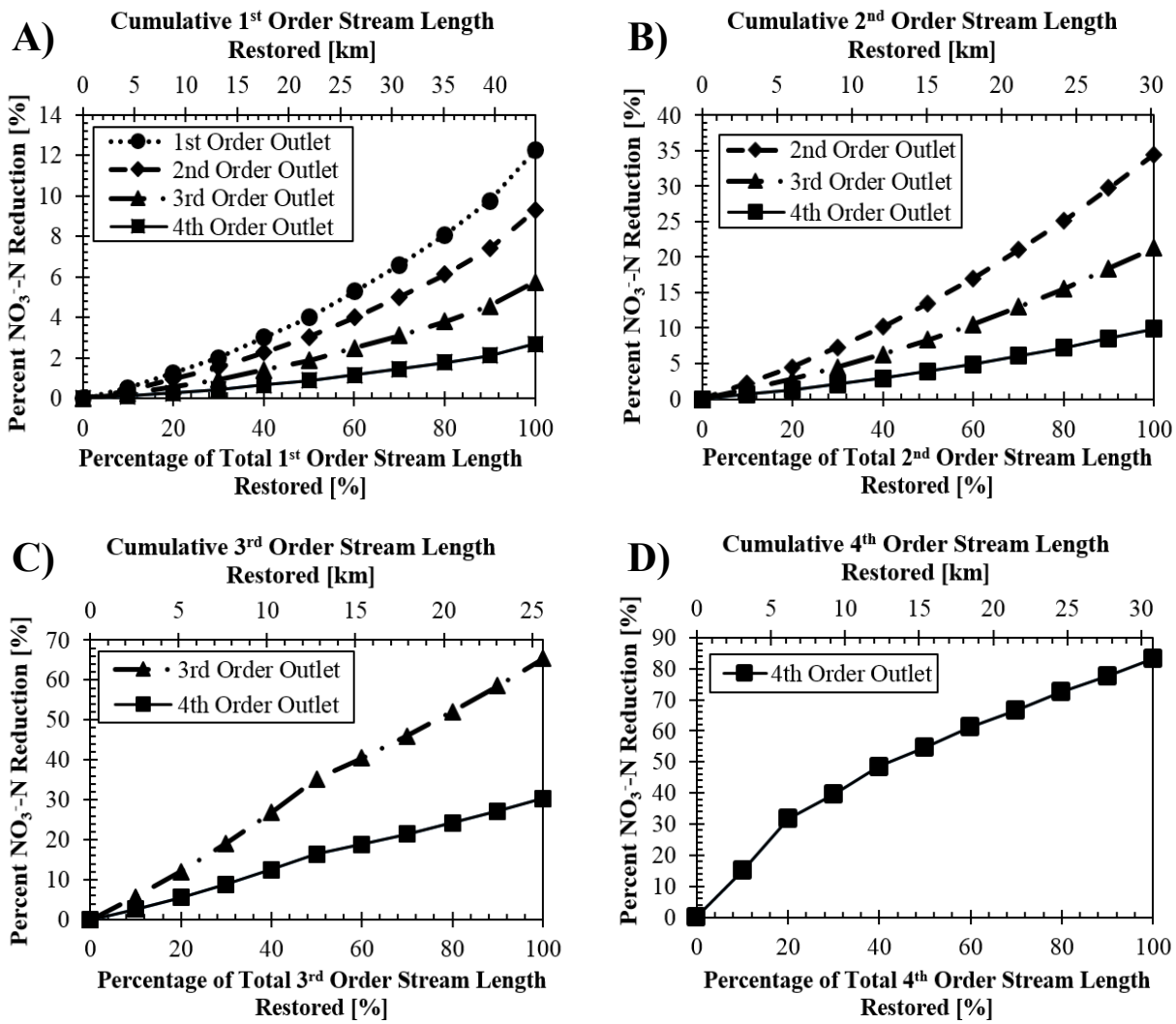

Figure 4: Percent nitrate-nitrogen (NO_3^--N) reduction in both concentration and mass at the furthest downstream cross-section of the A) 1st order rivers, B) 2nd order rivers, C) 3rd order rivers, and D) 4th order river due to restoration only in that respective stream order. All Y-axis percent reductions are on both a concentration and load basis since we used a base concentration of 1 mg/L. X-axis is percent of the cumulative channel length of that stream order that was restored, which is equal to the percent restored of each individual HEC-RAS river. Multiple lines in each panel distinguish conditions at the downstream end of the HEC-RAS rivers where restoration occurred from effects further downstream.

When considering increasing cumulative restoration of all order streams in the 4th order watershed, concavity in each order river matched that when restoration of each order was considered separately except in the 4th order river (compare Figure 4 and Figure 5A). In particular, trends were nonlinear concave-up in the 1st, 2nd, and upper reach of the 3rd order rivers where no surface water recycling takes place, and linear in the lower 3rd order reach as they were

in Figure 4A-C. The trend differed from the individual 4th order restoration (Figure 4D) in that percent reduction along the entire river was linear with no changes in slope.

The total cumulative NO_3^--N reduction from restoring all streams in the 4th order watershed (83.0%, rightmost end of solid black line in Figure 5A) was only about 0.5% higher than from restoring only the 4th order river by itself (83.5% rightmost end of red dashed line). In other words, restoring just the 4th order river reduced NO_3^--N concentration and load by 83%, whereas the 4th order river in the context of the fully restored watershed only provided 52% reduction (surface water entering the river had already been reduced 31%).

Since restoration is more commonly carried out in 1st through 3rd order streams due to practical challenges associated with restoring larger channels [*Craig et al.*, 2008], we rescaled our results to show effects in a 3rd order watershed (Figure 5B). In this case, 69% NO_3^--N concentration/load reduction was observed at the outlet of the 3rd order watershed (solid black line). Note this rescaling did not involve any new model runs, and 69% at the outlet of the restored 3rd order watershed corresponds to 31% at the 3rd order outlet in the restored 4th order watershed; there is just less total NO_3^--N in the model when ignoring the 4th order river. Similarly to the restored 4th order watershed, the effects of upstream restoration are not very apparent at the downstream end of the restored 3rd order watershed due to surface water recycling. In other words, restoring only the 3rd order streams (red dashed line) resulted in 65% reduction at their outlet by themselves, i.e. only 4% less than restoring everything upstream as well.

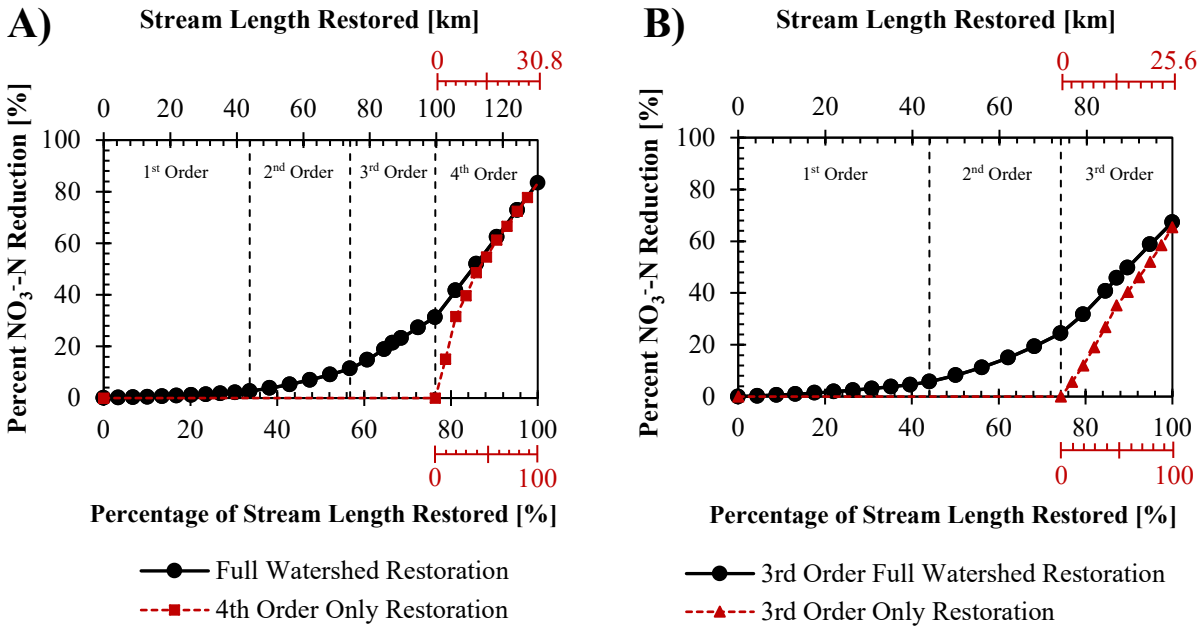

Figure 5: Percent nitrate-nitrogen (NO_3^--N) load/concentration reductions at the A) 4th order watershed outlet and B) 3rd order watershed outlet resulting from increasing percentages of the overall watershed restored, i.e. starting in the 1st order rivers and moving down to the outlet of the respective watershed. The red dashed line is for the individual A) 4th order restoration and B) 3rd order restoration by themselves (i.e. replotted from Figure 4C and D) as a comparison, and corresponds to the red x-axes.

2.3.2 Spatial Trends

Spatial plots were created to highlight spatial patterns within the stream network. A representative flow path was chosen from the upstream end of one of the most distal 1st order rivers to the downstream end of the 4th order river (Figure 6). Given the uniform 30-m spacing of hyporheic flow-inducing structures throughout the watershed, this flow path is the same as every flow path from the most distal 1st order rivers to the outlet of the 4th order river.

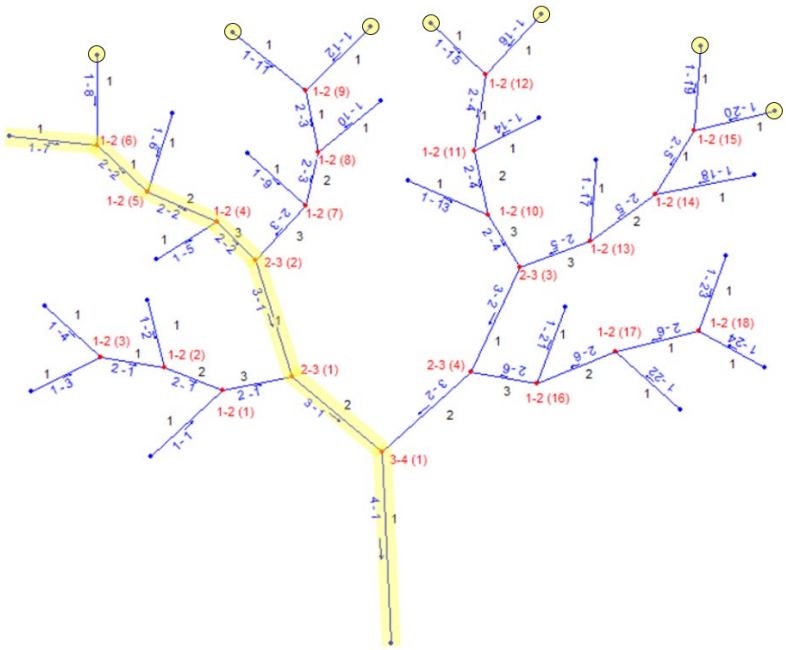

Figure 6: Plan view schematic showing the flow path chosen to display spatial patterns of surface water nitrate-nitrogen (NO_3^--N) concentration. NO_3^--N concentrations along this flow path (yellow highlight) would be the same as those starting from Rivers 1-8, 1-11, 1-12, 1-15, 1-16, 1-19, or 1-20 (yellow dots).

When considering 100% restoration of just individual stream orders, surface water NO_3^--N concentrations remained at 1 mg/L upstream of the respective stream order restored and decreased with distance downstream within the restored stream order (Figure 7A-D). Concentrations dropped more in higher-order rivers, i.e. 0.12 mg/L (12%) in the 1st order restoration (Figure 7A), versus 0.35 mg/L (35%) in the 2nd order restoration (Figure 7B), 0.65 mg/L (65%) in the 3rd order restoration (Figure 7C), and 0.83 mg/L (83%) in the 4th order restoration (Figure 7D). Concentrations then rebounded downstream of the restoration due to unmitigated gaining from groundwater (Q_{lat}). The magnitude of concentration rebound was highest after the 3rd order restoration (0.35 mg/L), versus 0.24 mg/L after the 2nd order restoration and 0.09 mg/L after the 1st order restoration. This in part reflects the fact that there was more rebound possible downstream of the higher order restored rivers, given that the higher order restored rivers removed more NO_3^--N in the first place. However, there was a higher percentage of rebound from the low order restorations, i.e., 75% after the 1st order restoration, 69% after the 2nd order restoration, and 54% after the 3rd order restoration. Channel flow

increased in the downstream direction, with both vertical step increases at each confluence and uniform lateral inflows from groundwater along each reach.

In the 2nd and 3rd order restorations there were bumps in surface water concentration where tributaries join the mainstem within the restored reaches (Figure 7B-C). These were due to unrestored lower order tributaries contributing flow with 1 mg/L NO_3^--N. Unrestored 1st order tributaries bumped the 2nd order surface water concentration by about 0.01 mg/L (Figure 7B), and unrestored 2nd order tributaries bumped the 3rd order surface water by about 0.12 mg/L (Figure 7C). Also note the change in slope of NO_3^--N concentration with distance after the junction in the 3rd order restoration (Figure 7C). This is where flow started to be recycled. NO_3^--N concentration was decreasing at a higher rate before (upstream of where) this recycling began to occur. This decrease in slope was more drastic in the 4th order restoration where recycling began about 5 km into the 4th order river (after the fourth data point) (Figure 7D).

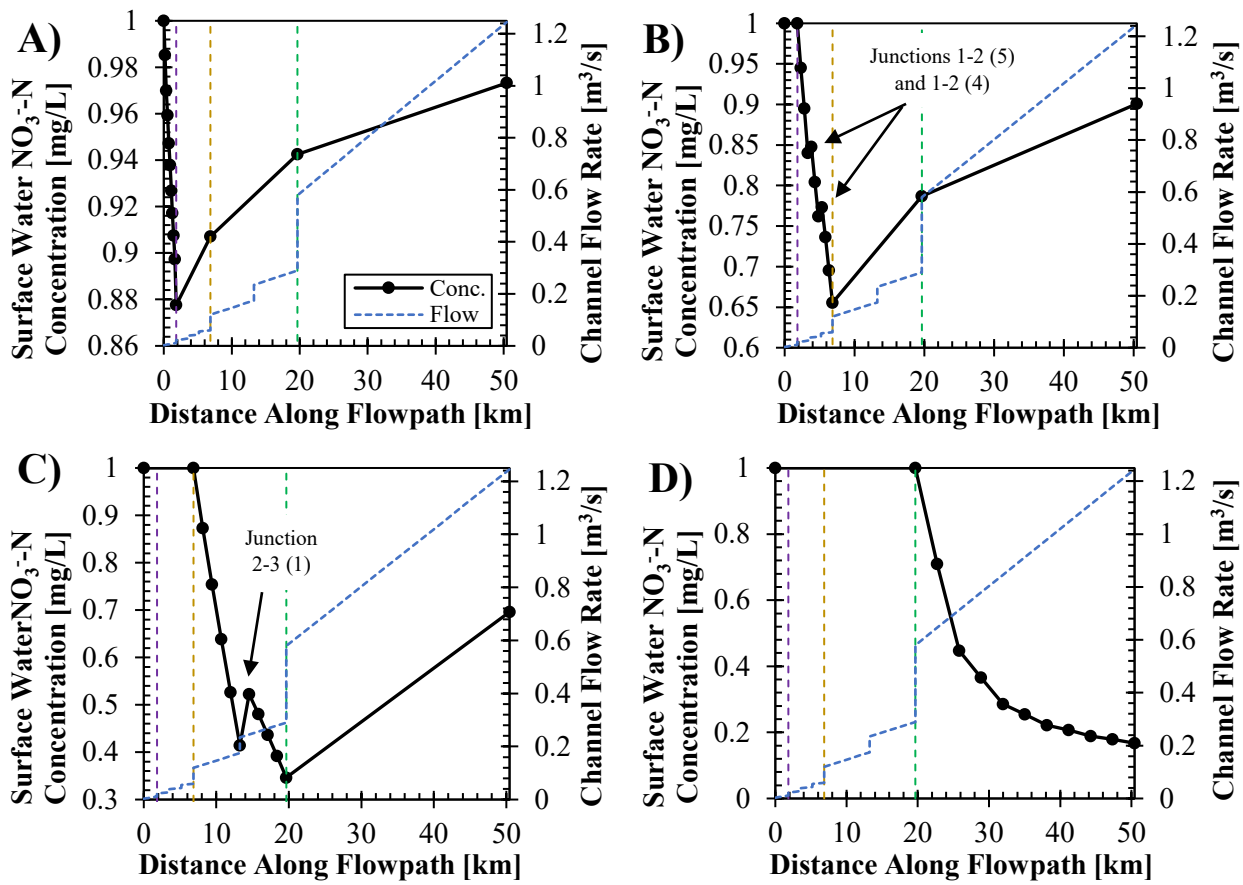

Figure 7: Surface water nitrate-nitrogen (NO_3^--N) concentration (left y-axes) and channel flow rate (right y-axes) versus distance downstream from the upstream end of 1st order River 1-7 resulting from: A) 100% of the 1st order rivers being restored, B) 100% of the 2nd order rivers being restored, C) 100% of the 3rd order rivers being restored, and D) 100% of the 4th order river

being restored. Dashed vertical lines indicate locations of junctions where a higher-order HEC-RAS river is formed from two lower-order rivers. From left to right, they indicate Junctions 1-2 (6) (purple), 2-3 (2) (gold), and 3-4 (1) (green). Labeled junctions are the locations of tributary inflows somewhere in the middle of the restored river. These locations would theoretically show as a vertical step change, however simulations were not run with the end of a restoration at the exact spatial location of the tributary confluence. Left y-axes scales vary among panels to enlarge effects of tributary inflows.

When considering the fully restored watershed, the rate of NO_3^--N concentration reduction with distance declined moving downstream (Figure 8). Despite lower concentrations entering the upstream end of the higher order rivers, the slope of concentration versus distance leveled out and ended around the same value as the individual 4th order restoration (~0.17 mg/L, compare Figure 7D and Figure 8). In other words, restoring the 4th order river alone was able to reduce the NO_3^--N concentration from 1 mg/L to about 0.17 mg/L, but in the full watershed restoration, the 4th order river was only able to reduce the NO_3^--N concentration from about 0.35 mg/L to the same 0.17 mg/L. This is analogous to the similar NO_3^--N reductions at the outlet of the fully restored watershed and that for just restoring the 4th order river (Figure 5A). Even at the downstream end of the lower order rivers, the difference in concentration was similar, with only 0.05 mg/L and 0.02 mg/L differences at the 2nd and 3rd order river outlets, respectively.

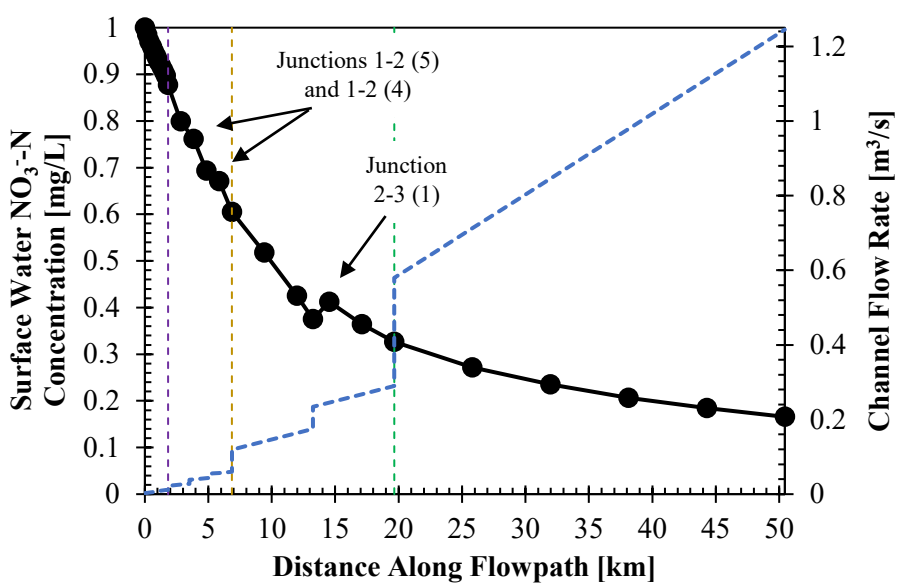

Figure 8: Surface water nitrate-nitrogen (NO_3^--N) concentration versus distance downstream where 100% of the watershed is restored (solid black line, left y-axis). Dashed blue line indicates surface water discharge (right y-axis). A flow path from a distal 1st order river stemming from River 2-1 or 2-6 would look very similar, the profile would just show a downward step at

Junction 2-3(1) from the 1st and 2nd order profile shown down to the concentration shown at that junction.

Finally, we quantified the NO_3^--N load (mass flux rate) along our representative flow path (Figure 6) to gain an understanding of the overall mass removal in the hyporheic zone (Figure 9). The NO_3^--N load in the unrestored watershed increased downstream proportionally to channel flow (Figure 8) as mass was continually being added at 1 mg/L from upwelling groundwater. The fact that the 100% restored line is below (has lower NO_3^--N load and concentration) than the 0% restored line is expected given restoration removes NO_3^--N mass from the surface water. Moving downstream from the headwaters, load did not significantly differ between the unrestored and fully restored watersheds until the 3rd and 4th order rivers where much of the channel length in the restored case maintains a relatively constant NO_3^--N load versus distance downstream. In the 4th order river, load only increased by about 20 mg/s from the beginning to the end of the restored reach, while in the 3rd order rivers the load was actually slightly decreasing by about 3 and 6 mg/s before and after the 2nd order junction, respectively. In these stretches where load is approximately constant, increases in flow (Q_{lat}) were being roughly balanced by reductions in the concentration (Q_{ho}). In other words, NO_3^--N mass coming in from groundwater gaining was almost completely in balance with NO_3^--N lost due to restoration (Equation 9). This is consistent with the linear approach to peak reduction in Figure 5A as well as the asymptotic approach to a minimum surface water concentration in Figure 8.

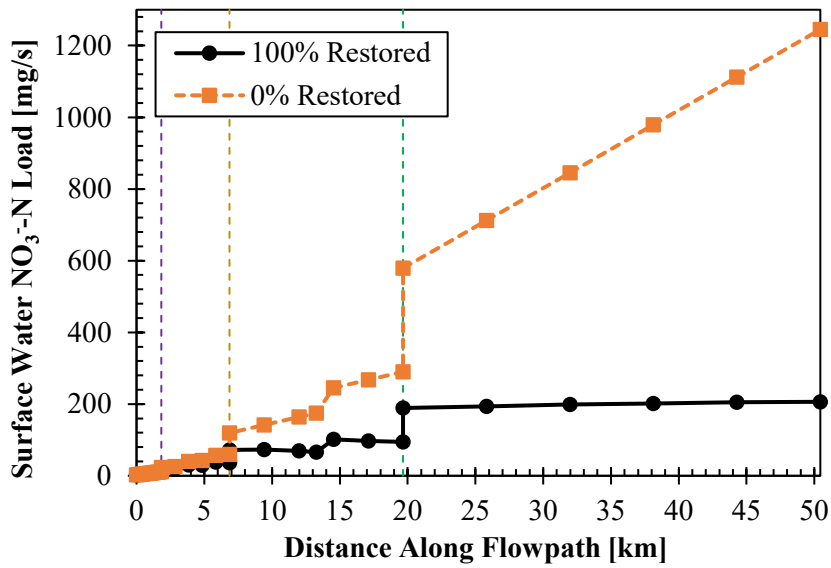

Figure 9: Surface water nitrate-nitrogen (NO_3^--N) load (mass flux rate) for the fully restored watershed (solid line) and fully unrestored watershed (dashed line). The percent difference between similar points along these two lines coincides with the percent reductions of the full watershed shown in Figure 5A. Dashed vertical lines indicate locations of junctions where a higher-order HEC-RAS river is formed from two lower-order rivers. From left to right, they indicate junctions 1-2 (6) (purple), 2-3 (2) (gold), and 3-4 (1) (green).

2.4 Discussion

2.4.1 Explanation of Trends and their Implication on Practical Stream Restoration

When comparing all the results from the percent reduction plots (Figure 4 and Figure 5) and spatial plots (Figure 7-Figure 9), the shape of the trends (i.e. concavity and linearity of the curves) suggest that recycling eventually sums to a watershed-scale maximum reduction in surface water nitrate-nitrogen (NO_3^--N) load specific to the properties of the watershed.

In the 1st and 2nd order rivers (Figure 4A-B), no recycling of surface water takes place and all reduction trends are concave-up, indicating high efficiency nitrate reduction with some remaining untapped capacity. These trends are concave-up due to the difference in mass flux between the constant, uniform 1 mg/L groundwater upwelling (source, Equation 9) and the continually increasing amount of water through the hyporheic zone relative to the surface water discharge that all returns at a concentration of 0 mg/L (sink, Equation 9). In particular, the observed exponential trend develops from the combination of a constant difference in the concentration components of flux and a continually increasing difference in the water flux components (Q and S_N, Equation 8).

By contrast, recycling of surface water begins to take place halfway through the 3rd order river and throughout most of the 4th order river, where the capacity for exponential reduction starts to disappear. Recycling specifically occurs when hyporheic outflow (Q_{ho}) equals the surface water discharge at that spatial location; hence the need for a new outflow point after all the water is sent back in from the previous hyporheic exchange cell. Repeatedly chaining these inflow and outflow points together keeps the amount of water in the channel in balance with the amount of water flowing through the hyporheic zone for the entirety of the reach. So here, in contrast with the 1st and 2nd order rivers, the water components of exchange and surface water flux remain equal, but the difference in concentration components continually decreases with each new inflow point moving downstream (decreasing $\frac{\partial \Phi}{\partial x}$, Equation 8), leading to the observed shift to a linear relationship (Figure 4C-D). The trend never completely levels off though due to the continually increasing amount of restoration-induced (0 mg/L) hyporheic water that re-enters the channel with each higher percent restored; it just becomes less efficient.

While the linear approach to the final percent reduction in both the full watershed restoration (Figure 5A) and individual 4th order restoration (Figure 4D) suggests that all the nitrate would eventually be removed if there were more stream length in the watershed, the spatial plots suggest otherwise. The concentration profiles of the full watershed restoration (Figure 8) and individual 4th order restoration (Figure 7D) both asymptotically approach a final concentration of ~0.17 mg/L, even with ~100 km less restoration upstream in the individual 4th order restoration. This suggests that the watershed was close to reaching some maximum possible nitrate load reduction. In the case of our modeled watershed, this maximum was ~83%. This levelling-off can be explained both by the decreasing difference in hyporheic outflow and inflow concentration with each hyporheic cell moving downstream, as well as the continually increasing rate of gaining with increasing river order (i.e. slope of channel flow rate in Figure 7 and Figure 8). Unmitigated 1 mg/L groundwater entered most rapidly in the 3rd and 4th order rivers, which is where the trend begins to occur. Based on the spatial plots, it appears that neither reduction nor rebound back to 1 mg/L will ever reach 100% based on the model parameters.

Such a maximum, and the approach to that maximum, would vary with the percentage of hyporheic exchange per feature (r_h), the percentage of denitrification per structure (r_N), and both the amount and concentration of gaining felt throughout a reach (Q_{lat}). While we did not run simulations that varied these parameters, we can qualitatively predict the outcomes. For example,

if we were to increase percent surface water cycling through the hyporheic zone per structure (r_h, 0.3% for our simulations, see also Section 2.4.3 below), surface water recycling would start to occur further upstream in the watershed, confining the upward concavity to lower and lower order rivers until it disappeared completely. Each order river would eventually show a linear approach to a new higher maximum reduction for that given set of parameters. A 100% reduction could potentially occur if the capacity to remove nitrate in the hyporheic zone was greater than the nitrate loading from diffuse sources; i.e., a negative slope on the 100% restored line (Figure 9). Decreasing r_h would have the opposite effect; i.e., upward concavity would spread lower in the watershed to higher order rivers simultaneously with a lower overall reduction (Figure 5) and a positive slope on the 100% restored load line (Figure 9). Decreasing r_N to less than 100% would likely have a similar affect as decreasing r_h as it would force equilibrium between surface water, upwelling and removal fluxes further downstream. Assuming the magnitude of Q_{lat} cannot be changed as it is determined by geologic and climatic controls, increasing or decreasing the concentration component of flux would likely show similar responses again. A higher background upwelling concentration would force equilibrium further down in the watershed (hence upward concavity moving downstream to a lower overall reduction), and a lower concentration would force equilibrium upstream and may even show downward concavity similar to the individual 4th order restoration (Figure 4D) depending on the magnitude of surface water versus hyporheic fluxes (Equation 9) in an approach to linearity and a higher overall nitrate reduction. Future studies could explore all of these possibilities, plus spatially heterogeneous variation in upwelling concentration due to patchy location of human nitrogen sources on the landscape.

1st and 2nd order rivers were efficient in processing their nitrate loads (i.e. had no recycling and were thus concave up in Figure 4A-B), but had very little impact on the efficiency of the watershed as a whole to eventually reach its maximum reduction. The latter is shown by individual 3rd and 4th order restorations (Figure 4C-D) reaching nearly the same reductions as restoring the full watershed restoration (Figure 5A-B). In the higher order reaches where some equilibrium is reached between all fluxes (100% restored line of Figure 9), the watershed takes a less efficient, linear approach to its maximum value, but the magnitude of water (and therefore load) is so much greater than in the headwaters that the linear reduction does more overall work to attaining max reduction.

The watershed in its current state reached a state of equilibrium between nitrate inputs and outputs around the beginning of the 3rd order river (Figure 9), and has the capability to reduce a maximum of ~83% of NO_3^--N based on the asymptotic behavior of the spatial plots (Figure 8). Increasing or decreasing model parameters such as r_h, r_N, the amount of background gaining (Q_{lat}), or concentration of background gaining (C_{lat}) are the only ways to significantly affect that final amount of reduction. These parameters, particularly r_h and r_N, might be controlled to a certain extent by restoration practitioners by varying channel morphology or carbon sources [*Hester & Doyle*, 2008; *Robertson & Merkley*, 2009]. Yet varying such parameters can often have much less effect on nitrate loads than overall watershed conditions such as degree of gaining that dominate surface water-groundwater interaction and hyporheic denitrification [*Hester et al.*, 2018]. Importantly, the asymptotic behavior of all the spatial plots (Figure 7 and Figure 8) suggests that restoring additional length of stream cannot necessarily result in 100% NO_3^--N reduction under the current conditions. Even if 100% NO_3^--N reduction from hyporheic stream restoration is not the goal, these results still indicate that diminishing returns will occur under certain watershed conditions, and therefore restoring a given length of stream will have different effects depending on how much restoration has already occurred. This is distinct from Protocol 2 of the Chesapeake Bay protocols [*Berg et al.*, 2014], and emphasizes the importance of viewing watershed as a whole.

2.4.2 Comparison of Methods to the Current Nitrogen Mitigation Credit Protocol under the Chesapeake Bay TMDL

One of the most criticized aspects of the current nitrogen mitigation credit system outlined in Protocol 2 of the Chesapeake Bay protocols [*Berg et al.*, 2014] is that it tends to over-predict nitrogen removal [*Stack*, 2019; *USEPA*, 2018]. Studies have shown that in order to accurately determine the degree of hyporheic exchange and denitrification, numerous characteristics of the channel need to be taken into consideration such as sediment hydraulic conductivity (K), channel planform, the degree of gaining or losing along the reach, and in-stream features that cause some degree of hydraulic head gradient [*Hester & Doyle*, 2008]. The natural variation of any of these channel characteristics directly affects the key parameters we used in our study to model these practical aspects of restoration (r_h, r_N, Q_{lat}, Section 2.4.3).

Simply put, hyporheic denitrification scales more with discharge than channel geometry, as expected from Protocol 2.

In order to benchmark our modeling approach against the Chesapeake Bay protocols, we applied Protocol 2 of Berg *et al.* (2014) to individual rivers in our model (Figure 10). The protocol rewards credit based on a uniform "hyporheic box" that extends down 1.5 m beneath the restored channel bed and 1.5 m horizontally to each side, with box dimensions being based on the extent of simultaneous improved surface floodplain connectivity measured by a bank-height ratio less than or equal to 1.0. In our case we multiplied that cross-sectional area of the hyporheic box (i.e. bankfull widths from Table 2 plus the protocol width multiplied by the protocol depth) by the length of the restored reach (i.e. channel lengths from Table 2 times percent restored), the bulk density of the bed material (ρ_b, either 1300 or 2000 kg/m^3 as discussed below), and an average denitrification rate of 48.2 µg N/kg of soil/day from Berg *et al.* (2014) to determine a nitrogen removal rate of the restored reach. We did this for each percent restored in Figure 4 and then divided by the watershed's total nitrogen load (0% restored load at the outlet location of each restoration, Figure 9) and converted to percent to generate the green lines in Figure 10. Note that here we define the "watershed" as all upstream drainage area from the outlet of the restoration because Protocol 2 uses the "unit area nitrogen load derived for the river basin segment in which the project is located." This contrasts with Figure 4 where the watershed was defined at the downstream end of whatever stream-order HEC-RAS river the restoration was located. Thus, to make a proper comparison, we converted our model results in Figure 4 to this new definition of watershed delineated from the downstream end of the restored reach, which are the black lines in Figure 10.

The only value not set as a constant in the protocol is the bulk density of the bed material, so we varied it over a representative range for soils that contain some amount of gravel as that would most closely match the bed material of Piedmont streams [*Lotspeich*, 2009]. In an example outlined within Berg *et al.* (2014), the panel of experts suggested using ρ_b equal to 2000 kg/m^3. Other resources have shown that ρ_b in stream beds containing at least some gravel rarely drops below 1300 kg/m^3 [*Bunte & Abt*, 2001; *Dragun*, 1998; *StructX*, 2019]; hence the range we show in Figure 10. To their credit, the panel of experts placed a cap of 40% nitrogen reduction on any hyporheic restoration (red lines in Figure 10), but the value is based on the results of one restoration completed on their study site at Minebank Run in Towson, MD.

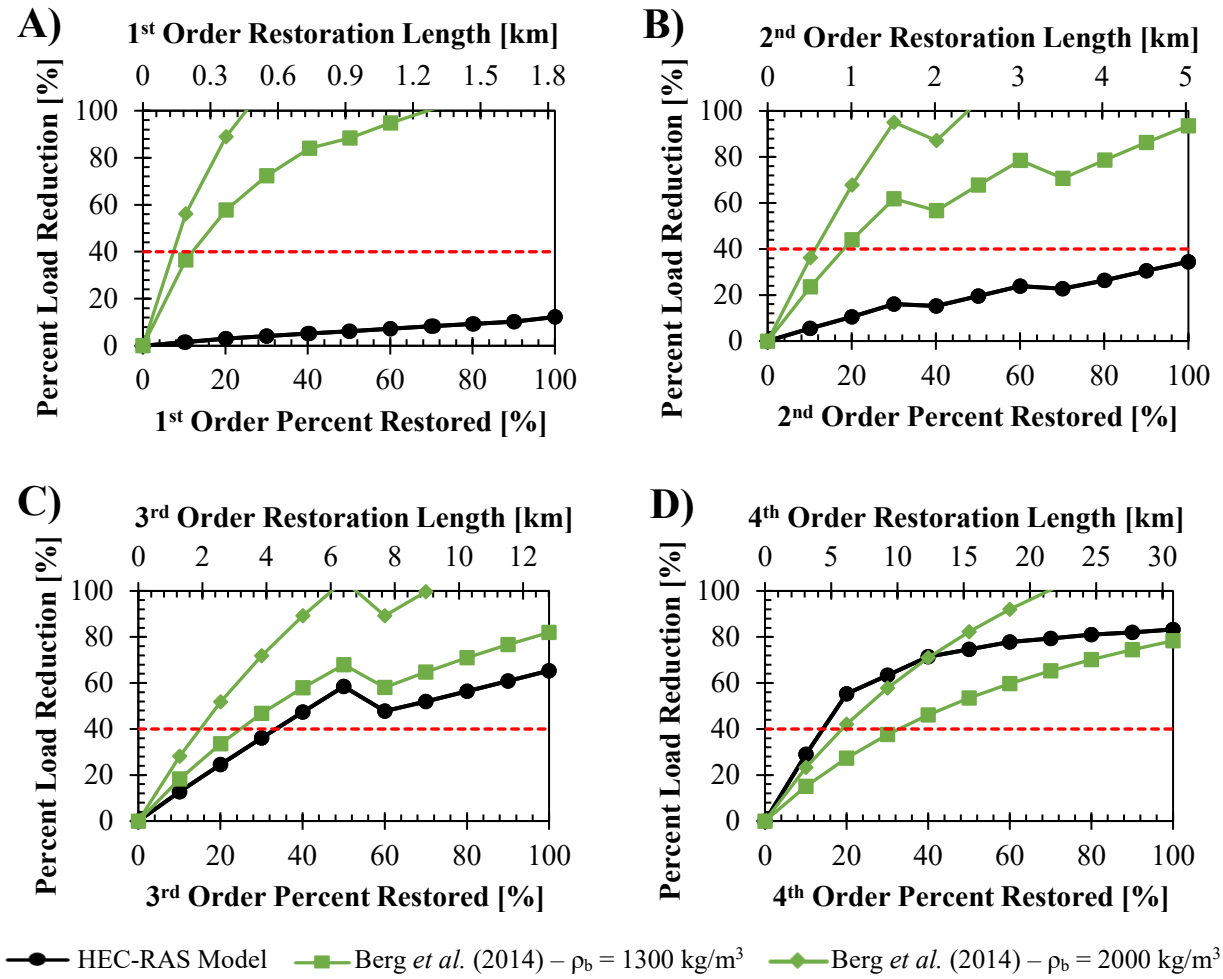

Figure 10: Application of Protocol 2 of the Chesapeake Bay protocols [Berg et al., 2014] to an individual A) 1st order river, B) 2nd order river, C) 3rd order river, and D) 4th order river within our theoretical watershed. Black trendlines are the results from our simulations developed from channel concentrations and discharges immediately following a restoration (hence the slight difference in the trends approaching the same outlet reductions shown in Figure 4), and green trendlines show load reductions attained from using the current nitrogen mitigation protocol with a range of soil densities corresponding a high value (i.e. the value suggested in Berg *et al.* (2014)) and a lower representative value of soil containing some gravel. The red dashed line at 40% is the reduction cap set by the expert panel [*Berg et al.*, 2014].

The Chesapeake Bay protocol [*Berg et al.*, 2014] generally did predict greater nitrogen removal than our model (Figure 10), especially on the lower order reaches where restoration is most common (Figure 10A-B) [*Craig et al.*, 2008]. In the 1st order river, the protocol's threshold of 40% reduction was reached at only about 300 m of restoration in even the most conservative trial (ρ_b = 1300 kg/m^3). Since our model geometries and flow characteristics were developed using resources that most practitioners would use in restoration design, i.e., NHD*Plus*, regional

curves, and other USGS and USDA resources, these results show that it would be very easy to attain the maximum credit for a relatively short restoration project (<1 km in most cases for 1st and 2nd order streams) that may not even be close to the actual nitrate removal occurring from their restoration.

Our modeling results for higher order rivers more closely matched the results from the Chesapeake Bay protocols [*Berg et al.*, 2014] (Figure 10C-D). Each of these trials reached the 40% threshold at around 4-5 km of restoration, which was roughly 1.5 times the average of Protocol 2 in the 3rd order river and slightly less than the Chesapeake Bay protocol in the 4th order river. This could mean that the protocol is more reliable for higher order streams, although it seems more likely that our assumption of 0.3% of surface water flowing through the hyporheic zone per structure is less accurate in these higher order systems. As stream order increases, the K of the bed material tends to decrease as the average bed material size decreases [*Charlton*, 2008], and the degree of gaining increases as seen in our data from the Virginia baseflow data (Table 3) [*Nelms et al.*, 1995]. Both of these factors in turn would decrease the amount of hyporheic exchange per structure [*Hester & Doyle*, 2008]. While 0.3% was roughly the median of all the sources we used [*Azinheira et al.*, 2014; *Gordon et al.*, 2013; *Hester & Doyle*, 2008; *Wondzell & Swanson*, 1996], it is reasonable to expect that value to decrease by up to an order of magnitude in higher order systems based on the physical properties just mentioned. A lower hyporheic exchange percentage in turn would likely change the concavity of the trendlines since less water would cycle through the hyporheic zone multiple times, and would also decrease the overall percent reduction at the outlet of each river. This could result in our model predicting nitrate reductions less than the Chesapeake Bay protocols [*Berg et al.*, 2014], similar to what we found for lower order reaches (Figure 10A-B). Although we chose not to introduce this added level of natural variability in this study, our modeling approach allows for spatially-varying hyporheic exchange percentages to be tested in future studies.

2.4.3 Evaluation of Model Parameters

Since this was a first of its kind approach to modeling effects of watershed-scale hyporheic restoration and its ability to induce denitrification, we chose to keep as many parameters constant as possible to avoid additional variation within an already complex model, while still obtaining results that were within an acceptable range of natural conditions. In any

watershed, spatial and temporal variations can strongly influence the degree of exchange and denitrification occurring in a given hyporheic zone, which in turn would affect the overall nitrate reduction experienced in downstream waterbodies. Here we discuss how variation in key input parameters would affect our results and how they could be addressed in future studies.

Hyporheic exchange (i.e. bidirectional exchange along relatively short flow paths) requires circumneutral (slightly gaining or losing) hydrologic conditions [*Hester & Doyle*, 2008], which is a reasonable assumption in our model given the alluvial channels and humid climate of the eastern USA [*Nelms et al.*, 1995]. In losing streams there is minimal possibility of return flow after surface water enters groundwater, and denitrification in these regions would be augmented by long-term storage in subsurface soils, so our approach would require modifications in arid regions. Azinheira *et al.* (2014) found that as background gaining increased from mildly gaining summer baseflow to more strongly gaining winter baseflow, the percent of channel flow induced through the hyporheic zone per in-stream restoration feature (r_h) decreased from 0.3% to less than 0.01%. Hester and Doyle (2008) similarly showed that increasing the degree of upwelling (Q_{lat}) will eventually stop all hyporheic exchange. For this reason, when using our approach it is important to consider the temporal variation of Q_{lat} over the course of not only annual cycles but also storm events which could increase or decrease r_h. However, during storm flows in particular, floodplain attenuation becomes a significant sink of nitrate [*Jones et al.*, 2015], even more so than the hyporheic zone in some cases [*Azinheira et al.*, 2014]. Because our approach used HEC-RAS, it would be straightforward to extend it in the future to study storm flows and also floodplain restoration.

Perhaps an even more significant influence on the percentage of hyporheic exchange per structure is the bed material's hydraulic conductivity (K), which can vary naturally over orders of magnitude within a single stream [*Brunke*, 1999; *Calver*, 2001; *Genereux et al.*, 2008]. Hyporheic exchange per in-stream feature (r_h) exponentially decreases from around 0.015% where sand as the largest particle size ($K \leq 10^{-5}$ m/s) [*Hester & Doyle*, 2008], and such reduction would result in little to no load reduction at the watershed outlet. In beds dominated by gravel or larger particles ($K \geq 10^{-2}$ m/s), r_h can reach up to 50% of surface water. These beds however lack the tightly-packed interstitial network necessary for denitrifying microbes, so structure-induced hyporheic water would re-emerge at >0 mg/L nitrate [*Hester & Gooseff*, 2011]. Well-mixed beds with some gravel (allowing surface water to enter the hyporheic zone) and some sand (substrate

for denitrifying microbes to survive) create the conditions we assumed in our model with r_h equal to 0.3% and 100% denitrification through the hyporheic zone (r_N). Hydraulic conductivity often decreases moving downstream through a watershed due to natural sediment sorting, which would decrease the overall watershed load reduction due to less cumulative water being cycled through the hyporheic zone. This and can be fine-tuned in our model and auxiliary R code using field or literature data.

In our base case we assumed no hyporheic exchange existed prior to restoration. Yet in many watersheds there will be at least some pre-existing hyporheic exchange. If this existing exchange is significant, the results of our model would need to be considered as a net reduction relative to pre-restoration conditions. Furthermore, structure longitudinal spacing along the channel may vary from our constant value of ~30m based on USDA (2007) and Hester *et al.* (2016) typically applied to 2nd and 3rd order streams. For example, structure spacing increases with channel width such that higher order streams would exhibit less hyporheic exchange than in our model, in turn reducing the overall watershed load reduction. Conversely, restoration in 1st order streams might entail structures spaced less than 30 m apart, which would induce more hyporheic change and denitrification than simulated in our model. We chose to keep spacing constant to avoid the introduction of a new variable, but a different spacing can easily be implemented in the auxiliary R code.

It will generally be intractable to restore an entire watershed due to legal, cost, or infrastructure constraints. Because our model results indicated that hyporheic restoration of low order streams had little effect on nitrate loading at the watershed-scale, choosing restoration location is critical. In our results, restoring just the 4th order river alone was able to reduce NO_3^--N concentration and load by 83%, whereas the 4th order river in the context of the fully restored watershed only provided 52% reduction (surface water entering the river had already been reduced 31%). This presents a trade-off. Restoration of high order rivers is typically more expensive, and sediments may be lower K than in smaller order streams, yet it takes less channel length to reach the watershed's maximum reduction capacity. By contrast, restoration on low order rivers is typically less expensive, and sediment K may be higher, yet it is harder to achieve significant reductions, so at least some restoration on higher order systems may eventually be necessary. And if lower order streams are already restored, any subsequent higher order restorations will be less effective than if they were implemented alone (Figure 5A). Therefore it

may be most effective to focus on larger streams from the start. Yet we note that if K decreases and structure spacing increases in 4th order streams relative to what we simulated in our model, the outsized importance of the 4th order stream in our results (Figure 5A) would diminish, indicating the importance of assessing spatial variation of these parameters any watershed under consideration.

Understanding the maximum possible degree of hyporheic exchange, denitrification, and the location of any polluted tributaries is an important step in choosing the most effective location based on a project's goals, and cannot be done without viewing and analyzing the watershed as a whole. With more watershed-scale planning and a better understanding of these key characteristics, i.e. sediment (r_h), microbiota (r_N), and upwelling (Q_{lat}), we can choose restoration locations and strategies that will ultimately work more efficiently toward reaching a nutrient reduction goal.

2.5 Conclusions

We developed a modeling approach capable of predicting the spatially-explicit and cumulative effects of hyporheic restoration carried out throughout a watershed. Specifically, we used HEC-RAS to model exchange and denitrification around fully-spanning weirs (cross-vanes) implemented throughout a hypothetical 4th order watershed typical of the Piedmont physiographic province of the eastern USA. We studied the cumulative effects of hyporheic restoration on nitrate-nitrogen (NO_3^--N) loading to downstream waterbodies in response to different spatial configurations of restoration implemented in individual order streams, as well as throughout the full watershed. We then compared the results of our modeling approach to the current Chesapeake Bay nitrogen mitigation credit system outlined in Protocol 2 of Berg *et al.* (2014). We found that 1) restoration on higher order rivers had a more significant effect on NO_3^--N load reduction at the overall watershed outlet than restoration on lower order rivers, 2) certain watersheds characteristics (i.e., the percentage of surface water flowing thorough the hyporheic zone per in-stream feature, r_h; the extent of denitrification in the hyporheic zone, r_N; and the influence of background gaining, Q_{lat}) led to a threshold or maximum attainable NO_3^--N removal capacity, and 3) the current nitrogen mitigation protocol generally overestimated the removal rates estimated by our modeling (Figure 10).

We found that restoration on higher order rivers has a more significant effect on NO_3^--N load reduction than restoration on lower order rivers (Figure 4 and Figure 5), which is contrary to the current belief [*Craig et al.*, 2008]. Restoration of 100% of 1st order (Figure 4A) and 2nd order (Figure 4B) rivers in the watershed was able to reduce the NO_3^--N load at the watershed outlet by only about 2.5% and 10%, respectively, while restoring 100% of the two 3rd order rivers (Figure 4C) and single 4th order river (Figure 4D) was able to reduce NO_3^--N load at the watershed outlet by about 30% and 83%, respectively. Even though there was more channel length available to be restored in the lower (1st and 2nd) order reaches, the cumulative amount of water flowing through the hyporheic zone was <10% of that flowing through in the 3rd and 4th order rivers because of the much greater gaining of nitrate-polluted water from groundwater in those higher order rivers. This conclusion depends on being able to implement restoration on larger order streams and rivers, which may have more practical limitations than in smaller streams.

More importantly than the load reductions we found was the behavior of the reduction trends at the watershed-scale. With a constant structure spacing of 30 m, r_h equal to 0.3% of surface flow per structure, r_N equal to 100% (i.e. complete denitrification in restoration-induced hyporheic zones), and the backgrounding upwelling (Q_{lat}) of nitrate-polluted water (i.e. at a concentration of 1 mg/L) occurring at the rate needed to match regional baseflow data from Nelms *et al.* (1995), we found an overall NO_3^--N reduction threshold or maximum of roughly 83% at the watershed level (Figure 5A). In the higher order reaches where surface water recycling (i.e. surface water cycling more than once through the hyporheic zone) was most drastic, a balance was reached between channel and hyporheic exchange water and NO_3^--N fluxes (Figure 9) which caused surface water concentration to level out at around 0.17 mg/L regardless of what happened upstream (Figure 7D and Figure 8). This trend not only reinforces the conclusion that lower order restorations do not have a significant effect on downstream nitrate loading, but also emphasizes the importance of watershed-scale planning in stream restoration. Lastly, it would be nearly impossible to restore 100% of an entire watershed due to legal, cost, or infrastructure constraints. Considering we showed that low order restorations have little to no effect on NO_3^--N loading at the watershed-scale, this makes choosing the location even more important, which would be facilitated by watershed-scale planning and feasibility assessment. While restoration on a lower order reach may be cheaper or easier to carry out, if water quality improvement is a project goal, the investment may be worth it to restore a higher

order reach. Understanding the maximum possible degree of hyporheic exchange, denitrification, and the location of any polluted tributaries is an important step in choosing the most effective location based on a project's goals, and cannot be done without viewing and analyzing the watershed as a whole.

References

Azinheira, D. L., Scott, D. T., Hession, W., & Hester, E. T. (2014). Comparison of effects of inset floodplains and hyporheic exchange induced by in-stream structures on solute retention. Water Resources Research, 50(7), 6168-6190. doi:10.1002/2013WR014400

Bencala, K. E., & Walters, R. A. (1983). Simulation of solute transport in a mountain pool-and-riffle stream: A transient storage model. Water Resources Research, 19(3), 718-724. doi:10.1029/WR019i003p00718

Bennett, L. (2017). Algae, Cyanobacteria Blooms, and Climate Change. The Climate Institute.

Berg, J., Burch, J., Cappucciti, D., Filoso, S., Lisa, F.-M., Goerman, D., . . . Winters, J. (2014). Recommendations of the Expert Panel to Define Removal Rates for Individual Stream Restoration Projects. Retrieved from Chesapeake Bay Program:

Bernhardt, E. S., Palmer, M. A., Allan, J. D., Alexander, G., Barnas, K., Brooks, S., . . . Sudduth, E. (2005). Synthesizing U.S. River Restoration Efforts. Science, 308(5722), 636. doi:10.1126/science.1109769

Bohn, B. A., & Kershner, J. L. (2002). Establishing aquatic restoration priorities using a watershed approach. Journal of Environmental Management, 64(4), 355-363. doi:https://doi.org/10.1006/jema.2001.0496

Boulton, A. J. (2007). Hyporheic rehabilitation in rivers: restoring vertical connectivity. Freshwater Biology, 52(4), 632-650. doi:10.1111/j.1365-2427.2006.01710.x

Boyer, E. W., Howarth, R. W., Galloway, J. N., Dentener, F. J., Green, P. A., & Vörösmarty, C. J. (2006). Riverine nitrogen export from the continents to the coasts. Global Biogeochemical Cycles, 20(1). doi:10.1029/2005GB002537

Brunke, M. (1999). Colmation and Depth Filtration within Streambeds: Retention of Particles in Hyporheic Interstices. International Review of Hydrobiology, 84(2), 99-117. doi:10.1002/iroh.199900014

Bunte, K., & Abt, S. R. (2001). Sampling surface and subsurface particle-size distributions in wadable gravel-and cobble-bed streams for analyses in sediment transport, hydraulics, and streambed monitoring. Gen. Tech. Rep. RMRS-GTR-74. Fort Collins, CO: U.S. Department of Agriculture, Forest Service, Rocky Mountain Research Station.

Calver, A. (2001). Riverbed Permeabilities: Information from Pooled Data. Groundwater, 39(4), 546-553. doi:10.1111/j.1745-6584.2001.tb02343.x

Cardenas, M. B. (2009). A model for lateral hyporheic flow based on valley slope and channel sinuosity. Water Resources Research, 45(1). doi:10.1029/2008WR007442

Charlton, R. (2008). Fundamentals of fluvial geomorphology. London: Routledge.

Chesapeake Bay Foundation. (2019). Saving a National Treasure. Retrieved from https://www.cbf.org

Chow, V. T. (1959). Open Channel Hydraulics. McGraw-Hill, New York.

Christopher, S. F., Tank, J. L., Mahl, U. H., Yen, H., Arnold, J. G., Trentman, M. T., . . . Royer, T. V. (2017). Modeling nutrient removal using watershed-scale implementation of the two-stage ditch. Ecological Engineering, 108, 358-369. doi:https://doi.org/10.1016/j.ecoleng.2017.03.015

Cinotto, P. J. (2003). Development of regional curves of bankfull-channel geometry and discharge for streams in the non-urban, Piedmont Physiographic Province, Pennsylvania and Maryland (2003-4014). Retrieved from Reston, VA: http://pubs.er.usgs.gov/publication/wri034014

Craig, L. S., Palmer, M. A., Richardson, D. C., Filoso, S., Bernhardt, E. S., Bledsoe, B. P., . . . Wilcock, P. R. (2008). Stream restoration strategies for reducing river nitrogen loads. Frontiers in Ecology and the Environment, 6(10), 529-538. doi:10.1890/070080

Crispell, J. K., & Endreny, T. A. (2009). Hyporheic exchange flow around constructed in-channel structures and implications for restoration design. Hydrological Processes, 23(8), 1158-1168. doi:10.1002/hyp.7230

Diaz, R. J., & Rosenberg, R. (2008). Spreading Dead Zones and Consequences for Marine Ecosystems. Science, 321(5891), 926. doi:10.1126/science.1156401

Donovan, M., Miller, A., Baker, M., & Gellis, A. (2015). Sediment contributions from floodplains and legacy sediments to Piedmont streams of Baltimore County, Maryland. Geomorphology, 235, 88-105. doi:https://doi.org/10.1016/j.geomorph.2015.01.025

Dragun, J. (1998). The Soil Chemistry of Hazardous Materials (2nd ed.): Amherst Scientific.

Filoso, S., & Palmer, M. (2011). Assessing Stream Restoration Effectiveness at Reducing Nitrogen Export to Downstream Waters. Ecological applications: a publication of the Ecological Society of America, 21, 1989-2006. doi:10.2307/41416633

Genereux, D., Leahy, S., Mitasova, H., Kennedy, C., & Corbett, D. (2008). Spatial and temporal variability of streambed hydraulic conductivity in West Bear Creek, North Carolina, USA. Journal of Hydrology, 358, 332-353. doi:10.1016/j.jhydrol.2008.06.017

Gomez-Velez, J. D., Harvey, J. W., Cardenas, M. B., & Kiel, B. (2015). Denitrification in the Mississippi River network controlled by flow through river bedforms. Nature Geoscience, 8, 941. doi:10.1038/ngeo2567 https://www.nature.com/articles/ngeo2567#supplementary-information

Gordon, R. P., Lautz, L. K., & Daniluk, T. L. (2013). Spatial patterns of hyporheic exchange and biogeochemical cycling around cross-vane restoration structures: Implications for stream restoration design. Water Resources Research, 49(4), 2040-2055. doi:10.1002/wrcr.20185

Groffman, P. M., Dorsey, A. M., & Mayer, P. M. (2005). N processing within geomorphic structures in urban streams. Journal of the North American Benthological Society, 24(3), 613-625. doi:10.1899/04-026.1

Hack, J. T. (1957). Studies of longitudinal stream profiles in Virginia and Maryland (294B). Retrieved from http://pubs.er.usgs.gov/publication/pp294B

Hanson, J., Chair, R., Boomer, K., Mason, P., Clearwater, D., Denver, J., . . . Uybarreta, T. (2016). Wetlands and Wetland Restoration Recommendations of the Wetland Expert Panel for the incorporation of non-tidal wetland best management practices (BMPs) and land uses in the Phase 6 Chesapeake Bay Watershed Model Prepared for With: Additional Contract Support Provided by Wetland Expert Panel iii.

Herzog, S. P., Higgins, C. P., & McCray, J. E. (2016). Engineered Streambeds for Induced Hyporheic Flow: Enhanced Removal of Nutrients, Pathogens, and Metals from Urban Streams. Journal of Environmental Engineering, 142(1), 04015053. doi:10.1061/(ASCE)EE.1943-7870.0001012

Hester, E. T., Brooks, K. E., & Scott, D. T. (2018). Comparing reach scale hyporheic exchange and denitrification induced by instream restoration structures and natural streambed

morphology. Ecological Engineering, 115, 105-121. doi:https://doi.org/10.1016/j.ecoleng.2018.01.011

Hester, E. T., & Doyle, M. W. (2008). In-stream geomorphic structures as drivers of hyporheic exchange. Water Resources Research, 44(3). doi:10.1029/2006WR005810

Hester, E. T., & Gooseff, M. (2011). Hyporheic Restoration in Streams and Rivers (Vol. 194).

Hester, E. T., Hammond, B., & Scott, D. T. (2016). Effects of inset floodplains and hyporheic exchange induced by in-stream structures on nitrate removal in a headwater stream. Ecological Engineering, 97, 452-464. doi:https://doi.org/10.1016/j.ecoleng.2016.10.036

Hiscock, K., & Grischek, T. (2001). Attenuation of groundwater pollution by bank filtration. Journal of Hydrology, 266, 139-144. doi:10.1016/S0022-1694(02)00158-0

Howarth, R. W., Anderson, D. B., Cloern, J. E., Elfring, C., Hopkinson, C. S., Lapointe, B., . . . Walker, D. (2000). Issues in ecology: Nutrient pollution of coastal rivers, bays, and seas.

Jones, C. N., Scott, D. T., Guth, C., Hester, E. T., & Hession, W. C. (2015). Seasonal Variation in Floodplain Biogeochemical Processing in a Restored Headwater Stream. Environmental Science & Technology, 49(22), 13190-13198. doi:10.1021/acs.est.5b02426

Kasahara, T., & Hill, A. R. (2006). Effects of riffle–step restoration on hyporheic zone chemistry in N-rich lowland streams. Canadian Journal of Fisheries and Aquatic Sciences, 63(1), 120-133. doi:10.1139/f05-199

Kiel, B. A., & Bayani Cardenas, M. (2014). Lateral hyporheic exchange throughout the Mississippi River network. Nature Geoscience, 7, 413. doi:10.1038/ngeo2157 https://www.nature.com/articles/ngeo2157#supplementary-information

Knust, A. E., & Warwick, J. J. (2009). Using a fluctuating tracer to estimate hyporheic exchange in restored and unrestored reaches of the Truckee River, Nevada, USA. Hydrological Processes, 23(8), 1119-1130. doi:10.1002/hyp.7218

Li, J., Glibert, P. M., & Gao, Y. (2015). Temporal and spatial changes in Chesapeake Bay water quality and relationships to Prorocentrum minimum, Karlodinium veneficum, and CyanoHAB events, 1991–2008. Harmful Algae, 42, 1-14. doi:https://doi.org/10.1016/j.hal.2014.11.003

Lotspeich, R. R. (2009). Regional curves of bankfull channel geometry for non-urban streams in the Piedmont Physiographic Province, Virginia. (51 p.). Reston, VA

Maryland Dept. of Information Technology. (2019). Maryland Trust Fund Restoration Mapper (DNR). Retrieved from https://data.imap.maryland.gov/datasets/5d35e10a473e4630b90f67f3511ccd38

McCuen, R. H. (2005). Hydrologic analysis and design (3rd ed). Upper Saddle River, NJ: Pearson Education Inc.

Morén, I., Wörman, A., & Riml, J. (2017). Design of Remediation Actions for Nutrient Mitigation in the Hyporheic Zone. Water Resources Research, 53(11), 8872-8899. doi:10.1002/2016WR020127

Morisawa, M. E. (1962). Quantitative Geomorphology of Some Watersheds in the Appalachian Plateau. GSA Bulletin, 73(9), 1025-1046. doi:10.1130/0016-7606(1962)73[1025:QGOSWI]2.0.CO;2

Nelms, D. L., Harlow Jr, G. E., & Hayes, D. C. (1995). Base-flow characteristics of streams in the Valley and Ridge, Blue Ridge, and Piedmont physiographic provinces of Virginia (95-298). Retrieved from http://pubs.er.usgs.gov/publication/ofr95298

Newcomer Johnson, T., Kaushal, S., Mayer, P., Smith, R., & Sivirichi, G. (2016). Nutrient Retention in Restored Streams and Rivers: Global Review and Synthesis.

Oelsner, G. P., & Stets, E. G. (2019). Recent trends in nutrient and sediment loading to coastal areas of the conterminous U.S.: Insights and global context. Science of the Total Environment, 654, 1225-1240. doi:https://doi.org/10.1016/j.scitotenv.2018.10.437

Pierson, S. M., Rosenbaum, B. J., McKay, L. D., & Dewald, T. G. (2008). Strahler Stream Order and Strahler Calculator Values in NHDPlus. In.

Robertson, W. D., & Merkley, L. C. (2009). In-Stream Bioreactor for Agricultural Nitrate Treatment. 38(1), 230-237. doi:10.2134/jeq2008.0100

Schumm, S. A. (1956). Evolution of Drainage Systems and Slopes in Badlands at Perth Amboy, New Jersey. GSA Bulletin, 67(5), 597-646. doi:10.1130/0016-7606(1956)67[597:EODSAS]2.0.CO;2

Sheibley, R. W., Ahearn, D. S., & Dahlgren, R. A. (2006). Nitrate loss from a restored floodplain in the Lower Cosumnes River, California. Hydrobiologia, 571(1), 261-272. doi:10.1007/s10750-006-0249-2

Singh, N. K., Gourevitch, J. D., Wemple, B. C., Watson, K. B., Rizzo, D. M., Polasky, S., & Ricketts, T. H. (2019). Optimizing wetland restoration to improve water quality at a

regional scale. Environmental Research Letters, 14(6), 064006. doi:10.1088/1748-9326/ab1827

Stack, B. (Producer). (2019). Chesapeake Bay Program Stream Restoration Credits: Moving Toward Functional Lift? Retrieved from https://www.cwp.org/chesapeake-bay-program-stream-restoration-credits-moving-toward-functional-lift/

Stanford, J. A., & Ward, J. V. (1993). An Ecosystem Perspective of Alluvial Rivers: Connectivity and the Hyporheic Corridor. Journal of the North American Benthological Society, 12(1), 48-60. doi:10.2307/1467685

Strahler, A. N. (1957). Quantitative analysis of watershed geomorphology. Eos, Transactions American Geophysical Union, 38(6), 913-920. doi:10.1029/TR038i006p00913

StructX. (2019). Structural Engineering Resources - Density Ranges for Different Soil Types. Retrieved from https://structx.com/Soil_Properties_002.html

Thompson, J., Pelc, C. E., Brogan, W. R., & Jordan, T. E. (2018). The multiscale effects of stream restoration on water quality. Ecological Engineering, 124, 7-18. doi:https://doi.org/10.1016/j.ecoleng.2018.09.016

USACE. (2016a). HEC-RAS River Analysis System Hydraulic Reference Manual. U.S. Army Corps of Engineers Institute for Water Resources Hydrologic Engineering Center.

USACE. (2016b). HEC-RAS River Analysis System User's Manual. US Army Corps of Engineers Institue for Water Resources Hydrologic Engineering Center.

USDA. (2007). Stream Restoration Design. Part 654 National Engineering Handbook.

USEPA. (2010). Chesapeake Bay Total Maximum Daily Load for Nitrogen, Phosphorus and Sediment. . U.S. Environmental Protection Agency, Region 3.

USEPA. (2018). Midpoint Assessment of the Chesapeake Bay Total Maximum Daily Load. Retrieved from https://www.epa.gov/sites/production/files/2018-07/documents/factsheet-epa-midpoint-assessment-chesapeake-bay-tmdl.pdf

USEPA. (2019). Chesapeake Bay Total Maximum Daily Load (TMDL). Retrieved from https://www.epa.gov/chesapeake-bay-tmdl

USGS. (2019). Science in Your Watershed. Retrieved from https://water.usgs.gov/wsc/map_index.html

Wondzell, S. M. (2011). The role of the hyporheic zone across stream networks. Hydrological Processes, 25(22), 3525-3532. doi:10.1002/hyp.8119

Wondzell, S. M., & Swanson, F. J. (1996). Seasonal and Storm Dynamics of the Hyporheic Zone of a 4th-Order Mountain Stream. II: Nitrogen Cycling. Journal of the North American Benthological Society, 15(1), 20-34. doi:10.2307/1467430

Zarnetske, J. P., Haggerty, R., Wondzell, S. M., & Baker, M. A. (2011). Dynamics of nitrate production and removal as a function of residence time in the hyporheic zone. Journal of Geophysical Research: Biogeosciences, 116(G1). doi:10.1029/2010JG001356

3. Engineering Significance

Hundreds of years of excess nutrient loading to large downstream waterbodies (i.e. the Black Sea, East China Sea, Gulf of Mexico, etc.) presents a global threat to both humans and wildlife [*Oelsner & Stets*, 2019]. In the Chesapeake Bay in particular, the landmark TMDL has been dropped in the hands of ecological land managers and engineers to solve the problems that have arisen from excess nutrient loading such as eutrophication [*Li et al.*, 2015], dead zones [*Diaz & Rosenberg*, 2008], and widespread declines in important fishery species [*Chesapeake Bay Foundation*, 2019]. We have made substantial progress in sediment and phosphorous loading due to more sustainable and efficient best management practices (BMPs) (i.e. bioretention, permeable pavement, grass swales, etc.) [*Chesapeake Bay Program*, 2018], but have fallen short of the nitrogen reduction goals [*USEPA*, 2018]. Stream restoration has been looked at as one of the most effective potential solutions to reaching nitrogen reduction goals due to typical project goals (i.e. bank stabilization, floodplain reconnection, riparian zone improvement, and hyporheic restoration) [*Bernhardt et al.*, 2005] being significant sinks of nitrate-nitrogen (NO_3^--N) or limiting overland and legacy nutrient loads [*Craig et al.*, 2008; *Thompson et al.*, 2018]. Inducing hyporheic exchange in particular presents a unique opportunity for nitrogen reduction, as polluted surface water travels through microbial-rich bed and bank sediments that are often ideal regions for denitrification to permanently transform dissolved nitrogen to gaseous nitrogen [*Hester et al.*, 2018], rather than just storing it long-term. Yet the hyporheic zone is vastly heterogeneous in time and space, and a failure to account for this functional variability in the current protocol for nitrogen mitigation credit rewarding could be a reason it often over-predicts reductions and why we have failed to meet the TMDL's nitrogen goals [*Berg et al.*, 2014; *Stack*, 2019].

The results of this research have 1) emphasized the importance of watershed-scale planning in stream restoration; which it lacks right now, 2) provided evidence of where the most efficient and influential locations are in a watershed to implement a hyporheic restoration project, and 3) given practitioners a new method in HEC-RAS that has to capability of accounting for the wide range of spatial and temporal variation known to exist in any hyporheic zone.

The asymptotic behavior of the concentration profiles with distance down the watershed (Figure 7 and Figure 8) indicates that there is a maximum reduction possible in a watershed.

However, the linear behavior in the percent reduction profiles near the bottom of the 4th order and full watershed restorations (Figure 4D and Figure 5A) indicates the opposite. We explain this using the load relationship (Figure 9) and comparing the fully unrestored and fully restored scenarios. The fully restored scenario showed a levelling-off of the load curve where all input and output NO_3^--N fluxes had reached an equilibrium in the 3rd and 4th order rivers due to surface water recycling (multiple passes through hyporheic zone). In other words, even if there were more channel length available to be restored in the watershed, the parameters of the watershed (r_h, r_N, Q_{lat}) would allow for very little further reduction. To increase the possible magnitude of reduction, those parameters hold the most control, rather than simply spending money on more restoration. Without understanding the watershed as a whole, an engineer may be fighting a losing battle in a watershed already near its peak reduction (either due to existing hyporheic exchange or conditions that are suboptimal for hyporheic exchange, i.e. excessive Q_{lat} and/or low r_h or r_N).

The varying concavity of our curves indicated that the effects of restoration are not linearly additive, and that restoration on higher order rivers was more effective than restoration on lower order rivers. This contradicts the current belief in the industry [*Craig et al.*, 2008]. Even though there was more channel length available to be restored in the lower (1st and 2nd) order reaches, the cumulative amount of water flowing through the hyporheic zone in these lower order reaches was <10% of that flowing through in the 3rd and 4th order rivers, hence the higher removal under our assumed supply-limited (r_N = 100%) conditions. While lower order reaches removed NO_3^--N more efficiently (concave-up nature, Figure 4A-B), the magnitude was insignificant compared to that from the 3rd and 4th order restorations. Restoration on low order streams did however have a significant effect on the effectiveness of downstream restorations (Figure 5A). Given the previously-established maximum removal capacity of watersheds, restoring just the 4th order river alone was able to reduce NO_3^--N concentration and load by 83%, whereas the 4th order river in the context of the fully restored watershed only provided 52% reduction (surface water entering the river had already been reduced 31%). This presents a trade-off scenario. Restoration on high order rivers is typically more expensive, but it takes less distance to reach the watershed's maximum reduction capacity; whereas restoration on low order rivers is typically less expensive, but since they never seem to be able to reach significant reductions, at least some restoration on higher order systems will eventually be necessary. Those

restorations will actually be subsequently less effective than if they were implemented alone. Therefore it seems that it is likely better to pay less attention to low order streams, and just primarily focus on larger streams from the start.

Finally, we created a method that has the ability to account for the spatial and temporal hyporheic zone heterogeneity known to exist in nature that the current protocol does not. We also proved that the current protocol; Protocol 2 of Berg *et al.* (2014), likely does over predict NO_3^--N removals in the hyporheic zone (Figure 10). Using our R script and HEC-RAS, an engineer can test different sediment types (by varying r_h and r_N), groundwater upwelling magnitudes and concentrations (Q_{lat}), and in-stream feature spacing so long as there is data from the field or literature to support the choice of these parameters. This approach will allow policy-makers to develop more realistic goals and subsequent plans to achieve those goals. It can also be used in design by engineers to determine a restoration length (or in-stream feature linear density) necessary to achieve some nitrogen reduction project goal.

Appendix A: Detailed Methodology on Developing and Running HEC-RAS Model

Appendix A-1: NHD*Plus* Data for Representative Drainage Areas

Data from NHD*Plus* was gathered in English units and converted to metric in all sections presented above. Below are box plots of the unfiltered (Figure A - 1) and filtered (Figure A - 2) Piedmont datasets. More details of filtering were outlined in Section 2.2.1.2. These were kept in square miles because the regional curves, Hack's Law, and Virginia Baseflow paper required input units of mi^2.

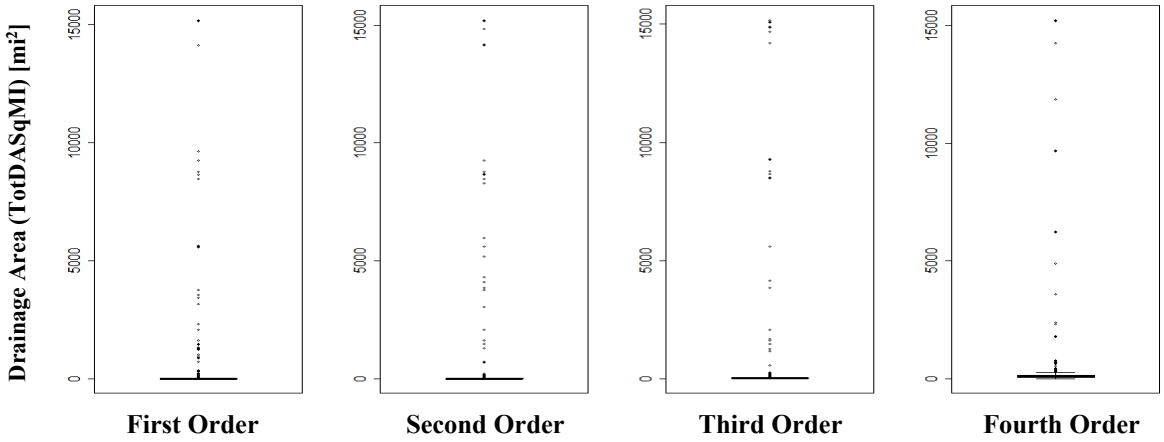

Figure A - 1: Unfiltered stream order data from NHDPlus for the HUCs associated with the Piedmont physiographic province. The median drainage areas of 1st through 4th order Piedmont streams from this dataset were 0.724 mi^2, 3.99 mi^2, 19.5 mi^2, and 83.3 mi^2, respectively.

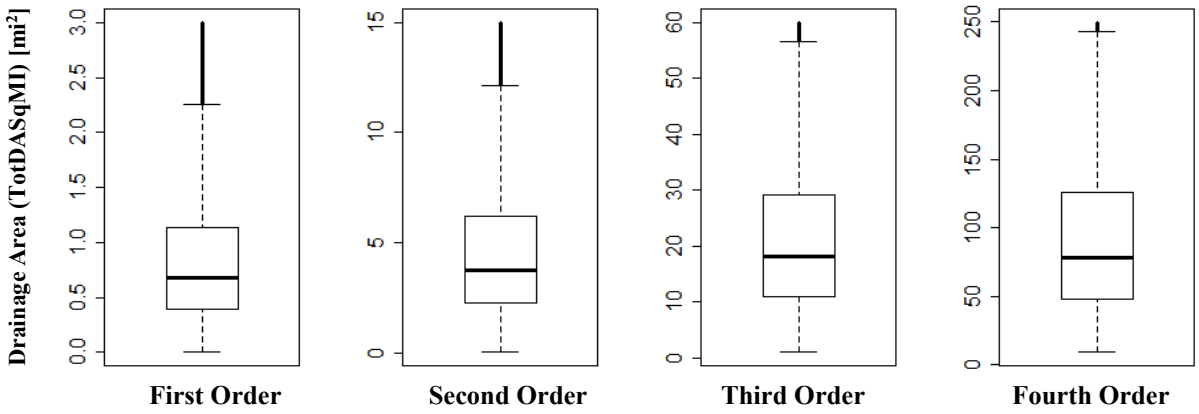

Figure A - 2: Filtered stream order data from NHDPlus for the HUCs associated with the Piedmont physiographic province. Those drainage areas determined to be a general representation of 1st through 4th order Piedmont streams (median value from filtered dataset) were 0.682 mi^2, 3.76 mi^2, 18.1 mi^2, and 78.0 mi^2, respectively.

Appendix A-2: Geometry Builder

The first step in developing a HEC-RAS model is to build a geometry file. Within the geometry file, "rivers" must be drawn from upstream to downstream, starting at the highest order rivers and filled in moving up the watershed. Each time a junction is created, HEC-RAS splits the existing river, and a new "reach" number must be specified for the new downstream reach of the river according to the numbering system described in Figure 1. For example, River 3-1 is cut in half by River 2-1 in the model. After River 2-1 is drawn to merge with River 3-1, HEC-RAS asks if River 3-1 should be split, and then asks the user to specify a reach number for the new downstream section, hence reaches 1 and 2 appearing in the model skeleton. Once a junction is created, new rivers need to be drawn to end there; no additional inputs are needed for the program to route flow through the system. The default setting of forcing equal water surface elevations at junctions for unsteady flow computations was left selected rather than using the conservation of momentum because the latter would vary based on tributary angles, and the latter were arbitrarily drawn. This avoided variability of flow conditions among junctions. The rest of the rivers were filled in according to the bifurcation ratios that are representative of a Piedmont watershed (Table 1).

Cross-sections were implemented next. Note that the model was built in English Units, therefore all Station numbering corresponds to spatial locations from the bottom of the watershed in units of feet. Starting with River 4-1, the furthest downstream cross-section was implemented first and given a "River Station (RS)" name according to the linear distance that cross-section was from the watershed outlet. Since this was the cross-section at the very bottom of the model, it was named "RS 0." For reference, the 4th order reach was determined to be 101,000 ft. long from Hack's Law, so the furthest upstream cross-section was named "RS 101000." That furthest upstream river station name then shares a name with the furthest downstream cross-section of the next order reach moving up the watershed. For example, the first river station in each of the 3rd order reaches is also named "RS 101000." This naming system was carried out the whole way up the model according to the cumulative lengths of each order river from the bottom of the watershed. The highest river station in the model is RS 165500 at the top of Rivers 1-7, 1-8, 1-11, 1-12, 1-15, 1-16, 1-19, and 1-20. The actual length between the cross-sections used by HEC-RAS in its flow routing is then input as the "downstream reach length" in the cross-section editor. Since there are only two cross-sections in each reach, the "downstream reach length" in

the upstream cross-section is the length of the channel, and the "downstream reach length" at the bottom of the reach is 0 ft.

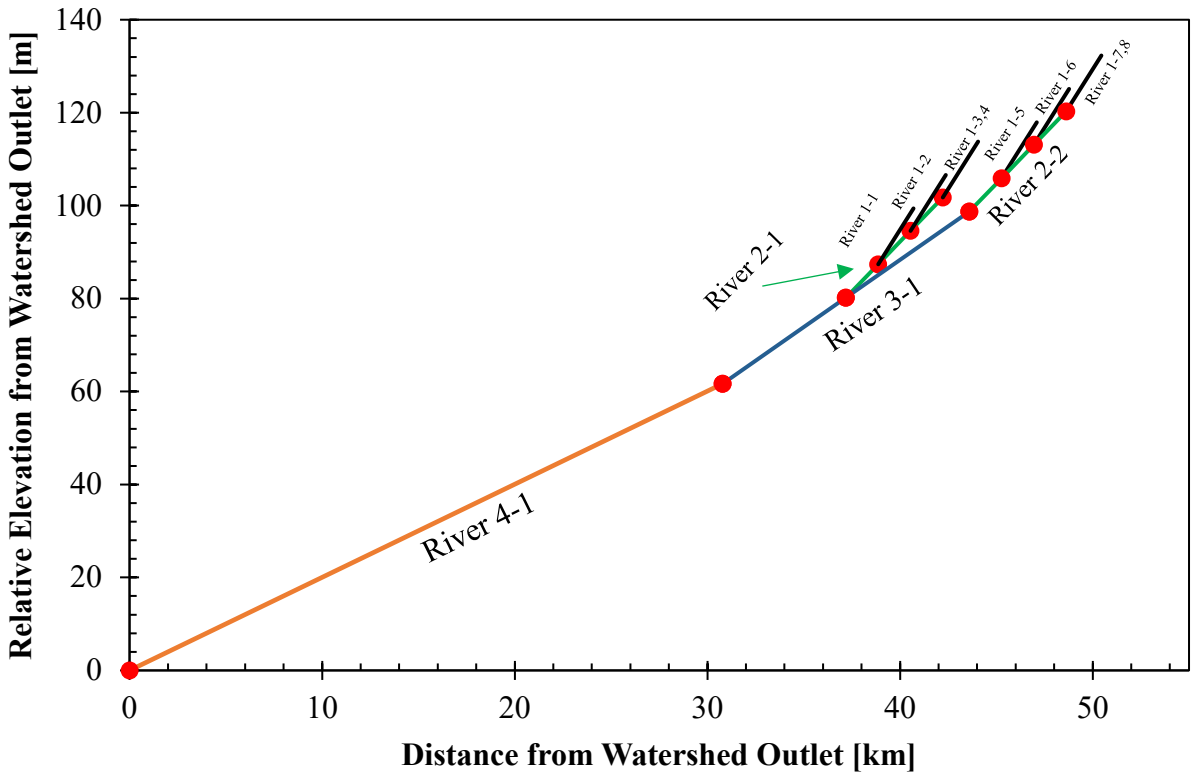

Figure A - 3: Longitudinal profile of watershed. The watershed in HEC-RAS was created symmetrical so this is the same longitudinal profile as traveling up River 3-2 after Junction 3-4(1). Orange is 4th order, blue is 3rd order, green is 2nd order, black is 1st order, red dots are junctions.

Cross-section "stations" were the final input needed in the cross-sectional geometry editor. These data points are the horizontal locations of some change in cross-sectional geometry. Looking upstream, the furthest left definition of some geometric feature is given a station of 0. Moving right across a cross-section of the river, each change in geometry is then assigned a station (horizontal distance measured in ft) and corresponding elevation. So each cross-section in the model had eight stations: (1) a left boundary station that was 10 ft higher in elevation than the floodplain, (2) the left edge of floodplain, (3) the left top of bank, (4) the left bottom of bank at an elevation equal to the death determined from the regional curve, (5) the right bottom of bank at a station equal to the width determined from the regional curve, (6) the right top of bank, (7) the right edge of the floodplain, and (8) the right floodplain boundary. A floodplain was included to mimic typical stream restoration practices and to provide us the opportunity to study overbank

events and floodplain restoration practices in future studies. We chose a floodplain width of 5 times the channel bottom width according to average values presented in [*USDA*, 2007]. Floodplains were assigned a Manning's n of 0.045 representative of a straight channel with pools and weeds [*Chow*, 1959]

Appendix A-3: Unsteady Flow Simulation

An unsteady flow file needed to be created first before the simulation could be ran. Due to the gaining nature of our watershed, each reach had to gain a certain amount of water in order to meet both the conditions of continuity at each junction as well as the channel flow rates determined from Nelms *et al.* (1995), therefore we could not use HEC-RAS's steady flow file because it had no way to implement lateral inflows. Due to multiple tributaries along each reach, the values in Table 3 needed to be equally split to keep the model as symmetrical as possible (Figure A - 4).

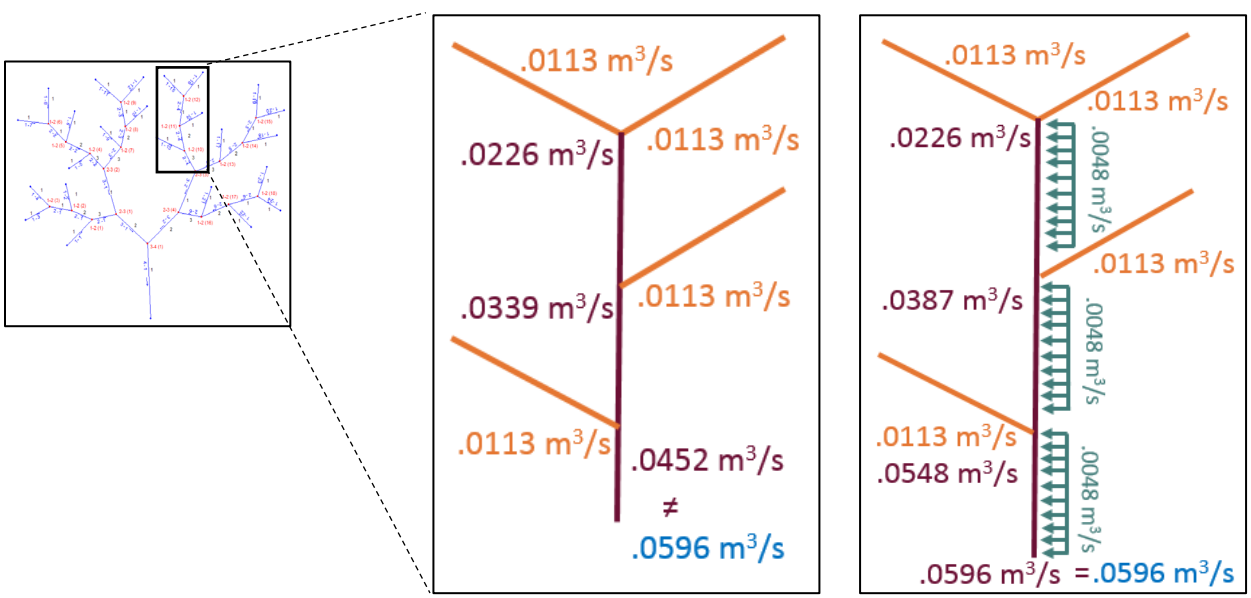

Figure A - 4: Example uniform lateral inflows for a 2nd order river showing flows that would result from no lateral inflows (left) and with actual lateral inflows used in the model (right). Orange values are surface water flow rates from 1st order rivers, red values are the resulting flows in the 2nd order river, green values are lateral inflows, and blue values are the required cumulative flow values from Table 3.

So in the unsteady flow setup, each 1st order river had a uniform flow hydrograph set to an arbitrary value of 0.0113 m^3/s at the first cross section as a boundary condition, a uniform lateral inflow starting at the second cross section and ending at the second to last cross-section according to Table 3, a uniform hyporheic outflow hydrograph at the 3rd cross-section according to the amount of water determined from the R code (Figure B - 3), and a hyporheic inflow hydrograph at the cross-section corresponding to the end of a restoration that was just the positive version of the outflow hydrograph. 2nd and 3rd order reaches had all of the same features, except they did not need an upstream boundary condition, just the uniform lateral inflow hydrograph needed to attain the proper values in Table 3. The 4th order reach was the same as the 2nd and 3rd order reaches, except it needed a downstream boundary condition that we set to the normal depth. The time of the hydrographs needs to equal or exceed the time window of the simulation. Since they are uniform, if the hydrograph exceeds the time window of the simulation, no effect will be felt.

Under these conditions, a minor unsteady peak appeared in the first few minutes of the 1st order cross-sections. It proceeded to propagate throughout the model, and eventually grew to a day-long ~20 cfs peak in the hydrograph at the final cross-section of the 4th order river. After the day-long peak, the flow was steady with only minor unsteadiness of +/- 0.005 cfs.

In order to remove this peak and make the model fully steady, a warm up period was added in the computation options and tolerances menu of the unsteady flow simulation window. After an iterative approach to determining how much of a warm up period was needed, it was found that 20,000 warm up steps at 0.1 hours each completely eliminated the unsteady peak that was propagating through the model. This warm up period had no effect on the actual time-span of the simulation, resulting in a completely steady flow model. Under this same window, the water surface calculation tolerance was set to 0.002 ft because of the small difference in flow between first order cross-sections. Without this tolerance, the model was unable to recognize the relatively small differences in flow between these closely-spaced cross-sections where flow changed very minimally compared to the rest of the model. After these tolerances and warmup period were implemented, the model could be run with a 10 second computation and mapping interval that produced a steady, baseflow scenario representative of a Piedmont watershed with only the minor unsteadiness of +/- 0.005 cfs described earlier.

Appendix A-4: Water Quality Simulations

The water quality model in HEC-RAS first asks the user to specify a constituent to study. We modeled nitrate-nitrogen (NO_3^--N) transport in the channel as an arbitrary conservative (non-reacting) constituent consistent that we called "Nitrogen." Concentration boundary conditions were needed at the upstream end of each 1st order river, at every flow change location, and for all uniform lateral inflows. We set all upstream and uniform lateral inflow boundary conditions to the same value (1 mg/L) to simulate a uniformly polluted watershed. The boundary condition for the hyporheic outflow was set to the upstream surface water concentration (1 mg/L in all initial flow cells, and the surface water concentration at the restoration outlet – read from the previous simulation results - for each successive outflow point where recycling occurred), and 0 mg/L at all hyporheic inflow points to model supply-limited denitrification in the hyporheic zone. Initial conditions were needed only at the upstream end of each reach, and were set to 1 mg/L, although because we ran the model until steady state, they did not affect our results. Dispersion coefficients were then specified for each reach in the model as the same relatively low value of 0.02 m^2/s to decrease model runtimes. For reference, typical dispersion coefficients for natural rivers are usually more than an order of magnitude higher than the value we chose [*Godfrey & Frederick*, 1970]. Sensitivity trials were completed to ensure that the same steady state was eventually reached no matter the dispersion coefficient.

After the arbitrary constituent, boundary and initial conditions, and dispersion coefficients were defined, the model had enough information to solve the advection dispersion equation (Equation 8) and produce spatial plots throughout the watershed. The water quality model was ran over the same time period as the hydraulics model, with all other default parameters selected. Similar to the hydraulic model, we ran the water quality model until steady state, when concentrations were no longer changing. After a model was ran, data was taken from the spatial plots and tables at key locations throughout the watershed that would later be needed to produce concentration profiles and percent reduction plots (Figure C - 1 through Figure C - 3).

Appendix B: Auxiliary R Code

Numerous studies have shown that denitrification is supply-limited in hyporheic sediment with $K \leq 10^{-4}$ m/s; i.e. complete denitrification within a hyporheic flow cell ($r_N = 100\%$) is reasonable [*Herzog et al.*, 2016; *Hester & Gooseff*, 2011; *Hester et al.*, 2016]. Yet as K increases, water flows through the hyporheic zone too quickly for complete denitrification to occur, and these coarse soils also lack the interstitial network necessary for microbial life [*Filoso & Palmer*, 2011; *Herzog et al.*, 2016; *Newcomer Johnson et al.*, 2016]. For this reason, in coarser beds where the r_h would increase, the assumption of 100% denitrification would not be applicable.

The auxiliary R code (Figure B - 3) was used to determine the amount of water to send through the hyporheic zone for each percent restored according to Equations 10 and 11. It also built on the water balance shown in the manuscript (Figure 2) and can account for possible variation in r_N. If r_N is anything less than 100%, HEC-RAS will need a downstream water quality boundary condition other than 0 mg/L as we used in this study. The R script will determine that based on the revised mass balance shown below (Figure B - 1). We also wrote the equation derivation that went into developing the loop in the code for a better understanding when using. All terms in the mass balance have units of [mg/s].

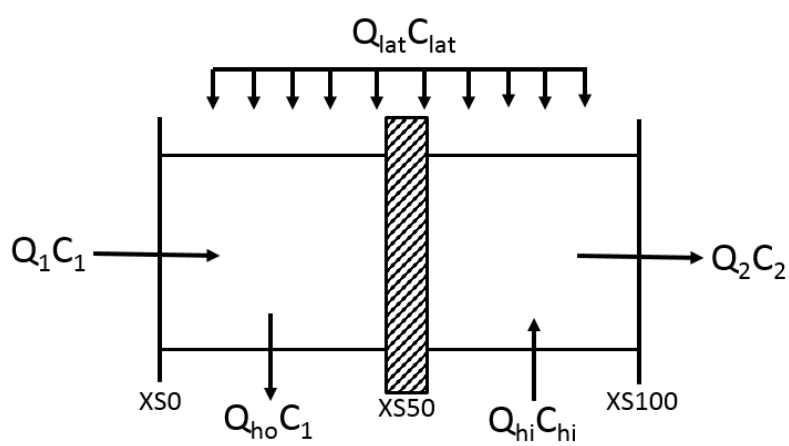

Figure B - 1: Conceptual mass balance of an in-stream restoration feature building on Figure 2 that includes concentrations.

$$Q_1C_1 - Q_{ho}C_1 + Q_{hi}C_{hi} + Q_{lat}C_{lat} = Q_2C_2 \quad \text{(B1)}$$

$$Q_{ho} = r_h{*}Q_1 \;\ldots\; Q_{ho} = Q_{hi} \;\ldots\; C_{hi} = r_N{*}C_1 \quad \text{(B2a…b…c)}$$

We assumed that all the water that entered the hyporheic zone upstream of a feature exited downstream, hence Equation B2b. Also note that throughout the thesis we defined r_N as the "percentage of denitrification per in-stream feature." This causes a problem in this mass balance as taking r_N = 100% (1.0), for example, would result in C_{hi} to equal C_1, hence no nitrate-nitrogen reduction. In the code we built in a line that subtracts r_N from 1 so that the downstream upwelling returns to the channel at the properly reduced concentration according to the denitrification percentage from field data or literature. Equation B3 is the full mass balance of the first restoration structure that comes from making the substitutions defined in Equations B2a-c into Equation B1.

$$Q_1C_1 - (r_hQ_1)C_1 + (r_hQ_1)[(r_N)C_1] + Q_{lat}C_{lat} = Q_2C_2 \quad \text{(B3)}$$

Chaining restorations together would result in a scenario such as the one described in Figure B - 2. The outlet load from the previous restoration segment (Q_2C_2) would now be the upstream load for the next restoration segment.

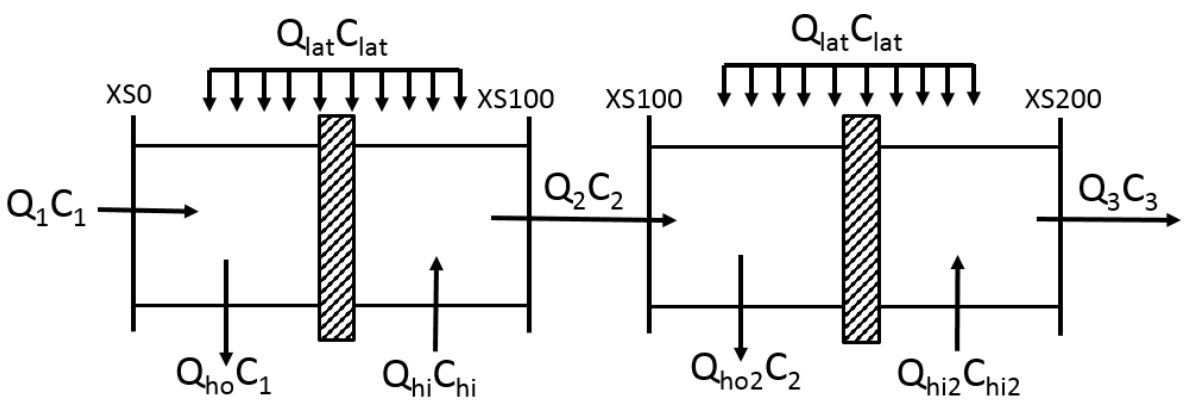

Figure B - 2: Conceptual model of the mass balance occurring from multiple restorations chained together.

We first took Equation B1 and gave the outlet flux a variable called "HYP1," shown below in Equations B4a-b because it begins to repeat within successive equations as more structures are added in a restoration.

$$Q_1C_1 - Q_{ho}C_1 + Q_{hi}C_{hi} + Q_{lat}C_{lat} = Q_2C_2 = \text{HYP1} \quad \text{(B4a)}$$

$$Q_1C_1 - (r_hQ_1)C_1 + (r_hQ_1)(r_NC_1) + Q_{lat}C_{lat} = Q_2C_2 = \text{HYP1} \quad \text{(B4b)}$$

We then defined the mass balance that would occur in the next section of stream before and after a restoration structure in Equation B5a-b. We gave the outlet load from this segment a

variable name of HYP2. We simply rearranged terms in Equation B5c to highlight the reoccurrence of Q_2C_2.

$$Q_2C_2 - Q_{ho2}C_2 + Q_{hi2}C_{hi2} + Q_{lat}C_{lat} = Q_3C_3 = HYP2 \quad \text{(B5a)}$$

$$Q_2C_2 - (r_hQ_2)C_2 + (r_hQ_2)(r_NC_2) + Q_{lat}C_{lat} = Q_3C_3 = HYP2 \quad \text{(B5b)}$$

$$Q_2C_2 - (r_h)Q_2C_2 + (r_hr_N)Q_2C_2 + Q_{lat}C_{lat} = Q_3C_3 = HYP2 \quad \text{(B5c)}$$

We then took the HYP1 variable that we defined in Equation B4a-b and plugged it into Equation B5c each time Q_2C_2 reappeared in the successive mass balance equation. This term already would have been defined with the known values from the model setup of the upstream flow rate (Q_1) and concentration (C_1), lateral inflow magnitude (Q_{lat}) and concentration (C_{lat}), removal per structure (r_N), and percentage of Q_1 flowing through the hyporheic zone per structure (r_h), such that Equation B6 could be defined.

$$HYP1 - r_hHYP1 + r_hr_NHYP1 + Q_{lat}C_{lat} = Q_3C_3 = HYP2 \quad \text{(B6)}$$

This same pattern would continue to occur as more structures were added (i.e. more stream was restored in our definition of restoration), such that we could develop Equation B7 that could be looped through however many structures were present in a restoration site (i).

$$HYP[i] - r_hHYP[i] + r_hr_NHYP[i] + Q_{lat}C_{lat} = HYP[i+1] \quad \text{(B7)}$$

After each loop cycle, the newly defined HYP[i+1] variable could be used to define the channel flow rate, channel concentration, and downstream upwelling concentrations by rearranging Equation B6. This is shown below in (Figure B - 3) for a fully restored 1st order stream. The code would be the same for any order stream, the initial variables would just need to be redefined based on the known upstream conditions for each order river.

```r
rm(list=ls(all=TRUE))

#First Order loop

#Initialize vectors
L_1 <- 6000                 #Length of 1st order stream [ft]
ss_1 <- 100                 #Spacing of structures according to literature [ft]
n_1 <- L_1/ss_1             #Number of Structures
n_array_1 <- c(1:n_1)       #Array for loop
HYP_1 <- c()                #Blank vector for "HYP" variable in mass balance
Qc_1 <- c()                 #Blank vector for "Qc" variable in mass balance. Channel Flow Rate
Cc_1 <- c()                 #Blank vector for "Cc" variable in mass balance. Channel concentration
Chi_1 <- c()                #Blank vector for "Chi" variable in mass balance. Concentration of water re-enterring channel after a structure.

#Initial Conditions
rh <- 0.003                 #Fraction of Water Traveling through the hyporheic zone over each structure [.3%]
rN <- 1                     #Fraction of Denitrification over each structure [100%]
rN <- 1-rN                  #Adjustor variable to make rN work properly in mass balance
Qlat_1_tot <- 0.3           #Amount of lateral inflow throughout the entire 1st order reach [cfs]
Qlat_1 <- Qlat_1_tot/n_1    #Amount of lateral inflow per structure (per 100 ft in the model) [cfs]
Clat <- 1                   #Concentration of GW enterring through lateral inflow [mg/L]
Qc_1[1] <- 0.1              #SW Flow rate at the top of each reach [cfs]
Cc_1[1] <- 1                #Concentration of SW at the begginign of the reach
Chi_1[1] <- Cc_1[1]*rN      #Concentration of the upwelling after a structure (Hec-RAS WQ Model Boundary Condition)

#Defininition of "HYP" varibale from mass balance under 1st structure -> HYP(n) = Qc(n+1)*Cc(n+1)
HYP_1[1] <- (Qc_1[1]*Cc_1[1])-(Qc_1[1]*Cc_1[1]*rh)+(Qc_1[1]*Cc_1[1]*rh*rN)+(Qlat_1*Clat)

#Loop through n number of structures
for (i in n_array_1) {
  HYP_1[i+1] <- HYP_1[i]-(HYP_1[i]*rh)+(HYP_1[i]*rh*rN)+(Qlat_1*Clat)
  Qc_1[i+1] <- Qc_1[i] + Qlat_1
  Cc_1[i+1] <- HYP_1[i]/Qc_1[i+1]
  Chi_1[i] <- ((Qc_1[i+1]*Cc_1[i+1])-(Qlat_1*Clat)+(rh*Qc_1[i]*Cc_1[i])-(Qc_1[i]*Cc_1[i]))/(rh*Qc_1[i])
}

#Vector of concentrations to enter as boundary conditions in the model
print(Cc_1, digits = 3)
CupBC_1 <- format(Chi_1[n_1], digits = 3)
cat("The concentration of the upwelling after the final structure (Hec-RAS BC) in the 1st order reaches is", CupBC_1, "mg/L")

#Determination of amount of water to send through the hyporheic zone in Hec-Ras
print(Qc_1[n_1+1], digits = 3)
SumQc_1 <- sum(Qc_1)
Q_hypo_1 <- SumQc_1*rh
print(Q_hypo_1, digits=3)

#Percent Reductions
Percent_Reduction_1 <- (1-(Cc_1/Cc_1[1]))*100
print(Percent_Reduction_1, digits = 3)
```

Figure B - 3: Auxiliary R code used to determine how much water to send through the hyporheic zone, as well as the downstream water quality boundary condition needed in model runs where r_N did not equal 100%

Appendix C: Interpreting Results from HEC-RAS

Below are a series of example spatial plots that are the default from the HEC-RAS water quality simulator. They show a trial where no surface water recycling occurred on an individual order restoration (Figure C - 1), a trial where surface water recycling did occur on an individual order restoration (Figure C - 2), and a trial from the full watershed restoration (Figure C - 2). All of the figures from the manuscripts were developed from the concentrations pulled from these plots. See figure captions and writing on the figures for detailed descriptions of what specific features mean.

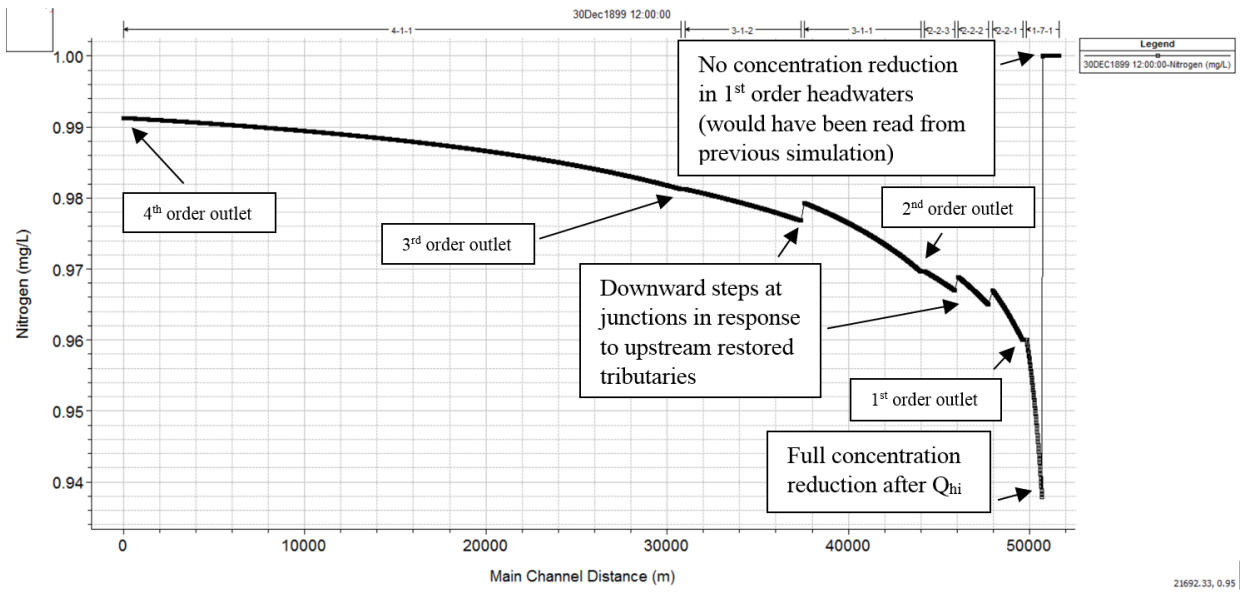

Figure C - 1: HEC-RAS concentration profile showing 50% of the individual 1st order rivers restored (i.e. restoration with no surface water recycling).

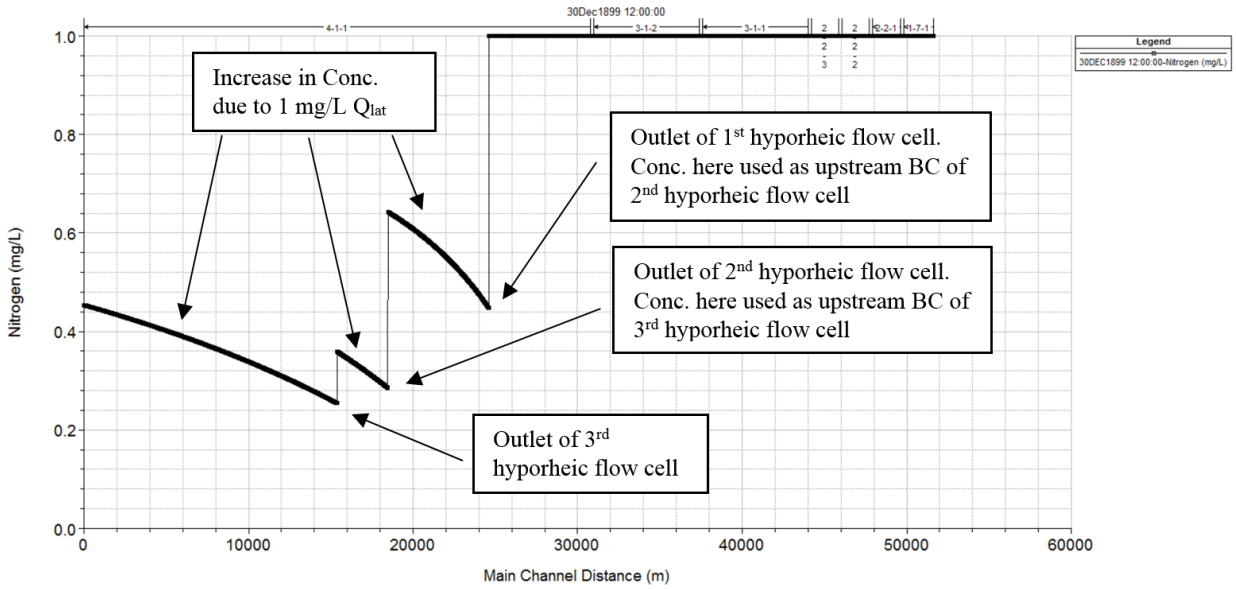

Figure C - 2: HEC-RAS concentration profile showing 50% of the individual 4th order restoration (i.e. restoration with surface water recycling)

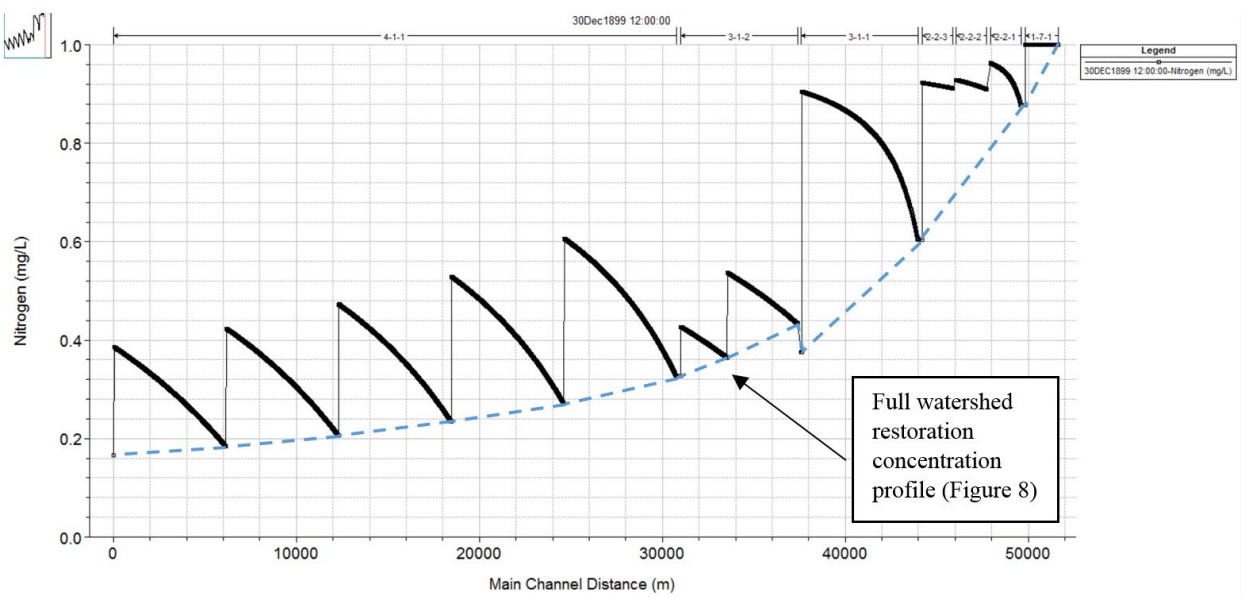

Figure C - 3: HEC-RAS concentration profile showing 100% of the full-watershed restoration (i.e. the raw data used to develop Figure 8). The detailed specifics of the 1st and 2nd order restorations are not shown in this plot, as no surface water recycling occurred (i.e. concentrations at specific spatial locations set as boundary conditions). Those concentrations needed to be recorded incrementally moving down the watershed as the concentrations at the outlet of a restoration as in Figure C - 1.

Appendix D: Details of Restoration Scenarios

Table D - 1: 1st order lengths, number of structures, and flow into and out of the hyporheic zone corresponding to certain percentages of channel length restored

Percent restored [%]	Cumulative length restored [m]	Length of restoration per individual 1st order reach [m]	Number of structures	Cumulative amount of water in/out of hyporheic zone [m^3/s]
0	0	0	0	0.00E+00
10	4,560	190	6	6.85E-05
20	8,880	370	12	1.44E-04
30	13,200	550	18	2.34E-04
40	17,760	740	24	3.40E-04
50	22,080	920	30	4.53E-04
60	26,400	1,100	36	5.97E-04
70	30,960	1,290	42	7.48E-04
80	35,280	1,470	48	9.15E-04
90	39,600	1,650	54	1.10E-03
100	43,920	1,830	60	1.30E-03

Table D - 2: 2nd order lengths, number of structures, and flow into and out of the hyporheic zone corresponding to certain percentages of channel length restored

Percent restored [%]	Cumulative length restored [m]	Length of restoration per individual 2nd order reach [m]	Number of structures	Cumulative amount of water in/out of hyporheic zone [m^3/s]
0	0	0	0	0.000
10	3,060	510	17	0.001
20	6,060	1,010	33	0.003
30	9,060	1,510	50	0.004
40	12,120	2,020	66	0.006
50	15,120	2,520	83	0.008
60	18,120	3,020	99	0.010
70	21,180	3,530	116	0.013
80	24,180	4,030	132	0.015
90	27,180	4,530	149	0.018
100	30,180	5,030	165	0.021

Table D - 3: 3rd order lengths, number of structures, and flow into and out of the hyporheic zone corresponding to certain percentages of channel length restored

Percent restored [%]	Cumulative length restored [m]	Length of restoration per individual 3rd order reach [m]	Number of structures	Cumulative amount of water in/out of hyporheic zone [m^3/s]
0	0	0	0	0.000
10	2,580	1,290	42	0.017
20	5,140	2,570	84	0.035
30	7,700	3,850	126	0.055
40	10,260	5,130	168	0.078
50	12,820	6,410	210	0.102
60	15,380	7,690	252	0.129
70	17,940	8,970	294	0.157
80	20,500	10,250	336	0.188
90	23,060	11,530	378	0.221
100	25,620	12,810	420	0.257

Table D - 4: 4th order lengths, number of structures, and flow into and out of the hyporheic zone corresponding to certain percentages of channel length restored

Percent restored [%]	Cumulative length restored [m]	Length of restoration per individual 4th order reach [m]	Number of structures	Cumulative amount of water in/out of hyporheic zone [m^3/s]
0	0	0	0	0.000
10	3,080	3,080	101	0.187
20	6,160	6,160	202	0.394
30	9,240	9,240	303	0.617
40	12,320	12,320	404	0.864
50	15,400	15,400	505	1.13
60	18,480	18,480	606	1.42
70	21,550	21,550	707	1.72
80	24,630	24,630	808	2.04
90	27,710	27,710	909	2.39
100	30,790	30,790	1010	2.76

Appendix E: Raw Data

All raw data presented came from the HEC-RAS water quality feature and was used to produce the figures within the manuscript. HEC-RAS reports concentration data out to the number of decimal places presented in all tables. All data is stored in a Microsoft Excel file which was where all figures were developed.

Table E - 1: Individual 1st order restoration raw data

Percent Restored [%]	Cumulative Length Restored [ft]	Cumulative Length Restored [m]	Nitrogen Concentration at end of 1st order reach [mg/L]	Percent Reduction at end of 1st Order	Nitrogen Concentration at end of 2nd order reach [mg/L]	Percent Reduction at end of 2nd Order	Nitrogen Concentration at end of 3rd order reach [mg/L]	Percent Reduction at end of 3rd Order	Percent Nitrogen Reduction at 4th Order Effluent [%]
0	0	0	1	0.00	1	0.00	1	0.00	0.00
10	14400	4389.12	0.9949984	0.50	0.9962074	0.38	0.9976121	0.24	0.11
20	28800	8778.24	0.9875128	1.25	0.9905308	0.95	0.994141	0.59	0.27
30	43200	13167.36	0.9800065	2.00	0.9848387	1.52	0.9906188	0.94	0.44
40	57600	17556.48	0.9700043	3.00	0.9772565	2.27	0.9859267	1.41	0.66
50	72000	21945.6	0.9599943	4.00	0.9696649	3.03	0.9812294	1.88	0.87
60	86400	26334.72	0.9472613	5.27	0.9600067	4.00	0.9752513	2.47	1.15
70	100800	30723.84	0.9340608	6.59	0.9499894	5.00	0.9690459	3.10	1.44
80	115200	35112.96	0.9193118	8.07	0.9388002	6.12	0.9621236	3.79	1.76
90	129600	39502.08	0.9025218	9.75	0.9260775	7.39	0.9542612	4.57	2.13
100	144000	43891.2	0.8775263	12.25	0.9071308	9.29	0.9425349	5.75	2.67

Table E - 2: Individual 2nd order restoration raw data

Percent Restored [%]	Cumulative Length Restored [ft]	Cumulative Length Restored [m]	Nitrogen Concentration at end of 2nd order reach [mg/L]	Percent Reduction at end of 2nd Order [%]	Nitrogen Concentration at end of 3rd order reach [mg/L]	Percent Reduction at end of 3rd Order [%]	Percent Nitrogen Reduction at 4th Order Effluent [%]
0	0	0	1	0.00	1	0.00	0.00
10	9900	3017.52	0.9777234	2.23	0.9862162	1.38	0.64
20	19800	6035.04	0.9549771	4.50	0.9721392	2.79	1.30
30	29700	9052.56	0.927479	7.25	0.955134	4.49	2.09
40	39600	12070.08	0.8985772	10.14	0.937246	6.28	2.92
50	49500	15087.6	0.864926	13.51	0.916423	8.36	3.89
60	59400	18105.12	0.8298675	17.01	0.89472	10.53	4.90
70	69300	21122.64	0.7895799	21.04	0.8697982	13.02	6.06
80	79200	24140.16	0.7488186	25.12	0.8445692	15.54	7.23
90	89100	27157.68	0.7023786	29.76	0.8158385	18.42	8.57
100	99000	30175.2	0.6554299	34.46	0.7868084	21.32	9.92

Table E - 3: Individual 3rd order restoration raw data

Percent Restored [%]	Cumulative Length Restored [ft]	Cumulative Length Restored [m]	Nitrogen Concentration at end of 3rd order reach [mg/L]	Percent Reduction at end of 3rd Order [%]	Percent Nitrogen Reduction at 4th Order Effluent [%]
0	0	0	1	0.00	0.00
10	8400	2560.32	0.9429125	5.71	2.66
20	16800	5120.64	0.8797614	12.02	5.60
30	25200	7680.96	0.8093746	19.06	8.87
40	33600	10241.28	0.7321526	26.78	12.47
50	42000	12801.6	0.6471174	35.29	16.42
60	50400	15361.92	0.5952598	40.47	18.84
70	58800	17922.24	0.5395237	46.05	21.43
80	67200	20482.56	0.4793888	52.06	24.23
90	75600	23042.88	0.4148373	58.52	27.23
100	84000	25603.2	0.3464241	65.36	30.42

Table E - 4: Individual 4th order restoration raw data

Percent Restored [%]	Cumulative Length Restored [ft]	Cumulative Length Restored [m]	Percent Nitrogen Reduction at 4th Order Effluent [%]
0	0	0	0.00
10	10100	3078.48	15.06
20	20200	6156.96	31.62
30	30300	9235.44	39.67
40	40400	12313.92	48.54
50	50500	15392.4	54.66
60	60600	18470.88	61.23
70	70700	21549.36	66.63
80	80800	24627.84	72.44
90	90900	27706.32	77.70
100	101000	30784.8	83.27

Table E - 5: Full 4th order watershed restoration raw data

Percent Restored [%]	Cumulative Length Restored [ft]	Cumulative Length Restored [m]	Percent Nitrogen Reduction at 4th Order Effluent [%]
0.00	0	0.0	0.00
3.36	14400	4389.1	0.11
6.73	28800	8778.2	0.27
10.09	43200	13167.4	0.44
13.46	57600	17556.5	0.66
16.82	72000	21945.6	0.87
20.19	86400	26334.7	1.15
23.55	100800	30723.8	1.44
26.92	115200	35113.0	1.76
30.28	129600	39502.1	2.13
33.64	144000	43891.2	2.67
38.27	163800	49926.2	3.81
42.90	183600	55961.3	5.24
47.52	203400	61996.3	6.98
52.15	223200	68031.4	9.02
56.78	243000	74066.4	11.38
60.70	259800	79187.0	14.77
64.63	276600	84307.7	18.93
66.59	285000	86868.0	21.33
68.55	293400	89428.3	23.18
72.48	310200	94549.0	27.33
76.40	327000	99669.6	31.34
81.12	347200	105826.6	41.69
85.84	367400	111983.5	51.97
90.56	387600	118140.5	62.42
95.28	407800	124297.4	72.86
100.00	428000	130454.4	83.42

Table E - 6: Full 3rd order restoration raw data

Percent Restored with 3rd Order the bottom of the watershed	Nitrogen Concnetration at 3rd order effluent [mg/L]	Percent Nitrogen Removal at Effluent [%]
0.00	1	0.00
4.40	0.9976121	0.24
8.81	0.994141	0.59
13.21	0.9906188	0.94
17.61	0.9859267	1.41
22.02	0.9812294	1.88
26.42	0.9752513	2.47
30.83	0.9690459	3.10
35.23	0.9621236	3.79
39.63	0.9542612	4.57
44.04	0.9425349	5.75
50.09	0.9180735	8.19
56.15	0.8874377	11.26
62.20	0.8501139	14.99
68.26	0.8060923	19.39
74.31	0.7553934	24.46
79.45	0.6826023	31.74
84.59	0.5932456	40.68
87.16	0.541785	45.82
89.72	0.5018767	49.81
94.86	0.4126933	58.73
100.00	0.3266759	67.33

Table E - 7: Nitrate-nitrogen (NO_3^--N) load raw data

Flowpath Length [m]	Channel Flow rate [cms]	Channel Flow Rate [l/s]	Mass Flow Rate 100% Restored [mg/s]	Mass Flow Rate Unrestored [mg/s]	Percent Reduction [%]
0.0	0.0028	2.83	2.83	2.83	0.00
182.9	0.0037	3.68	3.63	3.68	1.48
365.8	0.0045	4.53	4.39	4.53	3.01
548.6	0.0054	5.38	5.16	5.38	4.07
731.5	0.0062	6.23	5.90	6.23	5.28
914.4	0.0074	7.36	6.90	7.36	6.21
1097.3	0.0082	8.21	7.61	8.21	7.32
1280.2	0.0091	9.06	8.31	9.06	8.28
1463.0	0.0099	9.91	8.99	9.91	9.25
1645.9	0.011	10.76	9.65	10.76	10.28
1828.8	0.011	11.33	9.94	11.33	12.25
1828.8	0.023	22.65	19.88	22.65	12.25
2834.6	0.025	25.49	20.37	25.49	20.07
3840.5	0.040	39.64	30.19	39.64	23.84
4846.3	0.043	42.76	29.66	42.76	30.64
5852.2	0.057	56.92	38.18	56.92	32.92
6858.0	0.060	59.75	36.13	59.75	39.53
6858.0	0.12	119.50	72.26	119.50	39.53
9418.3	0.14	141.58	73.30	141.58	48.23
11978.6	0.16	163.95	69.67	163.95	57.50
13258.8	0.17	174.71	65.53	174.71	62.49
14539.0	0.25	245.51	101.24	245.51	58.76
17099.3	0.27	267.59	97.54	267.59	63.55
19659.6	0.29	289.68	94.63	289.68	67.33
19659.6	0.58	579.36	189.26	579.36	67.33
25816.6	0.71	712.17	193.43	712.17	72.84
31973.5	0.85	845.54	198.69	845.54	76.50
38130.5	0.98	978.63	201.78	978.63	79.38
44287.4	1.11	1112.00	205.06	1112.00	81.56
50444.4	1.24	1244.81	206.35	1244.81	83.42

Appendix F: Material Cited in Manuscript (Section 2) to be added to Supplemental Materials upon Publication

NOTE: There is no new information provided here. It is simply included for organizational purposes when the time comes to prepare supplemental materials for publication. All of these tables and figures are referenced in the Manuscript, and appear elsewhere in the Appendix.

LONGITUDINAL PROFILE – LOCATION: APPENDIX A. Cited on Page 33

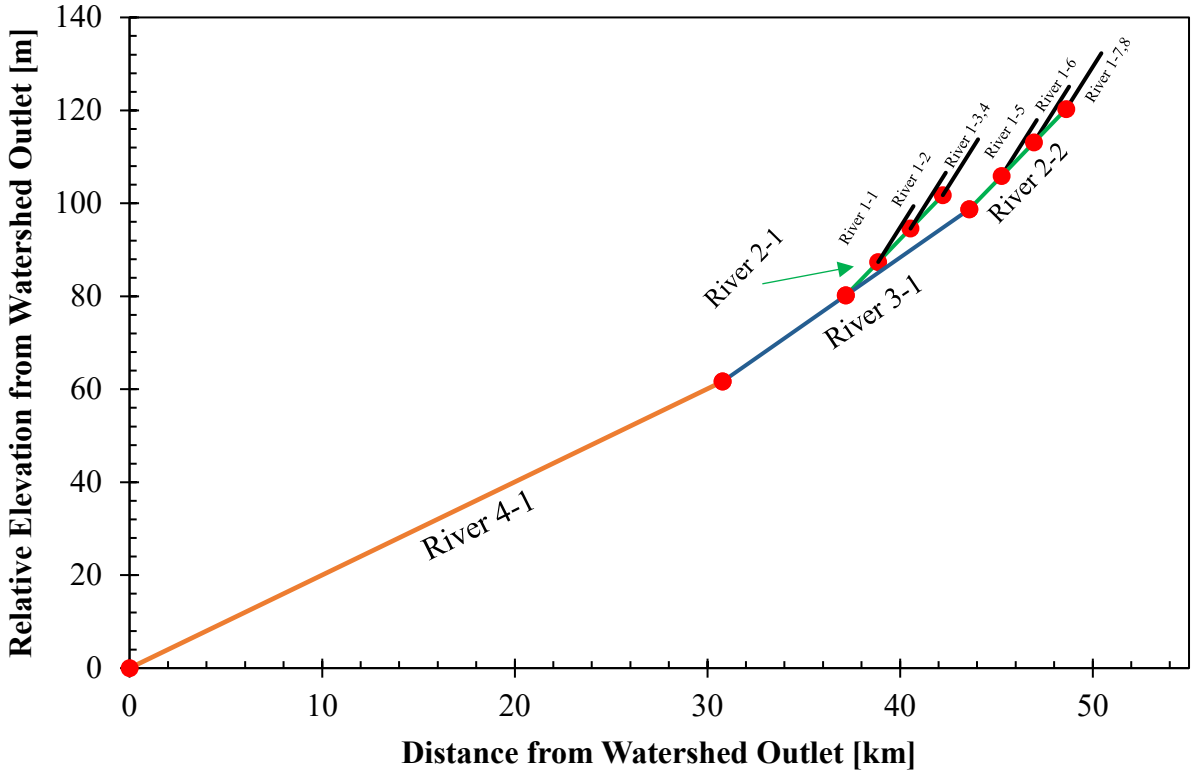

Figure A - 5: Longitudinal profile of watershed. The watershed in HEC-RAS was created symmetrical so this is the same longitudinal profile as traveling up River 3-2 after Junction 3-4(1). Orange is 4th order, blue is 3rd order, green is 2nd order, black is 1st order, red dots are junctions.

AUXILLIARY R CODE – LOCATION: APPENDIX B. Cited on Page 38

```
rm(list=ls(all=TRUE))

#First Order loop

#Initialize vectors
L_1 <- 6000                 #Length of 1st order stream [ft]
ss_1 <- 100                 #Spacing of structures according to literature [ft]
n_1 <- L_1/ss_1             #Number of Structures
n_array_1 <- c(1:n_1)       #Array for loop
HYP_1 <- c()                #Blank vector for "HYP" variable in mass balance
Qc_1 <- c()                 #Blank vector for "Qc" variable in mass balance. Channel Flow Rate
Cc_1 <- c()                 #Blank vector for "Cc" variable in mass balance. Channel concentration
Chi_1 <- c()                #Blank vector for "Chi" variable in mass balance. Concentration of water re-enterring channel after a structure.

#Initial Conditions
rh <- 0.003                 #Fraction of Water Traveling through the hyporheic zone over each structure [.3%]
rN <- 1                     #Fraction of Denitrification over each structure [100%]
rN <- 1-rN                  #Adjustor variable to make rN work properly in mass balance
Qlat_1_tot <- 0.3           #Amount of lateral inflow throughout the entire 1st order reach [cfs]
Qlat_1 <- Qlat_1_tot/n_1 #Amount of lateral inflow per structure (per 100 ft in the model) [cfs]
Clat <- 1                   #Concentration of GW enterring through lateral inflow [mg/L]
Qc_1[1] <- 0.1              #SW Flow rate at the top of each reach [cfs]
Cc_1[1] <- 1                #Concentration of SW at the begginign of the reach
Chi_1[1] <- Cc_1[1]*rN      #Concentration of the upwelling after a structure (Hec-RAS WQ Model Boundary Condition)

#Defininition of "HYP" varibale from mass balance under 1st structure -> HYP(n) = Qc(n+1)*Cc(n+1)
HYP_1[1] <- (Qc_1[1]*Cc_1[1])-(Qc_1[1]*Cc_1[1]*rh)+(Qc_1[1]*Cc_1[1]*rh*rN)+(Qlat_1*Clat)

#Loop through n number of structures
for (i in n_array_1) {
  HYP_1[i+1] <- HYP_1[i]-(HYP_1[i]*rh)+(HYP_1[i]*rh*rN)+(Qlat_1*Clat)
  Qc_1[i+1] <- Qc_1[i] + Qlat_1
  Cc_1[i+1] <- HYP_1[i]/Qc_1[i+1]
  Chi_1[i] <- ((Qc_1[i+1]*Cc_1[i+1])-(Qlat_1*Clat)+(rh*Qc_1[i]*Cc_1[i])-(Qc_1[i]*Cc_1[i]))/(rh*Qc_1[i])
}

#Vector of concentrations to enter as boundary conditions in the model
print(Cc_1, digits = 3)
CupBC_1 <- format(Chi_1[n_1], digits = 3)
cat("The concentration of the upwelling after the final structure (Hec-RAS BC) in the 1st order reaches is", CupBC_1, "mg/L")

#Determination of amount of water to send through the hyporheic zone in Hec-Ras
print(Qc_1[n_1+1], digits = 3)
SumQc_1 <- sum(Qc_1)
Q_hypo_1 <- SumQc_1*rh
print(Q_hypo_1, digits=3)

#Percent Reductions
Percent_Reduction_1 <- (1-(Cc_1/Cc_1[1]))*100
print(Percent_Reduction_1, digits = 3)
```

Figure B - 4: Auxiliary R code used to determine how much water to send through the hyporheic zone, as well as the downstream water quality boundary condition needed in model runs where r_N did not equal 100%

RESTORATION SCENARIO DETAILS – LOCATION: APPENDIX D. Cited on Page 39, 41

Table D - 5: 1st order lengths, number of structures, and flow into and out of the hyporheic zone corresponding to certain percentages of channel length restored

Percent restored [%]	Cumulative length restored [m]	Length of restoration per individual 1st order reach [m]	Number of structures	Cumulative amount of water in/out of hyporheic zone [m^3/s]
0	0	0	0	0.00E+00
10	4,560	190	6	6.85E-05
20	8,880	370	12	1.44E-04
30	13,200	550	18	2.34E-04
40	17,760	740	24	3.40E-04
50	22,080	920	30	4.53E-04
60	26,400	1,100	36	5.97E-04
70	30,960	1,290	42	7.48E-04
80	35,280	1,470	48	9.15E-04
90	39,600	1,650	54	1.10E-03
100	43,920	1,830	60	1.30E-03

Table D - 6: 2nd order lengths, number of structures, and flow into and out of the hyporheic zone corresponding to certain percentages of channel length restored

Percent restored [%]	Cumulative length restored [m]	Length of restoration per individual 2nd order reach [m]	Number of structures	Cumulative amount of water in/out of hyporheic zone [m^3/s]
0	0	0	0	0.000
10	3,060	510	17	0.001
20	6,060	1,010	33	0.003
30	9,060	1,510	50	0.004
40	12,120	2,020	66	0.006
50	15,120	2,520	83	0.008
60	18,120	3,020	99	0.010
70	21,180	3,530	116	0.013
80	24,180	4,030	132	0.015
90	27,180	4,530	149	0.018
100	30,180	5,030	165	0.021

Table D - 7: 3rd order lengths, number of structures, and flow into and out of the hyporheic zone corresponding to certain percentages of channel length restored

Percent restored [%]	Cumulative length restored [m]	Length of restoration per individual 3rd order reach [m]	Number of structures	Cumulative amount of water in/out of hyporheic zone [m^3/s]
0	0	0	0	0.000
10	2,580	1,290	42	0.017
20	5,140	2,570	84	0.035
30	7,700	3,850	126	0.055
40	10,260	5,130	168	0.078
50	12,820	6,410	210	0.102
60	15,380	7,690	252	0.129
70	17,940	8,970	294	0.157
80	20,500	10,250	336	0.188
90	23,060	11,530	378	0.221
100	25,620	12,810	420	0.257

Table D - 8: 4th order lengths, number of structures, and flow into and out of the hyporheic zone corresponding to certain percentages of channel length restored

Percent restored [%]	Cumulative length restored [m]	Length of restoration per individual 4th order reach [m]	Number of structures	Cumulative amount of water in/out of hyporheic zone [m^3/s]
0	0	0	0	0.000
10	3,080	3,080	101	0.187
20	6,160	6,160	202	0.394
30	9,240	9,240	303	0.617
40	12,320	12,320	404	0.864
50	15,400	15,400	505	1.13
60	18,480	18,480	606	1.42
70	21,550	21,550	707	1.72
80	24,630	24,630	808	2.04
90	27,710	27,710	909	2.39
100	30,790	30,790	1010	2.76